Gabriel Rodolfo Espinosa Espinoza

Molecular aspects of *Besnoitia besnoiti*-driven bovine neutrophil extracellular trap formation

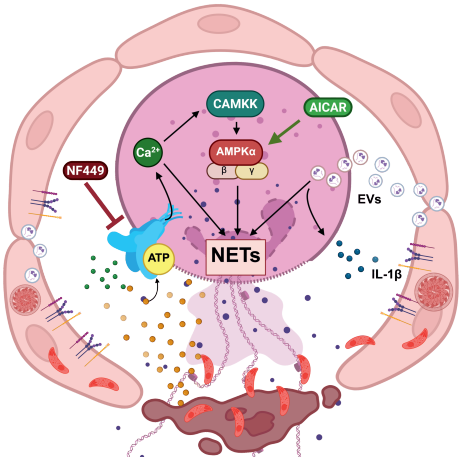

INAUGURAL DISSERTATION
submitted to the Faculty of Veterinary Medicine
in fulfilment of the requirements for the PhD degree
Doctor of Philosophy
of the Faculties of Veterinary Medicine and Medicine
of the Justus Liebig University Giessen, Germany

édition scientifique
VVB LAUFERSWEILER VERLAG

1. Auflage 2026

1st Edition 2026

Printed in Germany

édition scientifique
VVB LAUFERSWEILER VERLAG

STAUFENBERGRING 15, 35396 GIESSEN, GERMANY
Tel: 0641-5599888 Fax: 0641-5599890
email: redaktion@doktorverlag.de

www.doktorverlag.de

Molecular aspects of *Besnoitia besnoiti*-driven bovine neutrophil extracellular trap formation

INAUGURAL DISSERTATION

submitted to the Faculty of Veterinary Medicine

in fulfilment of the requirements

for the PhD degree

Doctor of Philosophy

of the Faculties of Veterinary Medicine and Medicine

of the Justus Liebig University Giessen, Germany

by

Gabriel Rodolfo Espinosa Espinoza

Biochemist from Angol, Chile

Gießen, 2026

From the Institute of Parasitology,
Faculty of Veterinary Medicine, Justus Liebig University Giessen
Managing Director: Prof. Dr. Anja Taubert

Chair: Prof. Dr. Ralph Schermuly
Vice-chair / Co-supervisor: Prof. Dr. Stephan Pleschka
First reviewer / Supervisor: Prof. Dr. Anja Taubert
Second reviewer: Prof. Dr. Marc Hübner

Date of Doctoral Defense: 27.02.2026

LIST OF PUBLICATION AND CONFERENCE CONTRIBUTIONS

Most data of this dissertation have already been published and presented at conferences:

Original papers

1. **Espinosa, G.**, Conejeros, I., Rojas-Barón, L., Hermosilla, C. R., Taubert, A. (2023). *Besnoitia besnoiti*-induced neutrophil clustering and neutrophil extracellular trap formation depend on P2X1 purinergic receptor signaling. *Frontiers in Immunology*, *14*, 1244068.
2. Conejeros, I., Velásquez, Z. D., Rojas-Barón, L., **Espinosa, G.**, Hermosilla, C., Taubert, A. (2024). The CAMKK/AMPK Pathway Contributes to *Besnoitia besnoiti*-Induced NETosis in Bovine Polymorphonuclear Neutrophils. *International Journal of Molecular Sciences*, 25(15), 8442.
3. **Espinosa, G.**, Salinas-Varas, C., Rojas-Barón, L., Preußer, C., Pogge von Strandmann, E., Gärtner, U., Conejeros, I., Hermosilla, C., Taubert, A. (2024). Bovine PMN responses to extracellular vesicles released by *Besnoitia besnoiti* tachyzoites and *B. besnoiti*-infected host cells. *Frontiers in Immunology*, 15, 1509355.
4. Conejeros, I., Velásquez, Z. D., **Espinosa, G.**, Rojas-Baron, L., Grabbe, M., Hermosilla, C., Taubert, A. (2025). AMPK and CAMKK activation participate in early events of *Toxoplasma gondii*-triggered NET formation in bovine polymorphonuclear neutrophils. *Frontiers in Veterinary Science*, 12, 1557509.

Please note:

Previously published content (text passages, illustrations) will be appropriately referenced throughout this document, citing the above-mentioned publications. Text passages are referenced paragraph-by-paragraph, illustrations in the respective figure legends.

Conference contributions

1. **Espinosa, G.**, Conejeros, I., Hermosilla, C., Taubert, A. P2X1 receptor antagonist NF449 inhibits *Besnoitia besnoiti*-induced anchored neutrophil extracellular trap (NET) formation. Conference of the DVG Specialist Group "Parasitology and Parasitic diseases", Berlin, Germany. 23-25/05/2022.
2. **Espinosa, G.**, Conejeros, I., Hermosilla, C., Taubert, A. P2X1 receptor antagonist NF449 inhibits *Besnoitia besnoiti*-induced neutrophil chemotaxis and anchored extracellular trap (NET) formation. 15th GGL Annual Conference, Justus Liebig University Giessen, Giessen, Germany, 14-15/09/2022
3. **Espinosa, G.**, Conejeros, I., Hermosilla, C., Taubert, A. P2X1 receptor antagonist NF449 inhibits *Besnoitia besnoiti*-induced neutrophil clustering and anchored extracellular trap (NET) formation. Conference of the German Society of Parasitology (DGP), Giessen, Germany, 15-17/03/2023
4. Conejeros, I., Velásquez, Z., **Espinosa, G.**, Hermosilla, C., Taubert, A. Parasitic molecular triggers of coccidia-induced NETosis: a role for cell surface glycans. Conference of the German Society of Parasitology (DGP), Giessen, Germany, 15-17/03/2023
5. **Espinosa, G.**, Conejeros, I., Hermosilla, C., Taubert, A. P2X1 receptor antagonist NF449 inhibits *Besnoitia besnoiti*-induced neutrophil clustering and anchored extracellular trap (NET) formation. European Phagocyte Workshop, Budapest, Hungary, 29/03-01/04/2023
6. **Espinosa, G.**, Conejeros, I., Rojas-Barón, L., Hermosilla, C., Taubert, A. P2X1 receptor antagonist NF449 inhibits *Besnoitia besnoiti*-induced neutrophil clustering and anchored extracellular trap (NET) formation. Conference of the DVG Specialist Group "Parasitology and Parasitic diseases", München, Germany, 15-17/05/2023
7. Conejeros, I., Velásquez, Z., Rojas-Barón, L., **Espinosa, G.**, Hermosilla, C., Taubert, A. Role of AMPK in *Besnoitia besnoiti* and *Toxoplasma gondii* tachyzoite-induced PMN responses. Conference of the DVG Specialist Group "Parasitology and Parasitic diseases". München, Germany, 15-17/05/2023
8. **Espinosa, G.**, Conejeros, I., Hermosilla, C., Taubert, A. Extracellular vesicles derived from *Besnoitia besnoiti*- and *Toxoplasma gondii*-infected host cells and -exposed PMN induce NOX-independent NET formation. 16th GGL Annual Conference, Justus Liebig University Giessen, Giessen, Germany, 20-21/09/2023

9. Conejeros, I., Velásquez, Z., Rojas-Barón, L., **Espinosa, G.**, Hermosilla, C., Taubert, A. Role of AMPK in *Besnoitia besnoiti* and *Toxoplasma gondii* tachyzoite-induced PMN responses. European Phagocyte Workshop, Visegrád, Hungary, 20-23/03/2024

10. **Espinosa, G.**, Salinas-Varas, C., Rojas-Barón, L., Preußer, C., Gärtner, U., Conejeros, I., Hermosilla, C., Taubert, A. *Besnoitia besnoiti* tachyzoites- and host cell-derived extracellular vesicles induce NOX-independent NET formation. Conference of the DVG Specialist Group "Parasitology and Parasitic diseases", Hannover, Germany, 08-10/07/2024

11. **Espinosa, G.**, Salinas-Varas, C., Rojas-Barón, L., Preußer, C., Gärtner, U., Conejeros, I., Hermosilla, C., Taubert, A. *Besnoitia besnoiti* tachyzoites- and host cell-derived extracellular vesicles induce NADPH oxidase-independent NET formation. 17th GGL Annual Conference, Justus Liebig University Giessen, Giessen, Germany, 11-12/09/2024

12. **Espinosa, G.**, Salinas-Varas, C., Rojas-Barón, L., Preußer, C., Gärtner, U., Conejeros, I., Hermosilla, C., Taubert, A. *Besnoitia besnoiti* tachyzoites- and host cell-derived extracellular vesicles induce NADPH oxidase-independent NET formation. International Symposium NEUTROPHIL, München, Germany, 17-19/09/2024

13. **Espinosa, G.**, Salinas-Varas, C., Rojas-Barón, L., Preußer, C., Pogge von Strandmann, E., Gärtner, U., Conejeros, I., Hermosilla, C., Taubert, A. Bovine PMN responses to extracellular vesicles released by *Besnoitia besnoiti* tachyzoites and B. besnoiti-infected host cells. Conference of the German Society of Parasitology (DGP), Würzburg, Germany, 11-14/03/2025

14. Conejeros I., Velásquez Z. D., Rojas L., **Espinosa G.**, Hermosilla C., Taubert A. The AMPK pathway plays a role in *Besnoitia besnoiti* and *Toxoplasma gondii* tachyzoite-induced PMN responses. Conference of the German Society of Parasitology (DGP), Würzburg, Germany, 11-14/03/2025

ABBREVIATIONS

$[Ca^{2+}]_i$: Intracellular Calcium Concentration

ADO: Adenosine

ADP: Adenosine Diphosphate

AICAR: Aminoimidazole Carboxamide Ribonucleotide

AMP: Adenosine Monophosphate

AMPK: AMP-Activated Protein Kinase

ANOVA: Analysis of Variance

AP2: Apetala 2

ATP: Adenosine Triphosphate

B.b.: *Besnoitia besnoiti*

BFD1: Bradyzoite-formation deficient 1

BKIs: Bumped Kinase Inhibitors

BUVEC: Bovine Umbilical Vein Endothelial Cell

CAMKK2: Calcium/Calmodulin-Dependent Kinase Kinase 2

cAMP: Cyclic Adenosine Monophosphate

CC: Compound C, Dorsomorphin

CD39: Cluster of Differentiation 39

CD73: Cluster of Differentiation 73

cGMP: Cyclic Guanosine Monophosphate

CLEC5A: C-Type Lectin Domain Family 5 Member A

CR: Complement Receptors

CRL: C-Type Lectins

CTSG: Cathepsin G

CXCL-: Chemokine (C-X-C Motif) Ligand

DAMPs: Damage-Associated Molecular Patterns

DCFH-DA: 2′,7′-Dichlorofluorescein Diacetate

DNA: Deoxyribonucleic Acid

EC: Endothelial Cell

ECGM: Endothelial Cell Growth Medium

EDTA: Ethylenediaminetetraacetic Acid

eIF2α: Eukaryotic Initiation Factor 2 Alpha

ELISA: Enzyme-Linked Immunosorbent Assay

ELQs: Endochine Like Quinolones

ER: Endoplasmic Reticulum

ERK1/2: Extracellular Signal-Regulated Kinase 1/2

ESCRT: Endosomal Sorting Complex Required for transport

EVs: Extracellular Vesicles

FBS: Fetal Bovine Serum

FcR: Fc Receptors

FCS: Fetal Calf Serum

fMLP: N-Formylated Peptides

GPCRs: G Protein-Coupled Receptors

HBSS: Hank's Balanced Salt Solution

HFF: Human Foreskin Fibroblast

HL-60: Human Promyelocytic Leukemia Cells

IC_{50}: Half Maximal Inhibitory Concentration

ICAM-1: Intercellular Adhesion Molecule 1

IFAT: Indirect Fluorescent Antibody Test

Ig-: Immunoglobulin-

IL-: Interleukin-

IST: Internal Transcribed Spacer

LC3: Light Chain 3

LKB1: Liver-Kinase-B1

LPS: Lipopolysaccharides

MAPK: Mitogen-Activated Protein Kinase

MDBK: Madin-Darby Bovine Kidney Cell

MHC-II: Major Histocompatibility Complex Class II

MPO: Myeloperoxidase

mPTP: Mitochondrial Permeability Transition Pore

mtDNA: Mitochondrial DNA

mtROS: Mitochondrial Reactive Oxygen Species

MVBs: Multivesicular Bodies

NADPH: Nicotinamide Adenine Dinucleotide Phosphate

NE: Neutrophil Elastase

NET: Neutrophil Extracellular Trap

NF-κB: Nuclear Factor Kappa B

OCR: Oxygen Consumption Rate

OXPHOS: Oxidative Phosphorylation

PAD4: Peptidylarginine Deiminase 4

PAMPs: Pathogen Associated Molecular Patterns

PBMC: Peripheral Blood Mononuclear Cell

PBS: Phosphate Buffered Saline

PCR: Polymerase Chain Reaction

PFKL: Phosphofructokinase-1 Liver Type

PI: Propidium Iodide

PI3K: Phosphoinositide 3-Kinase

PKC: Protein Kinase C

PMA: Phorbol-12-Myristate-13-Acetate

PMN: Polymorphonuclear Neutrophil

PR3: Proteinase 3

PRRs: Pattern Recognition Receptors

PVDF: Polyvinylidene Difluoride

PVM: Parasitophorous Vacuole Membrane

RNA: Ribonucleic Acid

ROS: Reactive Oxygen Species

RT: Room Temperature

SD: Standard Deviation

SEM: Scanning Electron Microscopy

SK3: Calcium-Activated Potassium Channel SK3

SOCE: Store-Operated Calcium Entry

TEM: Transmission Electron Microscopy

T.g.: *Toxoplasma gondii*

TLRs: Toll-Like Receptors

TRPM2: Transient Receptor Potential Melastatin 2

TxA2: Thromboxane A2

UDP: Uridine Diphosphate

UTP: Uridine Triphosphate

VCAM-1: Vascular Cell Adhesion Molecule 1

2-APB: 2-aminoethoxydiphenyl borate

TABLE OF CONTENTS

LIST OF PUBLICATION AND CONFERENCE CONTRIBUTIONS i

Original papers i

Conference contributions ii

ABBREVIATIONS iv

TABLE OF CONTENTS vii

LIST OF FIGURES xi

1. INTRODUCTION 1

1.1 Bovine besnoitiosis 1

1.1.1 Geographical distribution of bovine besnoitiosis 1

1.1.2 Epidemiological features, clinical signs and lesions 2

1.1.3 Diagnosis, treatment and control 3

1.2 *Besnoitia besnoiti* 4

1.2.1 Life cycle and transmission 6

1.3 Immune system 8

1.3.1 Polymorphonuclear neutrophils (PMN) biology: overview 8

1.3.1.1 Neutrophil granules and degranulation 10

1.3.1.2 Reactive oxygen species (ROS) 11

1.3.1.3 Phagocytosis 12

1.3.1.4 Neutrophil extracellular traps (NETs) 14

1.3.2 Intrinsic and extrinsic regulators of PMN activation 16

1.3.2.1 ATP and purinergic receptors 16

1.3.2.2 AMPK and autophagy 17

1.3.2.3 Extracellular vesicles 18

1.4 *Besnoitia besnoiti*-driven innate immune cell responses 20

1.4.1 The state of art of NET formation induced by protozoan parasites 21

1.5 Aims of the current dissertation 25

2. MATERIAL AND METHODS 26

2.1 Primary bovine umbilical vein endothelial cell isolation and maintenance 26

2.2 Host cell culture, *B. besnoiti* and *T. gondii* tachyzoite maintenance 26

2.3 Bovine PMN isolation 27

2.4 Extracellular vesicle (EV) isolation and characterization 27

2.5 Scanning electron microscopy (SEM) 28

2.6 NET detection by immunofluorescence microscopy 28

2.7 Extracellular DNA quantification 30

2.8 Quantification of ROS production by EV-stimulated PMN 30

2.9 Flow cytometry-based measurement of neutrophil intracellular calcium concentration 31

2.10 Quantification of PMN oxygen consumption rates (OCR) and extracellular acidification rates (ECAR) 31

2.11 Measurement of total neutrophil and extracellular ATP concentration 32

2.12 Analysis of PMN apoptosis and necrosis by flow cytometry 32

2.13 Immunoblotting 32

2.14 Transmission electron microscopy (TEM) of EVs 34

2.15 EV labelling with far red 34

2.16 Analysis of neutrophil EV uptake 35

2.17 IL-1β, IL-6 and CXCL8 quantification in PMN and BUVEC supernatants 35

2.18 Statistical analysis 36

2.18.1 Statistical settings for Chapter 1: *B. besnoiti*-induced PMN clustering and NET formation depend on P_2X_1 purinergic receptor signaling 36

2.18.2 Statistical settings for Chapter 2: The CAMKK/AMPK pathway activation participate in early events of *B. besnoiti*- and *T. gondii*-triggered NET formation in PMN 36

2.18.3 Statistical settings for Chapter 3: PMN responses to EVs released by *B. besnoiti* tachyzoites and *B. besnoiti*-infected host cells 37

3. RESULTS 38

3.1 Chapter 1: *B. besnoiti*-induced PMN clustering and NET formation depend on P_2X_1 purinergic receptor signaling 38

3.1.1 *B. besnoiti* tachyzoite-exposed bovine PMN release NETs entrapping tachyzoites 38

3.1.2 Exposure to *B. besnoiti* tachyzoites induces oxidative responses in bovine PMN 40

3.1.3 *B. besnoiti* tachyzoite exposure does not affect total ATP concentration in bovine PMN 43

3.1.4 Non-hydrolyzable ATP (ATPγS) boosts *B. besnoiti* tachyzoite-induced anchored NET formation 43

3.1.5 P_2X_1 inhibition by its antagonist NF449 blocks *B. besnoiti* tachyzoite-induced anchored NET formation 46

3.1.6 NF449 blocks *B. besnoiti* tachyzoite-induced NET formation in a dose-dependent manner and without affecting cell viability 49

3.1.7 *B. besnoiti* tachyzoite exposure induces a P2X1-dependent clustering of bovine PMN 49

3.2 Chapter 2: CAMKK/AMPK pathway activation participates in early events of *B. besnoiti*- and *T. gondii*-triggered NET formation 52

3.2.1 PMN exposure to *B. besnoiti* tachyzoites induces neutrophil AMPK phosphorylation . 52

3.2.2 *B. besnoti* tachyzoite exposure drives CAMKK upregulation and phosphorylation in PMN 55

3.2.3 PMN exposure to *T. gondii* tachyzoites induces a rise in neutrophil intracellular calcium concentration in addition to AMPK and CAMKK phosphorylation 56

3.2.4 ULK1 expression is upregulated in *B. besnoiti* tachyzoite-exposed PMN 56

3.2.5 AICAR treatments trigger AMPK phosphorylation in bovine PMN 59

3.2.6 AICAR treatments induce metabolic responses in bovine PMN but do not synergize with *B. besnoiti*-induced OCR and ECAR 59

3.2.7 Pharmacological AMPK activation enhances *B. besnoiti* and *T. gondii* tachyzoite-induced NET formation 62

3.2.8 *T. gondii* tachyzoite-induced DNA release depends on MAPK- and SOCE-related pathways 63

3.3 Chapter 3: PMN responses to EVs released by *B. besnoiti* tachyzoites and *B. besnoiti*-infected host cells 64

3.3.1 Isolation and characterization of EVs 65

3.3.2 Exposure of PMN to EVs from different cellular sources does not affect neutrophil oxidative and glycolytic responses 65

3.3.3 Exposure of PMN to BUVEC- and *B. besnoiti* tachyzoite-derived EVs induce extracellular DNA release in a ROS-independent manner 68

3.3.4 PMN take up EVs from different cellular sources 69

3.3.5 EV exposure to PMN selectively induces the release of IL-1β and IL-6 but not of CXCL8 69

4. DISCUSSION 73

4.1 Chapter 1: *B. besnoiti*-induced PMN clustering and NET formation depend on P_2X_1 purinergic receptor signaling 74

4.2 Chapter 2: The CAMKK/AMPK pathway activation participate in early events of *B. besnoiti* and *T. gondii* tachyzoite-triggered NET formation in PMN 78

4.3 Chapter 3: Bovine PMN responses to EVs released by *B. besnoiti* tachyzoites and *B. besnoiti*-infected host cells 82

5. ZUSAMMENFASSUNG 87

6. SUMMARY 89

7. REFERENCES 91

8. EHRENWÖRTLICHE ERKLÄRUNG 124

9. FUNDING 125

10. ACKNOWLEDGMENTS 126

LIST OF FIGURES

Figure 1. Life cycle of *Besnoitia besnoiti*. 7

Figure 2. Neutrophil effector mechanisms. 10

Figure 3. Neutrophil effector mechanisms: granule content, NADPH oxidase activation and phagocytic mechanisms. 13

Figure 4. Mechanisms of neutrophil extracellular traps formation. 15

Figure 5. Summary of intrinsic and extrinsic regulators of NET formation evaluated in this study. 20

Figure 6. *B. besnoiti* tachyzoites are trapped in released NETs. 39

Figure 7. Exposure to *B. besnoiti* tachyzoites induces oxygen consumption in bovine PMN. 41

Figure 8. Exposure to *B. besnoiti* tachyzoites induces a metabolic shift towards aerobic carbohydrate catabolism in bovine PMN. 43

Figure 9. Total neutrophil ATP and extracellular ATP concentration in *B. besnoiti* tachyzoite-PMN co-cultures. 44

Figure 10. ATPγS supplementation induces NET release and boosts *B. besnoiti* tachyzoite-driven anchored NET formation. 46

Figure 11. Effects of purinergic receptor antagonist pre-exposure treatments on *B. besnoiti*-tachyzoite driven NET formation. 48

Figure 12. Effects of purinergic receptor antagonist post-exposure treatments on *B. besnoiti* tachyzoite-triggered NET formation. 48

Figure 13. NF449 does not affect PMN viability and inhibits *B. besnoiti*-driven NET formation in an ATP-independent but dose-dependent manner. 50

Figure 14. *B. besnoiti* tachyzoite-induced clustering of bovine PMN depends on P2X1-based purinergic signaling. 51

Figure 15. *B. besnoiti* tachyzoite exposure induces AMPK phosphorylation in bovine PMN. 53

Figure 16. Analysis of the catalytic and regulatory subunits of AMPK in *B. besnoiti*-exposed bovine PMN. 54

Figure 17. *B. besnoiti* tachyzoite exposure induces CAMKK expression and phosphorylation in bovine PMN. 55

Figure 18. *T. gondii* tachyzoite exposure induces cytoplasmic calcium increase, AMPK and CAMKK phosphorylation in bovine PMN. 57

Figure 19. *B. besnoiti* tachyzoite exposure induces ULK-1 expression in bovine PMN. 58

Figure 20. AICAR treatments drive AMPK phosphorylation and NET formation in bovine PMN. 61

Figure 21. AICAR treatments induce oxygen consumption (OCR) and extracellular acidification (ECAR) rates in bovine PMN. 61

Figure 22. AICAR treatments enhance *B. besnoiti* and *T. gondii* tachyzoite-induced NET formation. 63

Figure 23. *Toxoplasma gondii*-induced DNA release in bovine PMN depends on ERK- and SOCE-related signaling pathways. 64

Figure 24. Characterization of BUVEC-, PMN- and *B. besnoiti* tachyzoite-derived EVs. 67

Figure 25. Exposure to EVs does not affect oxidative and glycolytic responses in bovine PMN. 67

Figure 26. Exposure of bovine PMN to BUVEC- and *B. besnoiti* tachyzoite-derived EVs induced NET formation in a ROS-independent manner. 70

Figure 27. PMN-mediated uptake of far red-labeled EVs. 71

Figure 28. Selected EV exposure induced IL-1b and IL-6 release in bovine PMN. 72

1. INTRODUCTION

1.1 Bovine besnoitiosis

Bovine besnoitiosis is a protozoan disease caused by the tissue cyst-forming apicomplexan parasite *Besnoitia besnoiti* [1–4]. Infections predominantly affects cattle, resulting in chronic and debilitating clinical manifestations that significantly compromise animal health and welfare, particularly in endemic regions [1,2,5]. Clinically, the disease is characterized by an initial acute febrile phase, which progresses into a chronic stage, defined by typical dermatological lesions, infertility, and a gradual decline in overall health and productivity [6,7]. Bovine besnoitiosis has been widely reported across Sub-Saharan Africa, Asia, and Europe [8,9]. In Europe, it is a reemerging disease, exhibiting both an expansion in its geographical distribution and a rise in the incidence of clinical cases. The disease is associated with substantial economic losses, primarily attributed to reduced fertility rates and prolonged calving intervals in suckler cow herds [10].

1.1.1 Geographical distribution of bovine besnoitiosis

The first cases of bovine besnoitiosis were documented in the French Pyrenees by Besnoit and Robin, and in Portugal by Franco and Borges, during the early 20th century [11,12]. Few decades later, multiple cases on infected cattle imported from Angola to Portugal were reported [1]. Since the 1980s, the disease has become widely distributed across various Sub-Saharan African countries, including Angola, Kenya, Tanzania, Botswana, Namibia, Zimbabwe, Uganda, Sudan, Cameroon, and Nigeria [4,13,14]. In the same time period, cases of besnoitiosis were also reported in Asia, Venezuela, and Israel [15].

It was not until the 1990s and early 2000s that new cases of bovine besnoitiosis were recorded in Europe, notably in Portugal, Spain, and France [10,16,17], where the disease is now considered endemic. In Germany, a significant outbreak of besnoitiosis occurred after importation of cattle from France into a beef cattle herd in Bavaria, where almost all animals of the herd were affected [18]. Subsequent case reports have documented the re-emergence and spread of bovine besnoitiosis across Central Europe. Reports from Hungary, Ireland, Italy, Belgium, Portugal, Spain, France, and Switzerland underscore the ongoing geographic expansion of this disease [19–27]. Recent findings further emphasize its re-emergence, with notable reports from Central Europe [3].

1.1.2 Epidemiological features, clinical signs and lesions

The severity of clinical signs varies significantly among infected individuals. Most animals (80% to 95%) remain asymptomatic after infections, and those that present symptoms exhibit varying degrees of clinical signs. The ratio of symptomatic to asymptomatic cases may vary depending on the level of enzootic occurrence of the disease in a given geographic area [4,28,29]. Moreover, epidemiological data on prevalence and incidence in Europe and Africa are scattered. Hence, individual and herd seroprevalence data vary greatly, depending on whether the study area is endemic or non-endemic for bovine besnoitiosis [30–32]. In Europe, for instance, a study in southwestern France documented an increase in seroprevalence on a dairy cattle farm from 30% in March 2008 to 89.5% in May 2009, with the highest number of seroconversions occurring during spring [32]. In Northern Italy, the prevalence of bovine besnoitiosis in breeding bulls reached 36.5%, with an incidence of 39.6% [31]. Similarly, a large beef cattle farm in Portugal recently reported an overall prevalence of 16.89%, with significant differences between calves under one year of age (4.8%) and adult cattle (19.67%) [30].

In symptomatic animals, factors like parasite load transmitted by vectors, host resistance, and differences in virulence between strains contribute to the individual variation of clinical signs presentation [1,33]. The disease progresses through an incubation period of up to 13 days, followed by two clinical phases: the acute febrile and anasarca phase and the chronic scleroderma phase. The acute febrile phase is characterized by the presence of tachyzoites in endothelial cells, leading to vasculitis, hyperplasia, thrombosis, and necrosis of venules and arterioles [3]. This phase manifests with fever reaching up to 40°C and typically lasts between two and ten days, although it may extend up to two months. Clinical signs include photophobia, epiphora, ocular and nasal discharge, anorexia, cessation of rumination, increased heart and respiratory rates, and, in some cases, abortion [5,15,34]. Due to the nonspecific nature of these signs, diagnosis during this stage is challenging and related differential diagnoses may include diseases like bluetongue or malignant catarrhal fever [9].

Early consequences of increased vascular permeability in the acute phase include the development of oedema. Initially localized at the head and neck, oedema may expand to limbs and ventral regions, including the jowl, breast, and scrotum. Scrotal oedema can become severe, potentially resulting in necrotizing orchitis, azoospermia, and permanent bull infertility [35,36]. Limb and joint oedema often cause significant pain, reluctance to move, and in severe cases, laminitis, leading to lameness. Respiratory complications, including alveolar and

interstitial oedema, may arise in severe cases. This phase of infection typically lasts between one and four weeks, during which specific antibodies become detectable 15–18 days post-infection [1,15]. Furthermore, a recent publication evaluated the implication of naturally acquired acute, subacute, and chronic besnoitiosis on hematologic, biochemical, and enzymatic parameters [37]. In acute and subacute stages, leukopenia, anemia, hypoalbuminemia, hypocalcemia, and elevated aspartate transaminase and creatine kinase activities reflected systemic inflammation and tissue damage, whereas chronic infection was characterized by persistent alterations in erythrocyte parameters and marked hyperglobulinemia. These results indicated that besnoitiosis induces stage-dependent alterations blood biochemical parameters, consistent with acute inflammatory responses and chronic inflammatory disease [37].

The subsequent chronic scleroderma phase is characterized by the formation of numerous tissue cysts containing bradyzoites. These cysts are commonly found in the dermis, upper respiratory tract, connective tissues, scleral conjunctiva, muscles, and the mucosa of the vulva, and less frequently in the spleen, liver, and heart muscle [3,15,34]. Some cysts are surrounded by granulomatous inflammatory infiltrates. Pathognomonic scleral cysts are found 6–7 weeks post-infection and, along with cysts in the vulvar region and nasal mucosa, are visible during clinical examination. Additionally, cutaneous changes during the chronic phase include thickened skin with hyperkeratosis and alopecia, particularly on the face, neck, udder, teats, perineal area, and scrotum. Both the acute and chronic phases of the disease can be fatal, and affected animals often have to be culled due to their poor economic value stemming from severe deterioration in health [1,15,34,38].

1.1.3 Diagnosis, treatment and control

Laboratory diagnosis may confirm suspicion of besnoitiosis based on epidemiological history and clinical examination. Several diagnostic techniques are available for *B. besnoiti* infection, either based on the detection of the parasite via microscopic examination of biopsies, parasitic DNA via PCR, or specific antibodies via ELISA [39–42]. Diagnosis during the acute phase of infection includes PCR using peripheral blood samples considering the short-lasting parasitaemia, and serological tests that detect parasite-specific immunoglobulins G and M (IgG and IgM) by ELISA [43,44]. To detect tissue cysts in the chronic phase, direct diagnosis on skin biopsies from the base tail (*regio femoris*), histology or immunohistochemistry and molecular biology techniques (PCR) proved useful [45]. Additionally, serological techniques detecting anti-*B. besnoiti* antibodies in biopsies can confirm the diagnosis [46]. However,

cross-reactivity with closely related parasites, such as *Neospora caninum* and *Sarcocystis* spp., has been observed in several tests, including immunofluorescence assays and ELISAs [47,48]. For high-value animals, it is strongly recommended to confirm negative results [42,49].

Currently, there are no therapeutics available in Europe to treat bovine besnoitiosis. Experimental *in vivo* treatments of naturally or experimentally infected animals applying sulfonamides, toltrazuril, oxytetracycline, and parvaquone yielded inconclusive outcomes due to poorly reproducible *in vivo* models [3]. However, *in vitro* studies have demonstrated the efficacy of novel compounds in the preclinical stage, such as bumped kinase inhibitors (BKIs) [50]. Moreover, other promising but not yet commercially available compounds, such as decoquinate, diclazuril [51], thiazolides [52], arylimidamides [53], naphto-quinone buparvaquone [54] and endochine like quinolones (ELQs) [55] have been reported, showing positive effects related to parasite growth control and tachyzoite ultrastructure impairment.

Since there are no therapeutics or vaccines available and registered in Europe for bovine besnoitiosis, disease control currently relies on bioexclusion and biocontainment measures. For non-infected farms, bioexclusion strategies include thorough clinical and serological monitoring of newly introduced animals during quarantine, avoidance of communal pastures or bulls, pre-breeding clinical examinations - including bull sperm quality control -, and application of repellents and ectoparasiticides both indoors and outdoors. In infected herds, biocontainment measures should complement bioexclusion. These control measures include the rapid culling of clinically affected animals, of sterile/infertile bulls, and of qPCR-positive seropositive animals; regular serological testing to segregate seropositive from seronegative animals; restocking exclusively with seronegative cattle; and restricting natural mating on negative bulls for seronegative cows while applying artificial insemination for seropositive animals [3].

1.2 Besnoitia besnoiti

The causative agent of bovine besnoitiosis, *Besnoitia besnoiti*, is an obligate intracellular protozoan parasite belonging to the genus *Besnoitia*, within the family Sarcocystidae and the phylum Apicomplexa. *Besnoitia* spp. are closely related to other fast proliferating coccidia like *Neospora caninum* and *Toxoplasma gondii* [18,56]. Members of the genus *Besnoitia* parasitize a wide range of hosts, including cattle, goats, equids, reindeer, caribou, opossums, rabbits, rodents, and lizards [57]. To date, ten species have been described: *Besnoitia bennetti*, *Besnoitia jellisoni*, *Besnoitia wallacei*, *Besnoitia tarandi*, *Besnoitia darlingi*, *Besnoitia caprae*,

Besnoitia besnoiti, *Besnoitia oryctofelisi*, *Besnoitia akodoni*, and *Besnoitia neotomofelis* [58]. A putative novel *Besnoitia* species was recently reported in a southern black-eared opossum from Argentina based on *18S* rRNA and ITS1 sequence identity [59]. In the case of the *18S* rRNA region sequence, 100% identity with *B. darlingi* and *B. oryctofelisi* was observed. However, analysis of the complete ITS1 sequence revealed 99.2% identity with *B. oryctofelisi* and 97.7% with *B. darlingi* suggesting that this *Besnoitia* sp. indeed differs from *B. darlingi*, while being closely related to *B. oryctofelisi*. *B. besnoiti* tachyzoites represent the proliferative stage responsible for the acute phase of the disease. These stages measure approximately 7 × 3 µm [60] and can be cultivated *in vitro* using various mammalian cell types, such as Madin-Darby bovine kidney cells (MDBK) and bovine umbilical vein endothelial cells (BUVEC) [18,53,61,62]. When analyzing *B. besnoiti* tachyzoites via electron microscopy (TEM), classical hallmarks of apicomplexan parasites are observed, including the presence of micronemes, rhoptries, the conoid, and a microtubular cytoskeleton underlying the pellicle [5]. *B. besnoiti* tachyzoites typically invade host cells by their apical end, a process facilitated by actin, myosin, and tubulin motor proteins. Once inside, tachyzoites form a specialized intracellular compartment known as the parasitophorous vacuole, which is surrounded by a parasitophorous vacuole membrane. Within this vacuole, tachyzoites undergo endodygeny, a process of continuous intracellular division [5,18,60].

During the chronic phase of besnoitiosis, large tissue cysts containing thousands to millions of *B. besnoiti* bradyzoites are found in the skin and mucosa. Bradyzoites are thinner and longer than thachyzoites, measuring around 8 x 2 µm and proliferating within unseptated cysts with a diameter up to 600 µm [58]. The thick cyst walls are characterized by three distinct layers: an outer layer of host-derived connective tissue, an intermediate layer derived from the infected host cell, and an inner parasite-derived cyst wall lining the luminal side of the PVM, which encloses the bradyzoites [8]. Moreover, the analysis of 77 cutaneous locations in four chronically infected cattle by real-time PCR revealed a non-uniform distribution of *Besnoitia besnoiti* tissue cysts within the skin, with the highest concentrations of parasite DNA consistently being detected in the rump, distal parts of the hindlegs, and forelegs. Consequently, the rump region (*Regio femoris*) was identified as the optimal site for collecting skin biopsies for diagnostic purposes [45].

A recent study using AP-SMALDI MSI on bovine skin cysts reported significant compositional changes in 467 lipids and glycolytic metabolites when comparing samples from infected animals with non-infected controls [63]. This highlights the extensive metabolic alterations

induced by infection, which are crucial for understanding the host-parasite interactions during chronic infection.

The molecular triggers of *B. besnoiti* stage conversion (tachyzoite to bradyzoite and vice versa) remain unknown. Genomic and proteomic studies strongly suggest that the differentiation process from tachyzoites to bradyzoites involves pathways similar to the well-characterized and close related apicomplexan parasite *Toxoplasma gondii* [64,65]. In *T. gondii*, several studies have shown that tachyzoite-to-bradyzoite conversion is triggered by diverse stressors, such as alkaline pH, nutrient deprivation, immune mediators, heat shock, endoplasmic reticulum (ER) stress, and metabolic inhibitors [66–73]. These stimuli activate parasite signalling pathways, including cAMP/cGMP-dependent kinases and eIF2α phosphorylation, leading to preferential translation of stress-responsive regulators like apetala 2 (AP2) factors and the master regulator bradyzoite-formation deficient 1 (BFD1) [74–76]. *In vivo*, different factors like immune pressure, febrile responses, and host cell type - particularly neurons and skeletal muscle - act as critical modulators of tissue cyst formation [77].

1.2.1 Life cycle and transmission

The life cycle of *B. besnoiti* has not yet been fully elucidated, and its definitive host remains unidentified (Fig. 1). This is also the case for *B. benneti*, *B. caprae*, and *B. tarandi*, which infect ungulates as intermediate hosts as well. In case of *B. besnoiti,* cattle serve as the primary intermediate host for both asexual stages, i. e. tachyzoites and bradyzoites [1]. A carnivorous definitive host is hypothesized for *B. besnoiti*. Thus, it is presumed that, similar to other *Besnoitia* species (*B. darlingi*, *B. wallacei*, *B. oryctofelisi*, and *B. neotomofelis*), a felid - particularly a wild felid - may serve as the definitive host of *B. besnoiti* [1,9,78]. To identify potential definitive and intermediate hosts for *B. besnoiti*, several animal species (domestic dogs, cats, rabbits, guinea pigs, gerbils, common voles, and NMRI mice) were experimentally inoculated with *B. besnoiti* isolates obtained from naturally infected German cattle [79]. While no shedding of *B. besnoiti* oocysts was observed at all, serological analyses evidenced that cats might act as intermediate hosts for *B. besnoiti* [79]. Another study assessed the potential role of free-roaming carnivores as definitive hosts of *B. besnoiti* in Spain. Sera from 205 individuals across 10 species, including wolves, foxes, martens, badgers, genets, mongooses, wildcats, and feral cats, were analysed by indirect fluorescent antibody test (IFAT) and western immunoblots using tachyzoite and bradyzoite antigens. Twelve animals, mainly cats, showed seroconversion

by at least one assay, although none proved positive in both tests [80]. Moreover, the precise role of wild ruminants and rodents in the life cycle of *B. besnoiti* remains to be elucidated.

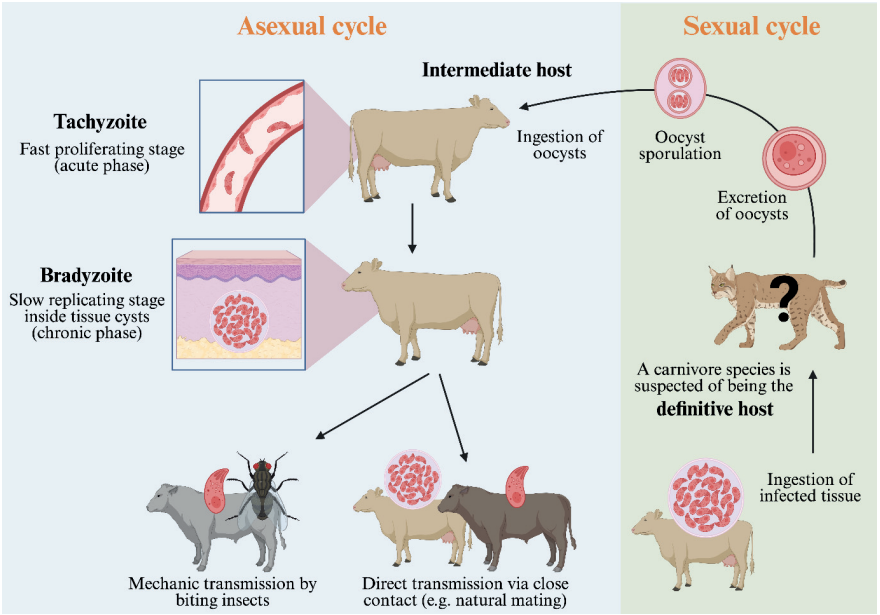

Figure 1. Life cycle of *Besnoitia besnoiti*. The full life cycle of the parasite remains unresolved. It is presumed that *B. besnoiti* follows a heteroxenous life cycle. The definitive host has not been identified so far, although it is suspected to be a carnivorous species, like in other *Besnoitia* species. Within intermediate hosts (bovids, cervids), two asexual stages develop: fast-replicating tachyzoites and slowly dividing bradyzoites, the latter of which assemble into macroscopic tissue cysts, e.g., located in subcutaneous connective or mucosal tissues. *Besnoitia besnoiti* can be transmitted horizontally between intermediate hosts, either through the bites of hematophagous arthropod vectors or by direct contact between infected and healthy animals. In case of horizontal transmission, bradyzoites located inside tissue cysts could be the infective stage since they are able to penetrate mucous membranes **[1,3]**.

B. besnoiti was shown to be transmitted horizontally between intermediate hosts, either through the bites of hematophagous arthropod vectors or via direct contact between infected and healthy animals [1]. Bradyzoites within tissue cysts are here considered the infective stage, as they are capable of penetrating mucous membranes [1]. Outbreaks of bovine besnoitiosis predominantly occur during seasons when biting flies are active. Several biting insects, including tsetse flies (*Glossina brevipalpis*), tabanids (*Atylotus nigromaculatus*, *Tabanocella denticornis*, *Haematopota albihirta*), and stable flies (*Stomoxys calcitrans*), seem capable of mechanical transmission of the parasite [5,81]. The fact, that tachyzoite stages were detected in lacrimal secretions [17], opens the possibility that non-biting flies like *Musca autumnalis* and *Musca domestica* might also contribute to mechanical transmission. Additionally, another

potential transmission route, though still scientifically unproven, involves direct animal-to-animal contact, e.g., during natural mating or by mucosal contact through licking [31,47]. Of note, neither venereal transmission nor transplacental transmission has been demonstrated so far and thus is currently considered unlikely [82].

1.3 Immune system

The immune system includes a coordinated network of cells, tissues, and organs in which innate and adaptive components interact to protect the host from pathogenic microorganisms. Innate immunity, an ancient form of host defence, has evolved to protect organisms against a wide range of infectious agents, including bacteria, fungi, viruses, and parasites [83]. The different components of the innate immune system comprise physical and anatomical barriers (e.g., skin, mucous membranes, endothelial cells from blood vessels), as well as humoral (e.g., the complement system) and cellular players. Endothelial cells represent a highly immunoreactive cell type, which - upon activation - initiate a cascade of proinflammatory responses, including the expression of adhesion molecules, cytokines, and chemokines. This activation mediates the recruitment of immune cells and orchestrates an acute inflammatory response [84]. Among the recruited cellular components, professional phagocytes, such as PMN, monocytes and macrophages, play pivotal roles in both parasite elimination (e.g., via phagocytosis) and the orchestration of inflammatory processes [83]. Conversely, adaptive immunity represents a highly specific, memory-based defence system that provides tailored protection against specific pathogens. It is mediated by lymphocytes, with T cells targeting infected cells directly and B cells producing antibodies that eventually neutralize extracellular pathogens. Together, these cell-mediated and humoral responses enable the host to mount a faster and more robust reaction upon re-exposure, thereby conferring long-term protective immunity [85].

The current work focuses on PMN-derived immune responses. Consequently, this cell type and its parasite-driven responses are here described in more detail.

1.3.1 Polymorphonuclear neutrophils (PMN) biology: overview

PMN are highly abundant leukocytes in bovine peripheral blood, reaching about ~30% of the total cell count [86–89]. They act as primary responders against invading pathogens including bacteria, fungi, and protozoa, particularly during acute inflammatory responses [90]. PMN originate from a myeloid progenitor cells in the bone marrow, being stimulated by a subset of

growth factors including granulocyte-macrophage colony stimulating factor in a process known as granulopoiesis [91]. PMN develop from mitotically active (promyelocytes, myelocytes) and postmitotic progenitor cells or immature neutrophils (metamyelocytes and banded neutrophils) into mature PMN, which circulate in the peripheral blood and migrate into tissues [92]. Mature PMN are characterized by their segmented nuclei, a diameter of approximately 7-10 μm in diameter, and a rather short life span of 12-14 h, which is significantly prolonged by cell activation. The cytoplasm of PMN is enriched with specific granules (see 1.3.1.1) and secretory vesicles that contribute to their antimicrobial functions [91,93].

In the past, PMN were considered as a uniform, finally differentiated cell population of the innate immune system with a pure pro-inflammatory function. Of note, recent studies elucidated that the total PMN population of a host is indeed characterized by a significant heterogeneity [94]. Strikingly, besides a maturation-related diversity of PMN, a regulatory, mainly immunosuppressive PMN subset is currently described in addition to classical pro-inflammatory PMN [92,94,95]. Thus, it has been proven for the murine and human system that PMN act beyond their classical function of direct pathogen abatement, thereby being actively involved in eliciting and shaping adaptive immune responses, e.g., by inhibiting lymphocyte functions like IFNγ production and T cell proliferation. Recent studies also characterized peripheral blood PMN as a heterogenous population exhibiting multiple phenotypes and functional capabilities [90,94]. Moreover, PMN aging is associated with distinct phenotypic and functional properties that vary with the circadian rhythm, influencing their responsiveness and clearance from circulation [96,97]. Hence, both neutrophil superoxide production and bacterial phagocytic activity display diurnal variations and are more pronounced during daylight hours [98].

In general, PMN are recruited from blood circulation into tissues (Fig. 2), mediated by endothelial cells in response to inflammatory cytokines and pathogen-derived molecules. This extravasation process is mediated by adhesion molecules (e.g., E- and P-selectins, VCAM1) on the endothelial luminal surface promoting PMN tethering, rolling and subsequent adhesion [90]. Upon adhesion, PMN flatten and polarize to transmigrate across the endothelial barrier (diapedesis), either via intercellular junctions or directly through endothelial cells. Once the endothelial cell barrier has been traversed, PMN migrates along chemotactic gradients towards the site of inflammation, guided by host-released cytokines [e.g., interleukin (IL)-8] and pathogen-derived chemoattractants. During this process, PMN release extracellular matrix-

degrading proteins, facilitating tissue infiltration. After reaching areas of high chemoattractant concentration, PMN assemble their oxidative burst machinery, a hallmark of PMN activation, and execute classical effector mechanisms like phagocytosis, reactive oxygen species (ROS) release, degranulation and neutrophil extracellular traps (NET) formation to fight pathogens [99–103].

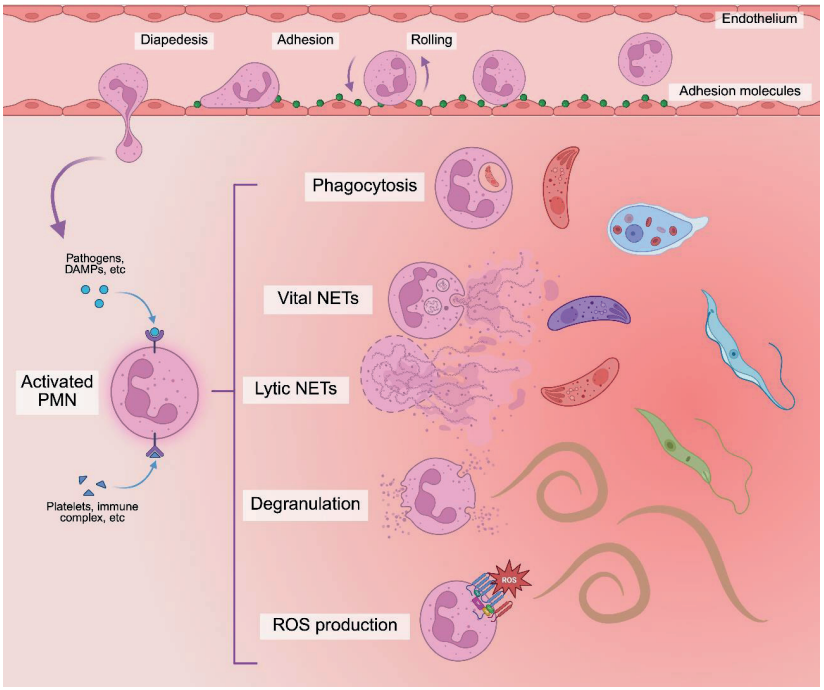

Figure 2. Neutrophil effector mechanisms. In response to chemokines being released by tissues suffering from unphysiological conditions (e.g., in case of tumor growth, inflammation, or acute injury), circulating PMN are attracted and migrate to affected sites performing sequential steps of tethering, rolling, adhesion, and transmigration. Once recruited, PMN recognize (mainly foreign) proteins and carbohydrates via pathogen recognition receptors, ranging from Toll-like receptors to specialized opsonized-molecules receptors and execute a wide array of antimicrobial mechanisms, thereby exposing pathogens to antimicrobial molecules like myeloperoxidase, neutrophil elastase, or reactive oxygen species. Moreover, other effector mechanisms include direct actions to immobilize or kill pathogens, like phagocytosis, neutrophil extracellular trap formation and degranulation [90].

1.3.1.1 Neutrophil granules and degranulation

PMN granules are membranous vesicles formed during PMN maturation, which carry a rich variety of enzymes, antimicrobial proteins, and signaling molecules that play a pivotal role in pathogen killing (Fig. 3A) [99]. There are three fundamental types of granules, classified by

their resident cargo: azurophilic granules (primary granules), specific granules (secondary granules), and gelatinase granules (tertiary granules) [99,104]. Azurophilic granules contain myeloperoxidase (MPO), lysozyme, and different serine proteases like neutrophil elastase (NE), proteinase 3 (PR3), and cathepsin G (CTSG). Neutrophil specific granules contain the iron-binding proteins lactoferrin and lipocalin-2, but, more importantly, are also characterized by the presence of the gp91^{phox} and p22^{phox} heterodimer, a main component of the nicotinamide adenine dinucleotide phosphate (NADPH) oxidase complex [99,105,106]. Gelatinase granules serve to store metalloproteases like gelatinase and leukolysin [107,108]. MPO is critical for the oxidative burst process since it catalyzes the production of hypochlorous acid, thereby increasing the antimicrobial activity of ROS, such as superoxide free radical, produced by NADPH oxidase [109]. Along with NE, these enzymes are principal components of NET structures [110]. When PMN progress through the activation process, granules are mobilized and fuse either with phagosomes or the plasma membrane. Degranulation of primary and secondary granules facilitates the generation of an antimicrobial milieu at the inflammatory site and produces an adverse environment for invading pathogens [111,112].

1.3.1.2 Reactive oxygen species (ROS)

Activated neutrophils represent one of the most relevant producers of superoxide radicals. ROS are synthesized by the NADPH oxidase, an enzymatic core complex constituted by both membrane-bound and soluble subunits (Fig. 3B) [106,113,114]. Its catalytic core consists of the transmembrane heterodimers gp91^{phox} and p22^{phox} (*phox* stand for phagocyte oxidase) and its soluble trimeric core is assembled by p47^{phox}, p67^{phox} and p40^{phox} [106,115]. NADPH oxidase activation is a tightly regulated process, triggered by specific receptors upon binding of microorganism-derived molecules, and soluble inflammatory mediators, leading to a downstream activation of distinct kinases like the protein kinase C (PKC), ERK1/2, MAPK, and phosphoinositide 3-kinase (PI3K). Activated kinases phosphorylate all cytosolic NADPH oxidase subunits, allowing the core to assemble with the plasma membrane and the phagocytic vacuole membrane, thereby forming the phagosome [113]. Besides this pathway, phagocytosis-mediated NADPH oxidase activation also takes place upon activation of phagocytic receptors [e.g., FcγR for immunoglobulin G (IgG) and the β2 integrin CR3], leading to downstream kinase activation, NADPH oxidase subunit phosphorylation and activation of the enzyme complex within the phagosome, even before it is fully sealed [114]. The transmembrane subunit gp91^{phox} chemically reduces NADPH from the cytosol to form $NADP^+$

and superoxide (O_2^-), contributing to generate ROS. Then, ROS are released either into the extracellular environment or into the phagosome [116]. The ROS entity includes several oxygen species. Apart from O_2^-, the most relevant reactive oxygen species are hydrogen peroxide (H_2O_2) and hypochlorous acid (HOCl), being HOCl production catalyzed by MPO [117]. Other ROS molecules are chloramines (R-NHCl), hypothiocyanite ($OSCN^-$), and organic radicals [116]. All these oxidants show antimicrobial activities by lipid peroxidation and protein / DNA damage, with HOCl being the fastest acting and most potent antimicrobial oxidant produced by PMN.

1.3.1.3 Phagocytosis

Phagocytosis is a cellular effector mechanism for ingesting and eliminating particles, including foreign substances, microorganisms, and apoptotic cells (Fig. 3C) [118–120]. This process is fulfilled by the coordination of neutrophil granules and phagosome fusion alongside with enhanced ROS production by NADPH oxidase [119]. PMN recognize pathogen associated molecular patterns (PAMPs) and opsonized molecules via phagocytic receptors like C-type lectins (CRL), scavenger receptors, complement receptors (CR) and Fc receptors (FcR) [121,122], thereby triggering a cascade of signals, changes in lipids composition in the cell membrane and the reorganization of actin cytoskeleton to expand the plasmatic membrane around the particle to be ingested [118]. After phagosome formation, phagosomes mature by sequential fusion steps, starting by the fusion of a new phagosome with azurofilic and specific granules, and, at the latest step, with lysosomes [123]. In the resulting phagolysosome, ingested microorganisms are finally degraded by both oxidative and non-oxidative mechanisms including acidification by V-ATPase (pumps hydrogen ions into the phagosome) and hydrolytic enzymes (e.g., from PMN granules) [119]. Recently, phagocytosis has been proposed to function as a kind of “sensor” for microbial size since, if phagocytosis fails, neutrophils switch to other mechanisms [124,125]. Thus, extracellular ROS production, PMN recruitment, and NET formation are typically performed in response to large pathogens, such as *Candida albicans* hyphae [124,126]. Whenever PMN encounter large pathogens, a lack of phagosome formation allows NE and MPO to be released into the neutrophil cytosol. This enables their translocation to the nucleus, where they drive chromatin decondensation - a key step in NET formation [124]. Moreover, NADPH oxidase assembles on the plasma membrane, leading to the extracellular release of ROS. In parallel, NF-κB activation amplifies IL-1β expression, promoting further neutrophil recruitment and clustering, which are essential for the

clearance of large pathogens [126]. These findings indicate that phagocytosis is a central regulator of the microbe size-dependent choice of neutrophil responses [110,125,127,128].

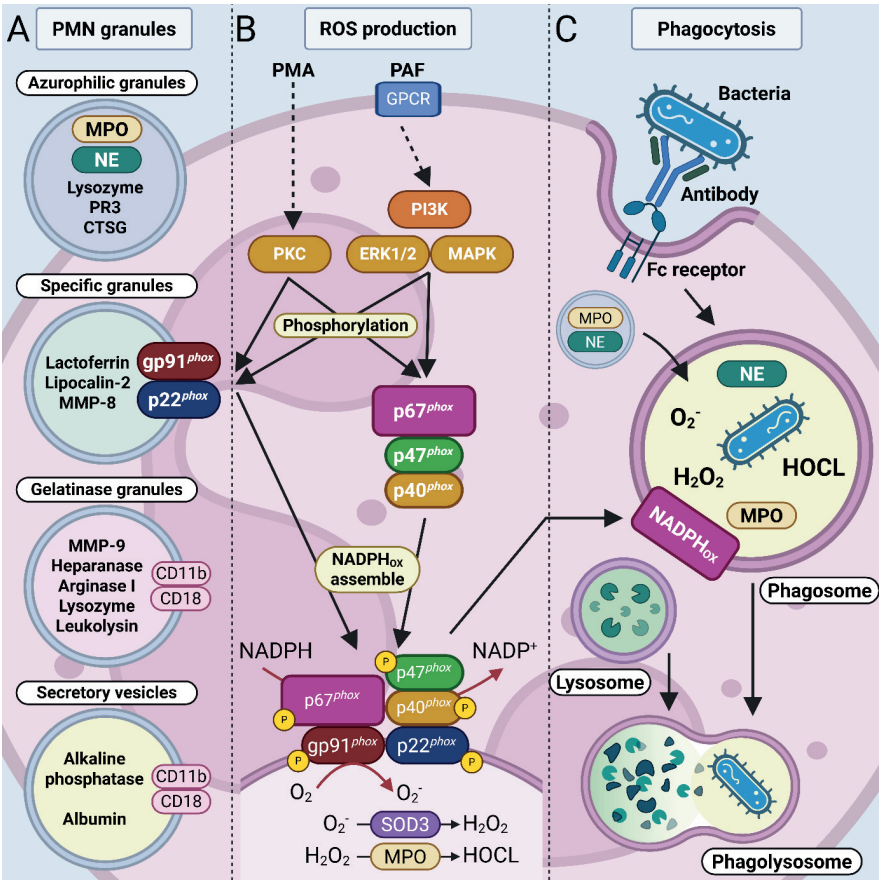

Figure 3. Neutrophil effector mechanisms: granule content, NADPH oxidase activation and phagocytic mechanisms. (A) Neutrophil granules and vesicles are categorized into azurophilic (primary), specific (secondary) and gelatinase (tertiary) granules, each containing distinct antimicrobial proteins such as myeloperoxidase (MPO), neutrophil elastase (NE), and lactoferrin. Upon activation, granules are mobilized and fuse with the plasma membrane or phagosomes, facilitating microbial killing and contributing to ROS production. (B) NADPH oxidase activation involves assembly of the transmembrane subunits gp91^{phox} and p22^{phox} with the cytosolic components p47^{phox}, p67^{phox}, and p40^{phox}. Upon receptor-mediated activation, all subunits are phosphorylated and translocate to the membrane, forming the active enzyme complex that generates reactive oxygen species (ROS), including superoxide (O_2^-) and hypochlorous acid (HOCl). These ROS exert antimicrobial activity within the phagosome and in the extracellular space. (C) Phagocytosis is initiated by the recognition of opsonized particles or pathogen-associated molecular patterns (PAMPs) via phagocytic receptors, triggering actin remodeling and membrane extension. Following internalization, phagosomes undergo sequential fusion with granules and lysosomes, forming phagolysosomes where pathogens are degraded through oxidative and non-oxidative mechanisms [99,106,112,113,118,120].

1.3.1.4 Neutrophil extracellular traps (NETs)

NETs are large extracellular web-like structures composed of neutrophil antimicrobial cytosolic and granule proteins assembled on a scaffold of decondensed chromatin [129]. NETs have been described as a defense mechanism capable of entrapping, neutralizing and eventually killing bacteria, fungi, viruses and parasites [129–132]. NET formation occurs via two distinct pathways: (1) NADPH oxidase-dependent NETosis, which critically involves ROS production, and (2) NADPH oxidase-independent NETosis, in which mitochondrial ROS (mtROS) [133] and peptidylarginine deiminase 4 (PAD4) play a crucial role in chromatin decondensation [110,128,134,135]. Originally, NET formation was considered as a cell death process. However, recent studies additionally described a fast (5-60 min), non-lytic fashion of NET formation where chromatin or mitochondrial DNA (mtDNA) is extruded from PMN without causing cell death, allowing neutrophils to remain functional on the level of phagocytic activity and locomotion [136–140].

NET formation is induced by several pro-inflammatory stimuli, including pathogen-associated molecular patterns (PAMPs) from bacteria, fungi, viruses, and parasites [e.g., lipopolysaccharides (LPS) or N-formylated peptides like fMLP]. Additionally, damage-associated molecular patterns (DAMPs), released by stressed or dying cells, also foster NET formation. PMN recognize these signals via pattern recognition receptors (PRRs), such as Toll-like receptors (TLRs), NOD-like receptors, and C-type lectin receptors and initiate signalling cascades leading to NET formation [141,142].

The best characterized pathway leading to NET formation - the lytic pathway - involves ROS production via NADPH oxidase (Fig. 4). Following NADPH oxidase activation, enhanced ROS levels trigger MPO-mediated oxidative activation of NE. Subsequently, NE degrades cytoplasmic actin cytoskeleton to block phagocytosis [124,125]. Once in the nucleus, NE cleaves histones, facilitating chromatin decondensation and DNA release [110,143]. Chromatin decondensation is also promoted by MPO, PR3 and CTSG binding (so-called azurosome), along with the activation of PAD4, which catalyzes citrullination of histones H3, H4 and H2A. This process converts arginine groups to citrulline, thereby neutralizing positive-charged histones and weakening DNA-histone interactions. As a result, chromatin expands, leading to nuclear membrane disruption. Then, chromatin is released into the cytosol, where it is decorated with a variety of granular and cytosolic proteins, and finally is extruded into the extracellular environment to perform anti-microbial functions [109,110,129,143,144].

Moreover, calcium is a crucial intracellular signaling molecule involved in NET formation (Fig. 4). A rise in cytosolic calcium concentration (originating from the endoplasmic reticulum), enhances PAD4 activity via calcium binding-induced conformational changes. Additionally, calcium promotes mitochondrial ROS production by facilitating the opening of the non-selective mitochondrial permeability transition pore (mPTP) and activating the small-conductance calcium-activated potassium channel SK3 (SK3). This process is implicated in NADPH oxidase-independent NET formation [127,134,145].

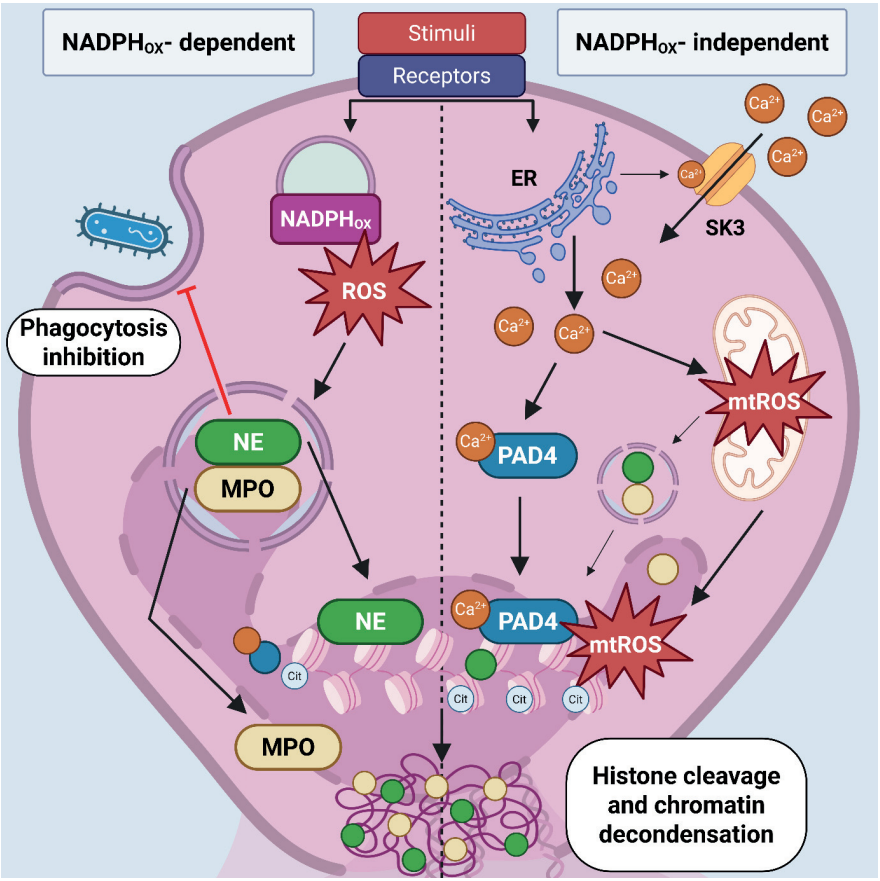

Figure 4. Mechanisms of neutrophil extracellular traps formation. Two main pathways of NET formation have been described: the NADPH oxidase-dependent and the NADPH oxidase-independent pathways. The NADPH oxidase-dependent mechanism, triggered by stimuli such as phorbol 12-myristate 13-acetate (PMA) and lipopolysaccharide (LPS), activates intracellular signaling cascades that lead to reactive oxygen species (ROS)-dependent release of myeloperoxidase (MPO) and neutrophil elastase (NE) from azurophilic granules. These enzymes mediate nuclear envelope disintegration, chromatin decondensation, and subsequent rupture of the plasma membrane. In addition, NE inhibits phagocytosis by degrading components of the cytoplasmic actin cytoskeleton. In contrast, the NADPH oxidase-independent pathway is initiated by cytokines such as interleukin

(IL)-6, IL-8, or tumor necrosis factor-alpha (TNF-α), as well as by calcium ionophores such as ionomycin. These stimuli promote an increase in cytoplasmic calcium concentration via mobilization from the endoplasmic reticulum (ER) and activation of the small-conductance calcium-activated potassium channel 3 (SK3), followed by mitochondrial ROS production. This, in turn, induces translocation of peptidylarginine deiminase 4 (PAD4) to the nucleus, where it catalyses histone citrullination. Both pathways converge on histone cleavage and chromatin decondensation, ultimately resulting in neutrophil cell death. [146–148].

1.3.2 Intrinsic and extrinsic regulators of PMN activation

1.3.2.1 ATP and purinergic receptors

The purinome of cells describes the entity of different representatives of purinergic receptors, which, together with membrane-bound ectonucleotidases, coordinate a complex network of reactions in response to extracellular ATP and adenosine levels, thereby regulating the purinergic signaling-based activation of effector functions. Purinergic cascades not only influence PMN phagocytosis, NETosis and ROS production, but also regulate neutrophil chemotaxis. In principle, PMN own various P_2X, P_2Y and P_1 adenosine (ADO) receptors [149,150]. Obviously, intracellular ATP serves as the primary energy source driving almost all cellular functions. However, ATP also plays a key role in purinergic signaling. In mammalian cells, ATP is mainly synthesized by glycolysis or by oxidative phosphorylation and stored at a high intracellular concentration of ~ 5 mM. Under physiological conditions, extracellular ATP levels remain low (~10 nM) due to the continuous hydrolysis of ATP to ADP, AMP and adenosine (ADO) by plasma membrane-anchored ectonucleotidases like CD39 (ectonucleoside triphosphate diphosphohydrolase, E-NTPDase1) and CD73(ecto-5′-nucleotidase) [151,152]. Under pathological conditions, such as trauma, ischemia, and infection, extracellular ATP concentrations rise dramatically and act as danger-associated molecular pattern (DAMP) and “find me” signal, thereby guiding the migration of purinergic receptor-expressing leukocytes, such as PMN [150].

Purinergic receptors are classified into three major families based on their signal transduction mechanism and structural properties. P_2X receptors ($P_2X_{1–7}R$) function as ATP-sensitive trimeric ion channels, facilitating the influx of sodium, potassium, and calcium. P_2Y receptors ($P_2Y_{1/2/4/6/11-14}R$) represent G protein-coupled receptors (GPCRs) that recognize ATP and several other nucleotides including ADP, UTP and UDP. Activation of P_2Y receptors triggers the phospholipase C/inositol trisphosphate/diacylglycerol pathway, leading to an endoplasmic reticulum-dependent rise in intracellular calcium (Fig. 5A). Moreover, P_1 receptors ($A_1/A_2A/A_2B/A_3R$) are also GPCRs but specifically recognize ADO [150,153–155]. Indeed, P_2R- and P_1R-mediated purinergic signaling often exerts opposing effects on immune cell

functions [150]. Specifically, ATP-mediated P_2R signaling predominantly enhances immune cell activation, while ADO-mediated P_1R signaling generally suppresses immune responses [156,157].

Purinergic signaling regulates diverse neutrophil activities like chemotaxis, rolling, adhesion, transmigration, ROS generation, NETosis, and apoptosis [158–164]. Recent studies on protozoa-driven PMN activation underlined an essential role of purinergic signaling in *Neospora caninum*-driven NET formation since tachyzoite-mediated NETosis was significantly blocked by a P_2Y_2 receptor inhibitor [165]. Additionally, P_2X_1 receptor blockage by the purinergic inhibitor NF449 significantly decreased NET formation induced by *Trypanosoma brucei brucei* trypomastigotes [166].

1.3.2.2 AMPK and autophagy

The main metabolic sensor in eukaryotic cells is the AMP-activated kinase (AMPK). It is a serine/threonine protein kinase consisting of three heterogenic subunits: a catalytic α-subunit as well as regulatory β- and γ-subunits, capable to directly bind AMP, ADP and ATP in a competitive manner [167]. AMPK is activated by phosphorylation in response to energetic stress after sensing a rise in AMP:ATP and ADP:ATP ratios. The AMPK-based regulatory system enables energy balance restoration by inhibiting anabolic processes, while promoting catabolic processes [168]. Moreover, AMPK activity is tightly regulated by upstream signals, including liver-kinase-B1 (LKB1), which responds to energetic stress [169], and calcium/calmodulin-dependent kinase kinase 2 (CAMKK2), which is activated by an increase in intracellular calcium levels (Fig. 5B) [170]. Thus, AMPK serves as a critical metabolic control system, allowing cells to dynamically adjust their energy metabolism in response to physiological demands [171]. This response can be triggered either by a reduction of ATP production (e.g., by hypoxia, glucose deprivation, heat shock or a reduced mitochondrial oxidative phosphorylation), or by an increased ATP consumption, as occurring during exercise or in cases of cellular metabolism upregulation [172]. Consequently, AMPK enhances energy-generating processes, including glucose uptake, glycolysis, fatty acid oxidation, and autophagy, while suppressing non-essential ATP-consuming pathways [167]. There is increasing evidence that AMPK participates in modulating acute inflammatory reactions and plays a major role in regulating PMN functions [172,173]. In mice, AMPK activation enhances PMN chemotaxis and bacterial killing *in vitro* and *in vivo* and counteracts chemotaxis inhibition induced by LPS (≥ 30 ng/mL). Accordingly, chemical blockage of AMPK activation

diminishes neutrophil chemotaxis [174]. On a mechanistic level, the pharmacological activation of AMPK by aminoimidazole carboxamide ribonucleotide (AICAR) drives actin polymerization, formation of PMN edges, phagocytosis, and bacterial killing in murine PMN [172,174,175]. Conversely, in human PMN, AMPK shows inhibitory effects on fMLP- and phorbol 12-myristate 13-acetate (PMA)-induced ROS production [176].

Autophagy represents a conserved intracellular degradation process that facilitates the recycling of cellular components, including proteins and organelles, and plays a crucial role in cellular responses to stress conditions [177]. At physiological states, the constitutive level of autophagic activity is usually low; however, it is markedly up-regulated in response to oxidative stress, nutrient starvation, and various other stimuli including pathogens [177]. During autophagy, cytosolic constituents are enclosed in double-membrane vesicles, called autophagosomes, and subsequently delivered to lysosomes for degradation (autolysosomes) [178]. Autophagy is primarily regulated by AMPK activation, which consequently leads to the inactivation of the mechanistic target of rapamycin (mTOR) [179]. Under nutritional or energy starvation, intracellular ATP levels decrease, resulting in AMPK activation which promotes autophagy by direct activation via the phosphorylation of regulatory kinases, such as unc51-like autophagy activating kinase 1 (ULK1) or Beclin 1, among others [171]. This process inhibits mTOR, thereby facilitating the recruitment of the activated ULK1 complex to nascent autophagosomal structures, driving the growth, elongation, and curvature of the forming autophagosome [177,180]. In general, neutrophil autophagy is linked to several PMN functions and can prime these innate immune cells to perform phagocytosis, ROS production and NET formation [62,177,181,182].

1.3.2.3 Extracellular vesicles

A broad range of different organisms and cells, including parasites, ECs and PMN, release extracellular vesicles (EVs) for communication purposes (Fig. 5C) [183–185]. In general, EVs comprise apoptotic bodies (50 nm – 5 μm), microvesicles (50 nm – 1 μm) and exosomes (30-150 nm), all containing a complex mixture of DNA, RNA, lipids, metabolites and proteins, with pivotal importance in cell to-cell communication [186].

EVs are nanoscaled, double-membraned vesicles that are constitutively generated from endosomes. Late endosomes accumulate intraluminal vesicles (ILVs) by inward budding their membranes, subsequently transforming into multivesicular bodies (MVBs). Throughout this

process, proteins commonly associated with EV biogenesis and secretion, such as Rab GTPases (Rab7, Rab11, Rab27a/b, Rab35), heat shock proteins, tetraspanins (CD9, CD63, CD81), and components of the endosomal sorting complex required for transport (ESCRT), are integrated into the invaginating membrane. Simultaneously, cell-specific cytosolic components, such as major histocompatibility complex class II (MHC-II) molecules - particularly in antigen-presenting cells - are encapsulated within the ILVs. Upon fusion of MVBs with the plasma membrane, the ILVs are released into the extracellular space, at which point they are classified as exosomes [187,188]. EV-based intercellular communication depends on effective delivery of genetic material, which can be achieved by receptor-ligand interactions, direct fusion of membranes, or internalization via endocytosis [189].

Emerging evidence indicates that EVs also modulate neutrophil effector functions [141]. Hence, it was reported that EV-driven reciprocal communication between platelets and PMN is enabled by neutrophil EV-based transfer of arachidonic acid to platelets, which is enzymatically converted into thromboxane A2 (TxA2). TxA2 release from platelets then propagates ICAM-1 upregulation on PMN, which binds to the EC surface and enables PMN extravasation to the site of inflammation [185]. Other studies have demonstrated that EVs from resting human PMN reduced ROS levels and IL-8 secretion in PMN isolated from venous blood. In contrast, EVs from PMN activated by opsonized particles enhanced ROS and IL-8 secretion in PMN and ECs, promoting antibacterial and proinflammatory responses [190,191]. These results highlight opposing EV effects, depending on the neutrophil activation state before their release. Furthermore, platelets secrete EVs after incubation with Dengue virus, LPS, and thrombin, activating the CLEC5A/TLR2 heterocomplex in human PMN, thereby enhancing NET formation and inducing the release of IL-1β and other proinflammatory cytokines from macrophages [192].

Notably, parasite-derived EVs can transfer virulence factors, drug-resistance genes and differentiation factors between parasites. Moreover, parasite-derived EVs modulate host immune responses by stimulating the release of anti-inflammatory cytokines, which may then assist parasites in evading the immune system [184–186,193–198].

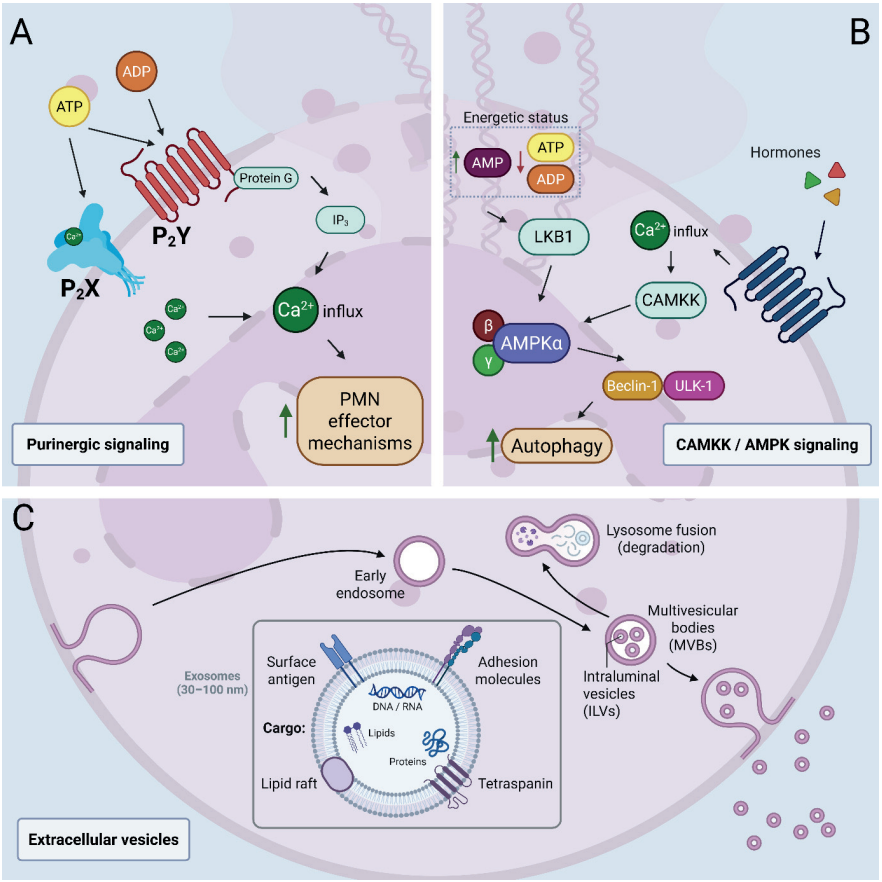

Figure 5. Summary of intrinsic and extrinsic regulators of NET formation evaluated in this study. (A) ATP and its metabolites released under pathological conditions like infection or tissue damage act as a danger-associated molecular pattern (DAMP) and signal via purinergic receptors. P_2X and P_2Y receptors promote PMN activation via a rise in intracellular calcium levels leading to enhanced chemotaxis, ROS production, and NET formation [150]. (B) AMPK serves as a central energy sensor being activated by metabolic stress and subsequent, CAMKK-mediated calcium influx. AMPK-mediated signaling suppresses anabolic processes while promoting catabolic pathways, including autophagy. In PMN, AMPK activation regulates chemotaxis, phagocytosis, ROS production, and bacterial killing, thereby highlighting its dual role in both metabolic adaptation and immune regulation [171,174]. (C) EVs released by PMN, ECs or parasites propagate intercellular communication by transferring proteins, lipids, and nucleic acids. Depending on their molecular content, EVs can enhance inflammatory and antimicrobial responses, or conversely, dampen immune activity [141,186].

1.4 Besnoitia besnoiti-driven innate immune cell responses

So far, relatively little is known on innate or adaptive immune responses during acute or chronic besnoitiosis. In *B. besnoiti*-infected animals, histological studies revealed the formation of

tissue cyst containing bradyzoites mainly in the skin, eye, tendons, and testicle during chronic besnoitiosis. In cysts-bearing tissues, immune cell infiltration was documented, characterized by the presence of macrophages, eosinophils, and scattered lymphocytes, thereby indicating a systemic activation of both, the innate and adaptive immune system [24,35,36,199].

In intermediate hosts like cattle, *B. besnoiti* tachyzoites predominantly infect host endothelial cells in various organs and blood vessels, replicating intracellularly via endodyogeny [45]. Previous studies have shown that tachyzoites are also able to invade monocytes and PMN, and are also present extracellularly in blood smears of infected animals [18,58]. Maksimov et al. (2016) reported that *B. besnoiti* infections drive an upregulation of the endothelial transcription of key genes associated with endothelial cell adhesion and leukocyte recruitment, such as P-selectin, intercellular adhesion molecule 1 (ICAM-1) and vascular cell adhesion molecule 1 (VCAM-1), as well as chemokines (CXCL1, CXCL8, CCL5), IL-6, and COX-2. Moreover, *B. besnoiti* infection promotes PMN rolling and adhesion to bovine endothelial cell layers [200]. In general, chemokines like CXCL1 and CXCL8, as well as adhesion molecules like ICAM-1 and VCAM-1 are known to play crucial roles in PMN recruitment and migration to the site of inflammation [90]. Consequently, their upregulation seems pivotal for the development of an appropriate and effective innate immune response.

1.4.1 The state of art of NET formation induced by protozoan parasites

Immune cells such as monocytes, macrophages and PMN are considered to be the first line of defence against pathogen invasion [201,202]. The early recruitment of neutrophils to the site of tissue invasion typically helps reduce the initial burden of protozoan parasites [201,202]. PMN effector mechanisms against protozoan parasites include degranulation, phagocytosis, ROS production, and, ultimately, NET formation [203]. Nevertheless, we have little knowledge on the molecular pathways involved in NET formation induced by protozoan parasites, and how these pathways can differ between different parasites.

Recent reports on *Leishmania amazonensis* (phylum Sarcomastigophora) promastigote-exposed PMN describe that inhibition of NE and PAD4 reduced the amount of NET formation [204]. *L. amazonensis* promastigotes caused an increase in H_2O_2 levels in PMN, and ROS were generated by both the NADPH oxidase complex and the mitochondrial respiratory chain. Nevertheless, only ROS derived from the NADPH oxidase complex appeared to be necessary for NET formation, as inhibition of other ROS sources did not affect NET release [204].

Moreover, a rapid NET formation was induced by promastigotes (within 10 minutes of stimulation), which depended on NE activity but was independent of NADPH oxidase-derived ROS and PAD4 activity, indicating that different pathways converge in the NET release triggered by the same stimulus [204]. In other studies, it has been demonstrated that *L. amazonensis* can induce NET formation through both NADPH oxidase-dependent and -independent pathways, depending on which PI3K subunit is activated [205]. The NADPH oxidase-dependent pathway involves the activation of PI3K-γ, which activates ERK via MAPK; subsequently, ERK activates PKC, and ROS are generated by NADPH oxidase [205]. On the other hand, NADPH oxidase-independent NETosis triggered by this parasite activates PI3K-δ, which leads to an increase in calcium mobilization [205].

In a different study that examined the interaction between PMN and *Trypanosoma cruzi* (phylum Sarcomastigophora), *T. cruzi* trypomastigotes and their soluble extracts were shown to induce NET formation in a dose-dependent manner [206]. This mechanism appears to be triggered by sensing via TLR2/4, phosphorylation of $p47^{phox}$ in a p38 MAPK-dependent manner, and involves ROS production and histone citrullination [206,207]. Furthermore, PMN possess Transient Receptor Potential Melastatin 2 (TRPM2) channels that can be activated by H_2O_2 produced through ROS generation under physiological conditions, allowing the flow of ions such as calcium, sodium, and magnesium [208]. This calcium influx through the TRPM2 channels may trigger the activation of PAD4, which leads to chromatin decondensation. Other studies have described that PMN are able to phagocytize both trypomastigote and amastigote forms of *T. cruzi* [209,210], killing the parasites in the phagolysosomal vacuole through a mechanism dependent on H_2O_2 [209,211]. It is unknown whether TRPM2 channels are activated during *T. cruzi*–neutrophil interaction; nonetheless, it could explain why neutrophils undergo NET formation [206,207], even when they are able to phagocytize trypanosomes [209,210,212].

Several publications describe NET formation as a key innate immune response against different developmental stages of protozoan parasites in the phylum Apicomplexa, such as *Eimeria bovis*, *Neospora caninum*, *Toxoplasma gondii*, *Cryptosporidium parvum*, *Plasmodium falciparum*, and *B. besnoiti*, with both shared and parasite- or host-specific characteristics.

In *E. bovis*-stimulated PMN, NET formation is NADPH oxidase-dependent, faster and stronger than PMA, requiring viable sporozoites and exhibiting time- and dose-dependent kinetics

[213]. NETs immobilize sporozoites and hamper them from host cell invasion [213]. The NET response is mediated by CD11b upregulation, ERK1/2 and p38 MAPK phosphorylation, and Ca^{2+} influx via store-operated calcium entry (SOCE), along with the presence of extracellular DNA co-localizing with histones and NE as demonstrated in both *in vitro* and *in vivo* studies [213–215].

N. caninum tachyzoites induce NET formation in PMN from various hosts in a time- and dose-dependent manner, characterized by DNA filaments co-localizing with NE, histones H3, and MPO. While canine PMN require ERK1/2, p38 MAPK, and SOCE, bovine PMN undergo NET formation in a dose-dependent manner, independent of NADPH oxidase, NE, MPO, PAD4, and key signalling pathways, suggesting species-specific regulatory mechanisms [165,216,217].

T. gondii induces NET release across multiple host species, exhibiting common NET characteristic and signalling pathways as *E. bovis* and *N. caninum*. In murine PMN, intranasal infection triggers fast PMN recruitment and NET formation, with reduced infectivity in tachyzoites recovered from lavage fluid [130]. Canine PMN respond with NET formation against *T. gondii in vitro*, but tachyzoites degrade zymosan-induced NETs, suggesting an evasion strategy [218]. Human and caprine PMN exhibit classical and rapid NET formation, with mechanisms involving Ca^{2+} signalling, PI3K, and NADPH oxidase-dependent ROS production, modulated by p38 MAPK and ERK1/2 [219,220]. Additionally, TLR 2/4 signalling and neutrophil glycolysis regulate this response in goats [219].

In *Cryptosporidium parvum*-stimulated PMN, NET formation occurs in a time- and dose-dependent manner, characterized by the release of extracellular DNA decorated with NE, MPO, and histones [221]. The process is calcium-dependent, requiring intracellular calcium influx and activation of the ERK1/2 and p38 MAPK signalling pathways for optimal activation [221]. *C. parvum*-induced NET formation immobilizes sporozoites and inhibits their excystation, preventing parasite invasion of host cells from both neonatal and adult PMN donors [162,222]. Moreover, inhibition of P2X1 receptors using specific antagonists, or blocking NE or MPO, results in a significant reduction in NET formation [162,222]. Additionally, the process was observed under both physiological (5% O_2) and hyperoxic (21% O_2) conditions, confirming that NET formation occurs regardless of oxygen levels [162].

A 2019 study describes the role of NET formation in the pathogenesis of malaria, a disease caused by *Plasmodium falciparum* [223]. The study shows that heme molecules from infected erythrocytes (a known malaria DAMP released during parasite egress) induce NET formation in a mitochondrial ROS-dependent manner, as PMN from granulomatous disease patients (who carry NADPH oxidase mutations) exhibit similar NET formation levels in comparison with PMN from control patients [223]. This result was later confirmed with a scavenger of mitochondrial ROS. In addition, heme-triggered NETs required the activity of protein kinase C (PKC), cyclin-dependent kinase 6 (CDK6), and NE/Proteinase 3 (PR3), but were independent of peptidyl arginine deiminase 4 (PAD4)-mediated citrullination [223]. These results were genetically confirmed by isolating peritoneal PMN from NE single-knockout and NE/PR3 double-knockout mice. NE/PR3−/− PMN failed to release extracellular chromatin, whereas NE−/− cells displayed a partial deficiency, demonstrating that these proteases have an essential nonredundant function in decondensing chromatin [223]. In contrast, there was no difference in NET formation between PAD4−/− and control PMN [223].

Recent studies have elucidated multiple aspects of *Besnoitia besnoiti*-induced NET formation. Both *B. besnoiti* tachyzoites and bradyzoites induce NET formation in a time- and dose-dependent manner, associated with increased NE and MPO activity, as well as enhanced ROS production [224,225]. This response occurs regardless of tachyzoite viability, but varies in amplitude [224]. Vital tachyzoites exhibit reduced endothelial infectivity after PMN interaction, an effect reversed by DNase treatment, highlighting the mechanistic role of NETs [224]. The metabolic requirements of *B. besnoiti*-induced NET formation rely on pyruvate- and lactate-mediated catabolic pathways [226]. Under physiological flow conditions, *B. besnoiti*-infected endothelial cells upregulate adhesion molecules (VCAM-1, P-selectin, ICAM-1, and E-selectin), promoting PMN adhesion. This interaction leads to endothelial damage via NET formation, with histone 2A identified as a key NET component. Interestingly, *B. besnoiti*-infected endothelium itself also induces NET release [62,227]. Furthermore, recent studies link autophagy and NET formation as bradyzoites-exposed PMN showed positive staining for microtubule-associated protein 1A/1B-light chain 3 (LC3), a key protein of autophagosome formation. Additionally, tachyzoite-exposed PMN release NET, featuring activation of calcium/calmodulin-dependent protein kinase kinase 2 / AMP-activated protein kinase (CAMKK/AMPK) pathway [225,228].

Collectively, while NET formation is a conserved response among Apicomplexan parasites, distinct regulatory pathways highlight host-specific variations in NET induction and efficacy.

1.5 Aims of the current dissertation

NET formation represents an essential component of the innate immune defense against pathogens. While the principal capacity of protozoan parasites like *Besnoitia besnoiti* to trigger NETs release has already been proven, the molecular mechanisms orchestrating this process remain only partially understood. In particular, the roles of distinct signaling pathways (e.g., purinergic signaling), metabolic regulators including AMPK, and parasite-host communication via extracellular vesicles have scarcely been addressed, so far.

This dissertation therefore aimed to add new data on the current understanding of the cellular and molecular mechanisms underlying *B. besnoiti*-induced NET formation in bovine PMN by focusing on the following topics:

Aim 1: To investigate the role of purinergic signaling and ATP as a master regulator of *B. besnoiti*-induced NET formation, addressed in Chapter 1: *B. besnoiti*-induced PMN clustering and NET formation depend on P2X1 purinergic receptor signaling

Aim 2: To elucidate the relevance of the AMPK-related signaling pathway as an early regulator of *B. besnoiti / T. gondii* tachyzoite-mediated PMN activation and NET formation, addressed in Chapter 2: The CAMKK/AMPK pathway activation participates in early events of *B. besnoiti*- and *T. gondii*-triggered NET formation in PMN

Aim 3: To evaluate the role of extracellular vesicles from different cellular origin (*B. besnoiti* tachyzoites, infected host cells and *B. besnoiti*-exposed PMN) in parasite-driven NET formation, addressed in Chapter 3: PMN responses to EVs released by *B. besnoiti* tachyzoites and *B. besnoiti*-infected host cells

2. MATERIAL AND METHODS

2.1 Primary bovine umbilical vein endothelial cell isolation and maintenance

Primary bovine umbilical vein endothelial cells (BUVEC) were isolated from umbilical veins obtained from calves born by *sectio caesarea* at the Justus Liebig University Giessen. Therefore, umbilical cords were stored at 4 °C in 0.9% Hank's balanced salt solution (HBSS)–HEPES buffer (H1641, Sigma-Aldrich; H4034, Sigma-Aldrich; pH 7.4) supplemented with 1% penicillin/streptomycin (P4333, Sigma-Aldrich) for a maximum of 16 h before use. For endothelial cells isolation, 0.025% collagenase type II (LS004174, Worthington Biochemical Corporation) suspended in Puck´s solution (137 mM NaCl, 5.37 mM KCl, 1.08 mM $CaCl_2$, 0.617 mM $MgSO_4$, 2.83 mM NaH_2HPO_4, 1.10 mM KH_2PO_4, 6.11 mM Glucose, pH 7.4) was infused into the lumen of ligated umbilical veins and incubated for 20 min at 37 °C/5% CO_2 atmosphere. Cells were collected in cell culture medium supplemented with 1 ml fetal calf serum (FCS, N4637, Sigma-Aldrich) to inactivate collagenase. After two washes (350 × g, 12 min, 20 °C), cells were re-suspended in complete endothelial cell growth medium (ECGM, C-22010, PromoCell) supplemented with 10% FCS. Then, cells were plated in 25 cm^2 tissue plastic culture flasks (C6481, Greiner) and cultured at 37 °C / 5% CO_2 atmosphere in modified ECGM medium (diluted at 30% in M199 medium, 2154, Sigma-Aldrich) supplemented with 5% fetal bovine serum (FBS, 10270-106, Gibco) and 1% penicillin/streptomycin. Medium was replaced every 2-3 days. BUVEC cell layers were used for infection after three passages *in vitro* [229].

2.2 Host cell culture, B. besnoiti and T. gondii tachyzoite maintenance

All experiments of the current study were performed with tachyzoite stages of the apicomplexan parasite *B. besnoiti* (Bb-Evora04 strain) and *Toxoplasma gondii* (RH strain). Madin-Darby bovine kidney (MDBK) and human foreskin fibroblasts (HFF) cells were used as host cells for *B. besnoiti* and *T. gondii* tachyzoite *in vitro* production, respectively. Host cell layers were cultured in 75 cm^2 plastic tissue culture flasks (C7231, Greiner) at 37°C/5% CO_2 atmosphere using RPMI 1640 medium (R0883, Sigma-Aldrich) or Dulbecco's modified Eagle medium (DMEM)-GlutaMAX (10566016, Gibco) supplemented with 5% fetal bovine serum and 1% penicillin/streptomycin for MDBK or HFF cells, respectively. Host cell layers were infected at 80% confluency with 2.4×10^7 tachyzoites. For tachyzoite harvest, infected host cells were scraped, cells and supernatants collected and filtered through a 5 µm syringe

filter (SLSV025LS, Merck), washed, and pelleted (400×g, 12 min) prior to re-suspension in supplemented RPMI 1640 cell culture medium. Tachyzoite numbers were determined in a Neubauer chamber (0640030, Marienfeld), and parasite stages were placed at 37 °C/5% CO_2 atmosphere for further experimental use [228–231].

2.3 Bovine PMN isolation

Healthy adult dairy cows served as blood donors. Animals were bled by puncture of the jugular vein and peripheral blood was collected in heparinized sterile plastic tubes (041551, Kabe Labortechnik). Heparinized blood was re-suspended at 1:1 ratio in 20 ml sterile PBS (D1408, Sigma-Aldrich) with 0.02% EDTA (8043.2, CarlRoth), carefully layered on top of 12 ml Histopaque-1077 separating solution (density = 1.077 g/l; 10771, Sigma-Aldrich) and centrifuged (800×g, 45 min) without brake. After removal of plasma and peripheral blood mononuclear cells, the volume of the cell suspension was adjusted to 10 ml with ice-cold HBSS (14065-049, Gibco). Then, 20 ml of lysis buffer (5.5 mM NaH_2PO_4, 10.8 mM KH_2PO_4, pH 7.2) were added and the sample was gently mixed for 60 s to lyse erythrocytes. Osmolarity was rapidly restored by addition of 10 ml hypertonic buffer (462 mM NaCl, 5.5 mM NaH_2PO_4, 10.8 mM KH_2PO_4, pH 7.2) and 10 ml HBSS. The lysis step was repeated twice. PMN were then suspended in 5 ml HBSS, counted in a Neubauer chamber and allowed to rest on ice for 30 minutes prior to any experimental use [228–231].

2.4 Extracellular vesicle (EV) isolation and characterization

To isolate EVs from B. besnoiti-infected BUVEC, 8 x 10^6 BUVEC (biological replicates = 3) in 75 cm^2 plastic tissue culture flasks were infected with tachyzoites (ratio: 1:6) in modified ECGM medium for 4 h (37 °C, 5% CO_2). After washing with sterile PBS, cells were resuspended in vesicle-depleted modified ECGM medium (EV medium) and incubated for 24 h. Equal numbers of plain tachyzoites and non-infected BUVEC were equally treated for controls. For isolation of EVs from tachyzoite-exposed PMN (n = 3), 5 x 10^7 PMN were exposed to tachyzoites (ratio 1:6) in EV medium for 4 h. Equal numbers of plain PMN and of zymosan-stimulated PMN (0.1 mg/ml, Z4250, Sigma-Aldrich) were used as controls. After incubation, EV-containing supernatants were collected and pooled per experimental condition and differentially centrifuged (300×g for 5 min, 2,000×g for 10 min and 10,000×g for 30 min) to eliminate cell debris. Supernatants were concentrated using Amicon Ultra-15 100 kDa MWCO filter devices (UFC9100, Millipore) to a final volume of 500 µl. Then, EV isolation

was performed by size-exclusion chromatography (SEC) with an Automatic Fraction Collector V2 (AFC-V2, Izon) using a qEV sepharose column (ICO-70, qEVoriginal/70 nm, Izon) according to IZON´s protocol. The columns were equilibrated with filtered (0.22 µm) PBS, pH 7.4, before loading EV samples (500 µl). After discarding 2.9 ml eluate, 0.5 ml fractions were collected into 2 ml eppendorf tubes. EV fractions were concentrated using Amicon Ultra-15 100 kDa MWCO filter devices to a final volume of 100-150 µl. EV samples were stored at −20°C until further use. For characterization of EV size and concentration, Nano-flow cytometry was conducted using a Flow NanoAnalyzer (NanoFCM Co., Ltd, Nottingham, UK) equipped with a 488 nm and a 638 nm laser at the Core Facility Extracellular Vesicles, Center for Tumor Biology and Immunology, Philipps University of Marburg, Germany. The instrument was calibrated using 200 nm polystyrene beads (NanoFCM Co. Ltd.) at a defined concentration of 2.08 x 10^8 particles/ml, serving as reference for particle concentration. Monodispersed silica beads (NanoFCM Co., Ltd) of four different diameters (68 nm, 91 nm, 113 nm and 155 nm) were utilized as size reference standards. Measurements of freshly filtered (0.1 µm) plain 1x TE buffer pH 7.4 (Lonza, Basel, Switzerland) were defined as background signals; consequently, respective values were subtracted from all other measurements. Particle concentration and size distribution of EV samples (diluted in 0.1 µm pore size-filtered 1x TE buffer) were calculated using NanoFCM software (NF Profession V2.0), based on data collected for one minute under a sample pressure of 1.0 kPa [229].

2.5 Scanning electron microscopy (SEM)

Bovine PMN were co-cultured with *B. besnoiti* tachyzoites at 1:4 ratio at 37°C and 5% CO_2 for 60 min on 10 mm coverslips (0111500, Marienfeld) pre-coated with 0.01% poly-L-lysine (P8920, Sigma-Aldrich). After incubation, cells were fixed in 2.5% glutaraldehyde (G5882, Merck), post-fixed in 1% osmium tetroxide (75632, Merck), washed in distilled water, dehydrated, critical point dried by CO_2-treatment and sputtered with gold. Finally, all samples were analysed via a Philips XL30 scanning electron microscope at the Institute of Anatomy and Cell Biology, Justus Liebig University Giessen, Germany [231].

2.6 NET detection by immunofluorescence microscopy

Bovine PMN were co-cultured with *B. besnoiti* tachyzoites (1:6 ratio) for 4 h (37 °C, 5% CO_2 atmosphere) on fibronectin- (2.5 ug/ml, F1141, Sigma-Aldrich) or poly-L-lysine-pretreated coverslips (15 mm diameter, 0111550, Marienfeld), fixed in 4% paraformaldehyde (158127,

Merck), and stored at 4 °C. To assess the effect of AMPK activation, *B. besnoiti* tachyzoite- or *T. gondii* tachyzoites-exposed PMN were stimulated with 1 mM of AICAR (A9978, Sigma-Aldrich). In an independent experiment, 2 x 10^5 PMN were co-cultured with BUVEC- and *B. besnoiti* tachyzoite-derived EVs (1 x 10^8 particles). Fixed samples were washed three times with blocking/permeabilization solution [PBS containing 3% BSA (A9418, Sigma-Aldrich), 0.3% Triton X-100 (X100, Sigma-Aldrich)]. For NET visualization samples were incubated in primary antibody solution diluted in blocking/permeabilization (overnight, 4 °C) applying anti-histone (1:1000, clone TNT-1, MAB3864, Merck) and anti-NE (1:1000, AB68672, Abcam) to stain DNA and respective proteins in NET structures. An in-house hyperimmune serum raised against *B. besnoiti* was used (1:100) to stain tachyzoites. In an independent experiment, primary antibody anti-histone (1:300, clone H11-4, MAB3422, Merck) were used. After three washings in PBS, samples were incubated for 1 h at RT in secondary antibody solution containing Alexa Fluor 488 goat anti-rabbit IgG (1:500, A11008, Life Technologies), Alexa Fluor 647 goat anti-mouse IgG (1:500, A21235, Life Technologies), or TRITC-conjugated anti-bovine (1:500, A18756, Invitrogen) antibodies. Occasionally, Alexa Fluor 594 goat anti-mouse IgG (1:500, A11005, Life Technologies) were used instead of Alexa Fluor 647. Finally, samples were washed three times in PBS, mounted in anti-fading buffer with 4′,6-diamidin-2-phenylindol (DAPI, 495952, Fluoromount G, Thermo Fisher), and sealed with coverslip sealant (23005-1, Biotium). Images were acquired by a Nikon Eclipse Ti2-A inverted microscope equipped with a white LED epifluorescence lamp, a ReScan confocal microscopic instrumentation (RCM 1.1 Visible, Confocal.nl) and a motorized z-stage (DI1500) controlled by the NIS-Elements v 5.11 software. Measurements of defined parameters (e.g., area, integrated density, and number) were performed with Fiji/Image J software (version: 1.53c) [232]. Histone-DNA and DAPI signals were acquired at the same time point for each image. A manual threshold was applied to each channel using the clustering algorithm of Otsu [233]. Sharpness of the images was adjusted and the percentage of cells releasing NETs for each experimental condition was assessed as described elsewhere [234] by determining the number of cells positive in the DNA-H1 channel relative to the total number of cells in the DAPI channel. Cells positive for DNA-H1 and showing an expanded non-multilobulated nucleus (>80 μm^2) were defined as NETotic. For EV-exposed PMN, image acquisition was achieved by a BZ-X800 microscope (Keyence), thereby applying identical brightness and contrast conditions within the datasets of each biological experiment. Percentages of NET-forming PMN were calculated semi-automatically by dividing the events counted in the histone channel (multiplied by 100) by the events counted in the DAPI channel [228–231].

2.7 Extracellular DNA quantification

Bovine PMN (2 x 10^5) suspended in RPMI 1640 medium without phenol red were confronted with *B. besnoiti* tachyzoites for 4 h (37°C, 5% CO_2) at a 1:6 ratio in the presence of non-modified ATP (0.05-50 µM, P1132, Promega), or non-hydrolyzable ATP (ATPγS; 0.05-50 µM; 4080, Tocris). Moreover, specific purinergic receptor antagonists were utilized to investigate receptor-mediated signalling pathways. The selective P_2Y_1 receptor antagonist MRS 2179 (0900, Tocris) and the P_2Y_6 receptor antagonist MRS 2578 (2146, Tocris) were employed for the inhibition of P_2Y-type receptors. For P_2X receptor inhibition, NF449 (1391, Tocris) was used as a selective P_2X_1 antagonist, 5-BDBD (3579, Tocris) as a P_2X_4 antagonist, and AZ10606120 (3323, Tocris) as a P_2X_7 antagonist. All antagonists were prepared at a concentration range of 0.1-100 µM. To investigate the role of EVs on NET release, bovine PMN (2 x 10^5) suspended in RPMI 1640 were confronted with 1 x 10^8 EV particles from all cellular sources (see 2.4) for 4 h (37°C, 5% CO_2). Independently, 2 × 10^5 bovine PMN were co-cultured with *T. gondii* (1:4) in RPMI 1640 medium but pretreated with the MAPK inhibitor UO126 (50 µM, 30 min; Sigma-Aldrich), the PI3K inhibitor LY294002 (1 µM, 30 min; CST) or the SOCE inhibitor 2-APB (50 µM, 30 min; Sigma) before exposure to *T. gondii*. To prove that the source of the fluorescence signal is extruded DNA from PMN, DNase I (90 U/sample, Roche Diagnostics) treatment was included as control. After incubation, sample supernatants were analysed for "cell-free" NETs. The remaining cells at the well bottoms were estimated for "anchored" NETs, as described elsewhere [235]. Therefore, picogreen [P7581, Invitrogen, 1:200 dilution in 10 mM Tris base (4855.2, Carl Roth)] buffered with 1 mM EDTA (50 µl/well) was added to each supernatant or pellet sample. Extracellular DNA was quantified by picogreen-derived fluorescence intensities using an automated multiplate reader (Varioskan, Thermo Scientific) at 480 nm excitation/ 520 nm emission [229–231].

2.8 Quantification of ROS production by EV-stimulated PMN

Total ROS measurement was performed by a chemiluminescence-based assay using luminol (A4685, Sigma-Aldrich). Therefore, 1 x10^7 PMN were suspended in 1 ml of HBSS; 100 µl (1 × 10^6 PMN) were transferred per well to a white 96-well plate. Then, 90 µl luminol (80 µM final concentration) were added per well. For negative controls, non-stimulated PMN were used. After 30 readings accounting for 12 minutes, 10 µl of 1 x10^8 EVs isolated from BUVEC controls, *B. besnoiti*-infected BUVEC, *B. besnoiti* tachyzoites or zymosan were added to PMN.

Chemiluminescence was measured for 3 h in a Luminometer (Luminoskan, Thermo Scientific) [229].

2.9 Flow cytometry-based measurement of neutrophil intracellular calcium concentration

1 x 10^7 PMN/mL were stained with 1 µM FLUO-4 AM (Invitrogen, UK) for 30 min at 37°C and 5% CO_2. Then, FLUO-4-loaded PMN were washed twice in HBSS and suspended at a concentration of 1 x 10^7 PMN/mL. For each assay, 5 x 10^5 PMN (50 µL PMN suspension) were dispensed in flow cytometry tubes (352052, Falcon, Corning) adjusting the volume to 400 µL with HBSS. After recording a baseline for 15 s, PMN were exposed to *T. gondii* tachyzoites (1:4) or stimulated with the calcium ionophore A23187 (25 µM, C9400, Sigma-Aldrich), thereby immediately registering changes in fluorescence intensity in the FL-1 channel. All calcium influx related experiments were performed in a BD Accuri C6 plus flow cytometer (BD Biosciences, Heidelberg, Germany) equipped with a non-pressurized peristaltic pump, allowing to add *T. gondii* tachyzoites without interrupting sampling. After experimentation, the mean intensity of fluorescence (MFI) after 5 min of stimulation was determined and graphed [230].

2.10 Quantification of PMN oxygen consumption rates (OCR) and extracellular acidification rates (ECAR)

Metabolic activation of bovine PMN was monitored using the Seahorse XF analyzer (Agilent). Briefly, 1 x 10^6 PMN from three blood donors were pelleted [500 x g, 10 min, room temperature (RT)]. PMN were re-suspended in 0.25 ml of XF RPMI assay medium (103576, Agilent) supplemented with 2 mM L-glutamine (103579, Agilent), 1 mM pyruvate (103578, Agilent), and 10 mM glucose (103577, Agilent). 2 x 10^5 cells were gently placed in each well of an eight-well XF analyzer plate (Agilent) pre-coated for 30 min with 0.001% poly-L-lysine. Then, XF RPMI assay medium was adjusted to 180 µl total volume per well and cells were incubated at 37°C without CO_2 supplementation for 45 min before Seahorse measurements. To evaluate the role of ATP (0.05-50 µM), ATPγS (0.05-50 µM), AICAR (10 mM), 1 x 10^8 EVs and *B. besnoiti* tachyzoites (1.2 x 10^6/well) on PMN activation, stimuli were suspended in XF RPMI assay medium and supplemented to PMN via instrument-own injection ports after baseline measurements. The total assay duration was 240 min (160 min in the case of EVs-exposed PMN). Background subtraction and determination of OCR/ECAR registries were

performed by using Seahorse Agilent analytics platform (https://seahorseanalytics.agilent.com) [228,229,231].

2.11 Measurement of total neutrophil and extracellular ATP concentration

1×10^6 bovine PMN were confronted with *B. besnoiti* tachyzoites (1:6 ratio) in HBSS and incubated at 37 °C/5% CO_2 for 15 s and 15 min. For positive controls, cells were stimulated with a combination of PMA (100 nM, P1585, Sigma-Aldrich) and ionomycin (5 µM, 10634, Sigma-Aldrich) in HBSS supplemented with 1 M NaCl. After incubation on ice for 5 min, cells were pelleted (600 × g, 5 min) and supernatants were recovered for extracellular ATP quantification using an ATP Determination kit (A22066; Invitrogen) according to manufacturer's instructions. For the estimation of neutrophil total ATP concentration, cell pellets were analysed by the CellTiter-Glo luminescent Cell viability assay (G7571, Promega) following manufacturer's instructions. All samples were analysed by luminometry using an automated reader (Luminoskan Flash) [231].

2.12 Analysis of PMN apoptosis and necrosis by flow cytometry

In order to determine potential NF449-driven effects on PMN apoptosis and necrosis rates, PMN suspensions (2×10^5/200 µl HBSS) were placed into 5 mL polystyrene round-bottom tubes (352052, Falcon, Corning) and treated with NF449 (10-100 µM) for 4 hours at 37°C/5%CO_2. In a separate set of experiment, apoptosis and necrosis rates in AICAR (1 mM)- and compound-C (10 µM , ab144821, Abcam)-treated PMN were determined after 4 h of incubation. PMN were then pelleted (600 x g, 8 min), stained by Annexin V-FITC/ propidium iodide (PI) double staining apoptosis detection kit (ab14085, Abcam) following the manufacturer´s instructions and analysed by a BD Accuri C6 Plus Flow Cytometer (BD, USA). FlowJo v10.8.1 software was used to determine apoptosis and necrosis rates [228,231].

2.13 Immunoblotting

Proteins from *B. besnoiti* or *T. gondii* tachyzoite-exposed and non-exposed bovine PMN (5×10^6), or PMN treated with AICAR (1 mM) and compound C (10 µM) were extracted in RIPA buffer (50 mM Tris-HCl, pH 7.4; 1% NP-40; 0.5% Na-deoxycholate; 0.1% SDS; 150 mM NaCl; 2 mM EDTA; 50 mM NaF; CarlRoth) supplemented with a protease inhibitor cocktail (Sigma-P8340, Aldrich), 1 mM sodium orthovanadate tyrosine phosphatase inhibitor

(ab120386, Abcam) and 1 mM phenylmethylsulphonyl fluoride (ab141032, Abcam) after 30 min of incubation. Protein extracts were sonicated for five cycles of 20 s with 20 s resting in between. Then, the samples were centrifuged (10,000 × *g*, 10 min, 4 °C) to sediment intact cells and nuclei. Supernatants were collected and their protein content was quantified via the Pierce™ Bradford Plus Protein Assay Kit (23236, Thermo Scientific) according to the manufacturer's instructions. For immunoblotting, samples were supplemented with 6 M urea. After boiling (95 °C, 5 min), 40 µg of total protein was electrophoresed per slot in 12% or 15% polyacrylamide gels (100 V, 90 min) using a Mini-PROTEAN Tetra Cell system (Biorad). Proteins were then transferred (300 mA, 2 h) to polyvinylidene difluoride (PVDF) membranes (IPVH08100, Merck) using a wet-tank tranfer system (Biorad). The blots were first incubated in blocking solution [3% BSA in TBS (50 mM Tris-Cl, pH 7.6; 150 mM NaCl containing 0.1% Tween 20; P9416, Sigma-Aldrich) for 1 h at RT], and then reacted with primary antibodies overnight at 4 °C. Primary antibodies were anti-AMPKα (1:1000, 50081, Cell Signaling), anti-AMPKα Thr172 (1:1000, 5831, Cell Signaling), anti-pAMPKα (1:1000, 2795, Cell Signaling), anti-pAMPKβ1 (1:1000, 4178, Cell Signaling), anti-pAMPKγ1 (1:1000, 4187, Cell Signaling), anti-CAMKK (1:1000, ab96531, Abcam), anti-pCAMKK (1:1000, abPA5-64569, Thermo Fischer), anti-Beclin-1 (1:1000, 3495, Cell Signaling), anti-p-Beclin-1 (1:1000, 14717, Cell Signaling), and anti-ULK1 (1:1000, 8054, Cell Signaling) diluted in blocking solution. The detection of vinculin (1:1000, sc-73614, Santa Cruz) was used for normalization of the samples. Signal detection was accomplished by incubation for 30 min at RT in the corresponding secondary antibodies conjugated with peroxidase (1:40000, 31430; and 1:40000, 31460, Pierce) and then applying an enhanced chemiluminescence detection system (ECL® plus kit, RPN2132, GE Healthcare). Protein signals were recorded in a ChemoCam Imager® (Biorad, Feldkirchen, Germany). Protein masses were controlled by a protein ladder (PageRuler®plus pre-stained protein ladder covering ~10–250 kDa, 26619, Thermo Fisher Scientific). Quantification of protein band intensities was performed by Image J® software (Fiji version) using the gel analyzer plugin [228,230].

In an independent experimental setup for EV protein characterization, the protein concentration of each EV isolate was estimated by the absorbance at 562 nm using the micro BCA protein assay kit (23235, Thermo Scientific) following manufacturer's protocol. EV-derived protein samples were supplemented with Laemmli-β-mercaptoethanol loading buffer (1x final concentration, 1610747, BioRad). Commercially available human EV-derived proteins (EV pos, EXOAB-POS-1, System Biosciences) and *B. besnoiti* tachyzoite protein extracts were

used as positive controls. After boiling (95 °C) for 5 min, proteins (20 µg/slot) were separated in 4-20% polyacrylamide gels (4561095, BioRad) via electrophoresis (120 V constant for 1 h, tetra system BioRad) and then transferred to 0.2 µm PVDF membranes (trans-blot turbo, 1704156, 2.5 A constant, up to 25 V, 7 min, BioRad). Samples were blocked in blocking solution, and then reacted with primary antibodies diluted in blocking solution (overnight, 4 °C). Primary antibodies were anti-CD9 (1:500, MA1-19301, ThermoFisher), anti-CD81 (1:500, MA5-28419, ThermoFisher) and anti-Vinculin (1:500). Vinculin was included as sample loading control. Following three washes in TBS-Tween 0.1% buffer, blots were incubated with secondary antibody solutions (dilution in blocking solution, 30 min, RT). Secondary antibodies included anti-mouse (1:40000, 31430, Pierce) and anti-rabbit (1:40000, 31466, Pierce) antibodies. After three further washes in TBS-Tween (0.1%) buffer, signal detection was accomplished by an enhanced chemiluminescence detection system (Clarity Max Western ECL substrate, 1705062, BioRad) and recorded using a ChemiDOC Imager (BioRad). Protein masses were controlled by a protein ladder (PageRuler Plus Prestained Protein Ladder ~10-180 kDa, 26616, Thermo Fisher Scientific) [229].

2.14 Transmission electron microscopy (TEM) of EVs

TEM analysis was performed on 1 x 10^{10} EVs derived from infected BUVEC and *B. besnoiti* tachyzoites. EV samples (10 µl) were fixed in a drop of 0.1 M cacodylate buffer (J60344, Sigma-Aldrich) containing 4 % formaldehyde and 1.5 % glutaraldehyde. Specimen suspensions were absorbed immediately after fixation on formvar-coated grids (TEM-FCF200CU50, Sigma-Aldrich) and stained with 1% ammonium molybdate (277908, Sigma-Aldrich). Negatively stained samples were inspected in a transmission electron microscope (EM 902N, Zeiss, Oberkochen, Germany) equipped with a slow-scan 2K CCD camera (TRS, Tröndle, Moorenweis, Germany) [229].

2.15 EV labelling with far red

1 x 10^9 EVs isolated from non-infected BUVEC, *B. besnoiti*-infected BUVEC and *B. besnoiti* tachyzoites were stained by far red (CellTrace™ far red, C34564, ThermoFisher) as described elsewhere [236]. Briefly, EVs (1 x 10^9/15 µl) in PBS were mixed with 15 µl far red dye solution (40 µM) and incubated for 2 h at 37 °C. To remove unbound dye, EVs were loaded on a qEV sepharose column (qEVoriginal/70 nm, Izon) and processed as described before (see 2.4). Cell Trace far red dye without EVs was used as dye control [229].

2.16 Analysis of neutrophil EV uptake

1 x 10^6 PMN were exposed to 1 x 10^9 far red-labelled EVs derived from non-infected BUVEC, *B. besnoiti*-infected BUVEC and *B. besnoiti* tachyzoites in RPMI-1640 medium (without phenol red) at 37 °C for 6 h. Far red dye without EVs was used as dye control, unstimulated/unstained PMN were used as negative controls and PMN directly stained with Far red dye were used as positive control. Samples were mixed by gently pipetting every hour. Cells were washed twice with PBS before analysis. Confocal microscopy was performed on 0.5 x 10^6 EV-stimulated PMN seeded in 24-well plates containing poly-L-lysine (0.01%, 20 min, RT and subsequent washing with PBS) -pretreated 15 mm coverslips. After allowing PMN to sediment for 30 min, cells were fixed in 4% paraformaldehyde and mounted in anti-fading buffer with DAPI (Fluoromount G). Images were acquired by a Nikon Eclipse Ti2-A inverted microscope equipped with ReScan confocal microscopic instrumentation (RCM 1.1 Visible, Confocal.nl) and a motorized z-stage (DI1500). Two channels were recorded for signal detection: DAPI/405 nm and far red dye/640 nm. Images were acquired by a sCMOS camera (PCO edge) using a CFI Plan Apochromat X20 and x60 lambda-immersion oil objective (NA 1.4/0.13; Nikon) controlled by NIS-Elements v 5.11 (Nikon, Tokyo, Japan) software. Identical brightness and contrast conditions were applied for each data set within one experiment using Fiji software [229].

2.17 IL-1β, IL-6 and CXCL8 quantification in PMN and BUVEC supernatants

1 x 10^6 PMN or BUVEC plated in 12 well plates were exposed to 1 x 10^8 EVs derived from non-infected BUVEC, *B. besnoiti*-infected BUVEC and *B. besnoiti* tachyzoites for 4 h (PMN) or 24 h (BUVEC) at 37°C, 5% CO_2. PMN stimulation with LPS (1 µg/ml, L2630, Sigma-Adrich) and PMA/ionomycin (100 nM/5 µM) or BUVEC stimulation with LPS (0.01 µg/ml) were used for positive controls. After incubation, aliquots (100 µl) of cell supernatants (each: $n = 3$) were analysed for the presence of IL-1β (bovine IL-1β ELISA Kit, ESS0027, Thermo Fisher Scientific), IL-6 (ESS0029, Thermo Fisher Scientific) and CXCL8 (IL-8, bovine IL-8 ELISA kit, ABIN6957183, Antibodies Online), following the manufacturer's instructions. In the case of IL-1β and IL-6 ELISA kits, high affinity binding 96 well plates (655061, Greiner bio one) were used. The samples were analyzed at 450 nm and 550 nm in an automated Varioskan Flash Reader (Thermo Fisher Scientific, MA, USA). Standard curves and sample

concentrations of IL-1β, IL-6 and CXCL8 were calculated using GraphPad PRISM® V10.3.0 software package (GraphPad software, USA) [229].

2.18 Statistical analysis

All experiments were repeated at least three times. Statistical significance was defined by a p value < 0.05. The p values were determined by applying the following analyses:

2.18.1 Statistical settings for Chapter 1: B. besnoiti-induced PMN clustering and NET formation depend on P_2X_1 purinergic receptor signalling

Unpaired two-way t-tests were used for Seahorse-based metabolic measurements. Unpaired two-way t-tests and one-way ANOVA followed by Tukey´s multiple comparison was applied on ATP quantification experiments. One-way ANOVA followed by a Dunnett´s multiple comparison was used to analyse extracellular DNA quantification experiments. Kruskal Wallis´s followed by a Dunn´s multiple comparison was applied on extracellular DNA quantification assays using purinergic receptors inhibitors. One-way ANOVA followed by a Tukey´s multiple comparison was used to analyse clustering experiments. Bars graphs represent the mean ± SD, and statistical analyses were generated using Graph Pad PRISM® V7.03) [231].

2.18.2 Statistical settings for Chapter 2: The CAMKK/AMPK pathway activation participate in early events of B. besnoiti- and T. gondii-triggered NET formation in PMN

In the Western blot experiments, the p-values were calculated via unpaired, two-tailed t-tests, comparing control PMN vs. PMN exposed to *B. besnoiti* tachyzoites at each time point, and via paired, two-tailed t-tests, comparing control PMN vs. PMN incubated with *T. gondii*. For Seahorse-based metabolic measurements, the p-values were calculated using the Mann–Whitney test. Kruskal-Wallis followed by Dunn's multiple comparisons tests were applied to NET quantification results. ANOVA followed by Dunnet multiple comparisons tests were applied to calcium influx and DNA release data. Bar graphs represent the mean ± SD, and statistical analysis was performed by GraphPad software (v. 7.03) [228,230].

2.18.3 Statistical settings for Chapter 3: PMN responses to EVs released by B. besnoiti tachyzoites and B. besnoiti-infected host cells

One-way ANOVA followed by a Dunnett´s multiple comparison test, with single pooled variance were applied on every experiment of this result section. Bars graphs represent the mean ± SD, and statistical analyses were generated using GraphPad PRISM® V10.3.0 [229].

3. RESULTS

3.1 Chapter 1: B. besnoiti-induced PMN clustering and NET formation depend on P_2X_1 purinergic receptor signalling

Intracellular ATP not only serves as the main source of cellular energy but also acts as a key signaling molecule. Under stress conditions, cells release ATP as a danger signal that attracts purinergic receptor-expressing leukocytes like PMN. In PMN, purinergic signaling modulates essential functions through paracrine and autocrine mechanisms, thereby regulating processes like chemotaxis, adhesion, transmigration, ROS production, NET formation, and apoptosis [158–164]. This chapter studies the role of purinergic signaling and the metabolic state of PMN in *B. besnoiti* tachyzoite-induced NET formation. Related data have been published in Espinosa et al., 2023.

3.1.1 B. besnoiti tachyzoite-exposed bovine PMN release NETs entrapping tachyzoites

To first re-confirm the functional capacity of *B. besnoiti* tachyzoites to induce NET formation in bovine PMN, we analyzed parasite-confronted PMN for NET formation by SEM and immunofluorescence analysis. SEM showed that *B. besnoiti* tachyzoite-exposed PMN indeed released NETs (Fig. 6C, D, white arrows) in comparison to unstimulated PMN (Fig. 6A) with several tachyzoites being firmly entrapped by these structures. Of note, the aberrant morphology of entrapped tachyzoites (Fig. 6D) strongly suggested that these stages were dead. To confirm NET identity, classical proteins of NETs were visualized by immunostaining. Here, co-localization of extracellular DNA with histone (i. e. H1) and NE was verified for *B. besnoiti* tachyzoite-driven NETs. Some of these NET fibers were in direct contact with *B. besnoiti* tachyzoites, potentially entrapping the parasites (Fig. 6E, F) [231].

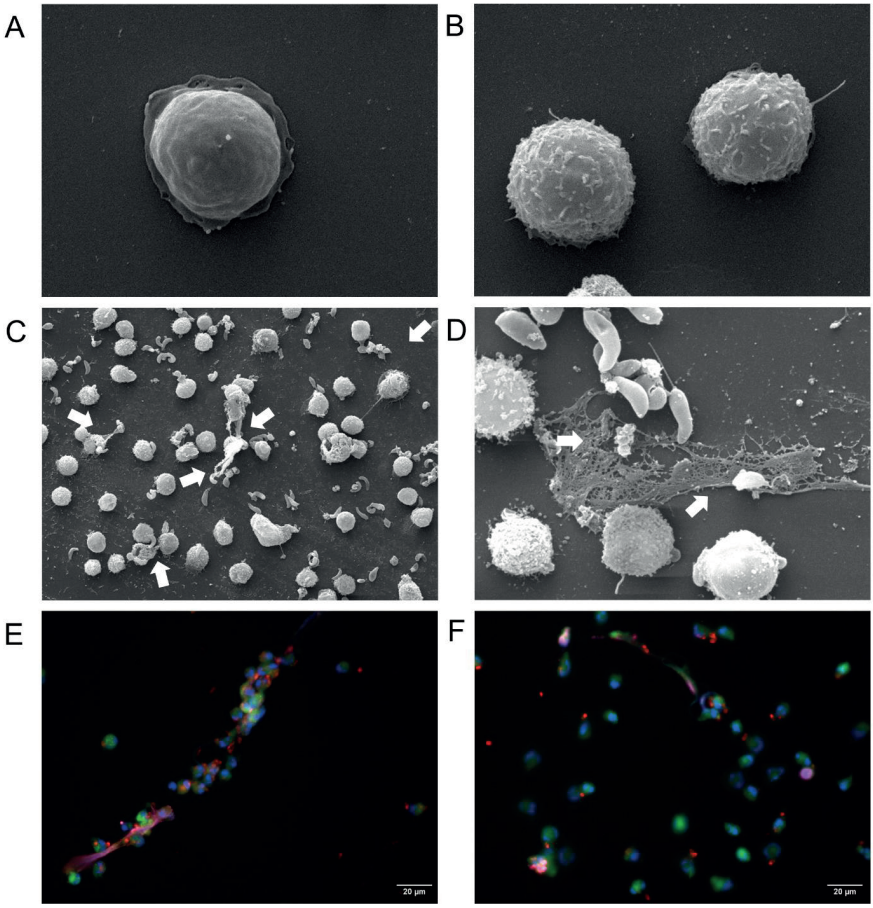

Figure 6. *B. besnoiti* tachyzoites are trapped in released NETs. (A) Unstimulated PMN and (B) activated PMN. NETs, defined as extracellular chromatin filaments containing NE and histone H1, were released and formed a network in contact with *B. besnoiti* tachyzoites, as visualized via SEM (C, D) and immunostaining (E, F). White arrows indicate entrapped *B. besnoiti* tachyzoites. Co-localization of DNA (DAPI, blue); *B. besnoiti* tachyzoites (red); Histone H1 (clone TNT-1, pink) and NE (green) [231]

3.1.2 Exposure to B. besnoiti tachyzoites induces oxidative responses in bovine PMN

To explore parasite-driven changes in the energetic status and oxidative responses of *B. besnoiti* tachyzoite-confronted PMN, we analyzed neutrophil metabolic parameters by means of oxygen consumption rates (OCR) and extracellular acidification rates (ECAR) (Fig. 7). *B. besnoiti* tachyzoite supplementation to PMN induced a significant increase in OCR ($p < 0.01$), whilst ECAR was not affected (Fig. 7A, B). Given that ATP is involved in both neutrophil metabolic reactions and purinergic signaling responses, the effect of non-modified ATP supplementation was evaluated at increasing concentrations. Overall, ATP supplementation failed to change oxidative responses (OCR) (Fig. 7C) but led to a significant ($p < 0.05$) increase in ECAR at a concentration of 50 μM (Fig. 7D) [231]. Based on these data, the influence of ATP on *B. besnoiti* tachyzoite-induced activation of PMN was evaluated on the level of additive effects. Therefore, PMN were pre-treated with ATP (50 μM) and then exposed to *B. besnoiti* tachyzoites (PMN:tachyzoites, 1:6). However, ATP pretreatments neither changed the parasite-driven increase in OCR nor ECAR levels (Fig. 8A, B). As expected, a rapid increase in ECAR after ATP supplementation (Fig. 8B, unfilled circles) was observed when compared to plain XF RPMI medium (Fig. 8B, filled black circles, $p < 0.05$). Energetic mapping indicated that *B. besnoiti* tachyzoite exposure induced a shift towards aerobic metabolism in PMN, whilst ATP supplementation rather shifted PMN into a glycolytic status (Fig. 8C). When the non-hydrolyzable variant of ATP (ATPγS; Fig. 8D, E) was used, a modest but significant increase in neutrophil OCR and ECAR was observed, indicating that PMN were activated and shifted to an energetic status. Again, addition of ATPγS did not alter the response to *B. besnoiti* tachyzoites (Fig. 8D, E). Overall, the tachyzoite-induced OCR increase was neither changed by ATP nor by ATPγS supplementation, thereby suggesting a pivotal role of oxygen consumption in parasite-driven activation of bovine PMN [231].

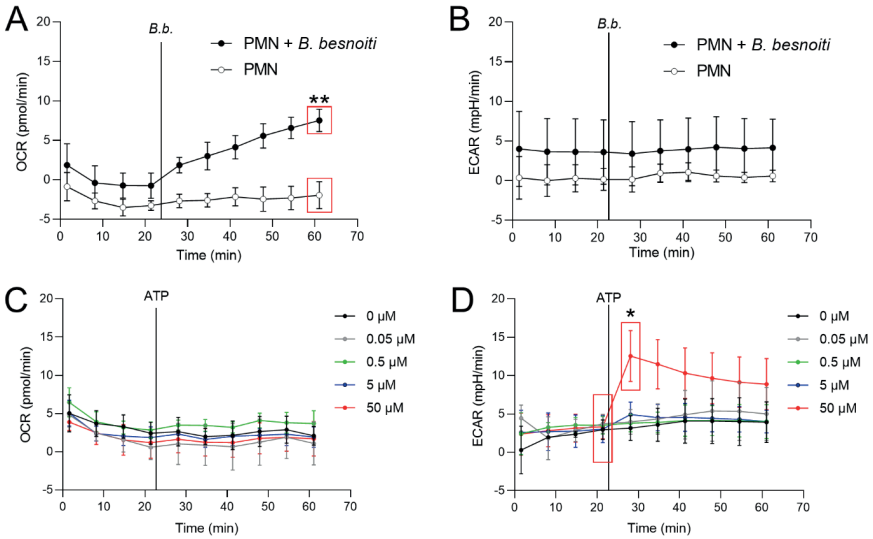

Figure 7. Exposure to *B. besnoiti* tachyzoites induces oxygen consumption in bovine PMN. In the absence of CO_2, 2 x 10^5 PMN were incubated in XF RPMI media for 45 min. Four basal measurements were performed and then either *B. besnoiti* tachyzoites (A, B) or ATP (0.05-50 µM; C, D) was supplemented at the time point indicated by a vertical line. OCR (A, C) and ECAR (B, D) values were obtained by Seahorse technology and plotted over time (n = 3, for each condition). All data are shown as mean ± SD; *p-values* were calculated by unpaired two-tailed t - test analysis (n = 3) [231].

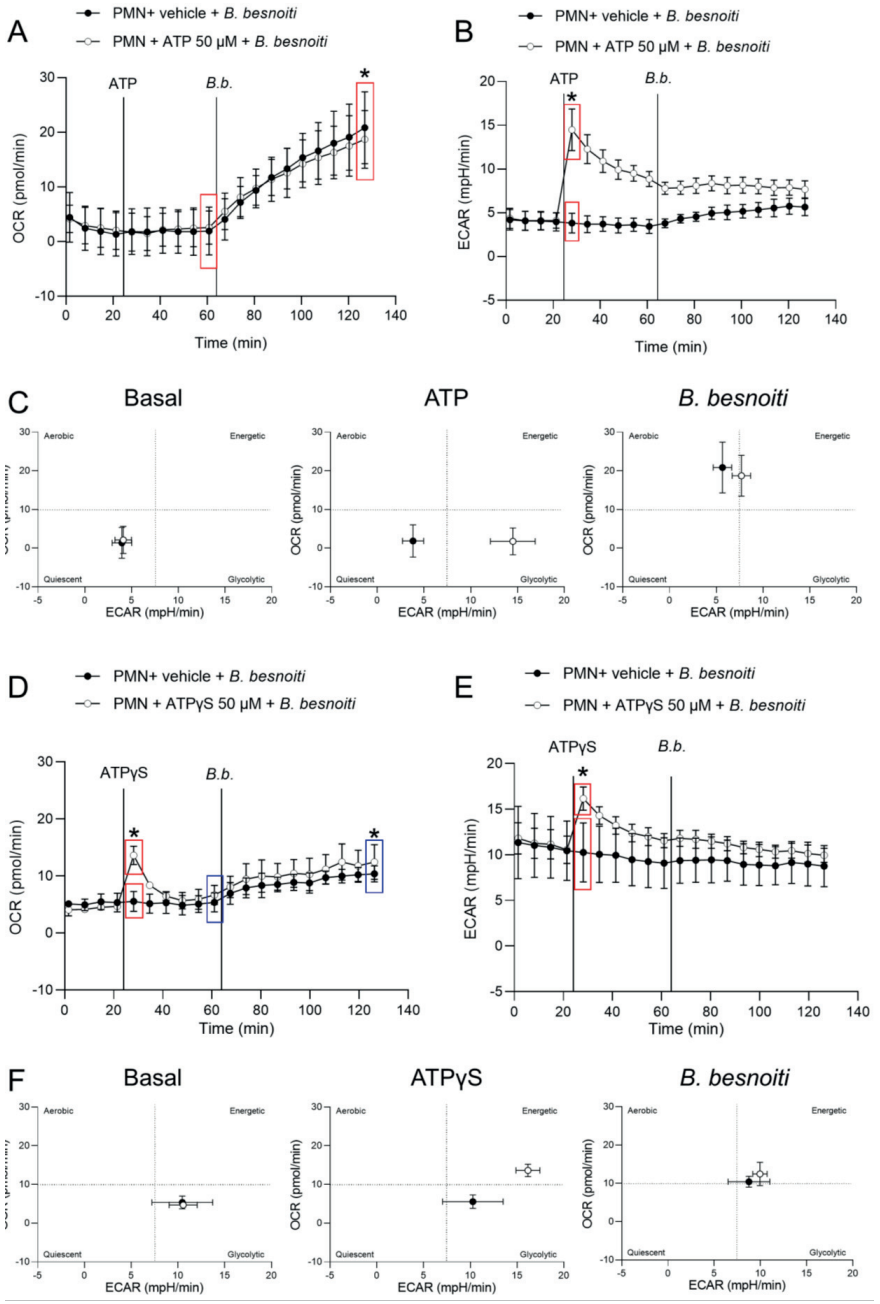
A
PMN+ vehicle + B. besnoiti
PMN + ATP 50 µM + B. besnoiti
ATP
B.b.
OCR (pmol/min)
Time (min)
B
PMN+ vehicle + B. besnoiti
PMN + ATP 50 µM + B. besnoiti
ATP
B.b.
ECAR (mpH/min)
Time (min)
C
Basal
ATP
B. besnoiti
Aerobic
Energetic
Quiescent
Glycolytic
OCR (pmol/min)
ECAR (mpH/min)
D
PMN+ vehicle + B. besnoiti
PMN + ATPγS 50 µM + B. besnoiti
ATPγS
B.b.
OCR (pmol/min)
Time (min)
E
PMN+ vehicle + B. besnoiti
PMN + ATPγS 50 µM + B. besnoiti
ATPγS
B.b.
ECAR (mpH/min)
Time (min)
F
Basal
ATPγS
B. besnoiti
Aerobic
Energetic
Quiescent
Glycolytic
OCR (pmol/min)
ECAR (mpH/min)

Figure 8. Exposure to *B. besnoiti* tachyzoites induces a metabolic shift towards aerobic carbohydrate catabolism in bovine PMN. After basal measurements, PMN were treated with ATP, ATPγS (both 50 μM), or vehicle, followed by supplementation of *B. besnoiti* tachyzoites as indicated by vertical lines. Differences in OCR and ECAR from means in the same curve and sharing boxes of the same colour were calculated (A, B, D, E). Energetic maps (C, F) were generated by presenting OCR (Y-axis) and ECAR (X-axis) as means of the different measurements over time. All data are shown as mean ± SD; *p-values* were calculated by unpaired *t* - test (A, B, *n* = 6; D, E *n* = 3) [231].

3.1.3 B. besnoiti tachyzoite exposure does not affect total ATP concentration in bovine PMN

To investigate a potential change in extracellular ATP and in total neutrophil ATP levels after tachyzoite exposure, ATP concentrations were analysed at 15 seconds or 15 minutes of confrontation by luminometry (Fig. 9). For positive controls, stimulations of PMN with hypersaline buffer and PMA/ionomycin were used. Exogenous ATP levels were measured in supernatants of PMN treated with a hypertonic buffer for 15 seconds. Here, indeed a significant rise ($p < 0.001$) in extracellular ATP were detected (Fig. 9A). Furthermore, total ATP levels of bovine PMN were estimated in PMN stimulated with PMA and ionomycin for 15 and 60 min and revealed a continuous drop in ATP levels signifying ATP consumption over time ($p < 0.0001$) (Fig. 9B). However, when PMN were exposed to *B. besnoiti* tachyzoites, neither changes in extracellular ATP concentration nor in total neutrophil ATP levels were detected (Fig. 9C-E) [231].

3.1.4 Non-hydrolyzable ATP (ATPγS) boosts B. besnoiti tachyzoite-induced anchored NET formation

Given that a high extracellular ATP concentration signifies a danger signal and may foster general PMN effector mechanisms, we here studied effects of exogenous ATP on parasite-driven NET formation. NET quantification based on picogreen-derived fluorescence intensities was performed, allowing for “cell-free” and “anchored” NETs differentiation, thereby reflecting the late phase of NET formation. Here, PMN were pre-stimulated with non-modified ATP or ATPγS in a dose-dependent manner and then confronted with *B. besnoiti* tachyzoites (Fig. 10). As expected, parasite-exposed PMN showed a significant increase in anchored NET formation ($p < 0.05$) compared to medium-stimulated controls (Fig. 10D). Dose-dependent treatments with exogenous non-modified ATP treatment neither affected basal nor tachyzoite-induced NET formation (Fig. 10A-D). In contrast, ATPγS treatments resulted in a significant increase of basal anchored ($p < 0.0001$) and cell-free ($p < 0.01$) NET formation in plain PMN at 50 μM concentration (Fig. 10E, G). Interestingly, in case of *B. besnoiti* tachyzoite-exposed

PMN, ATPγS treatments exclusively induced an increased in the release of anchored but not of cell-free NET formation ($p < 0.01$; Fig. 10H) [231].

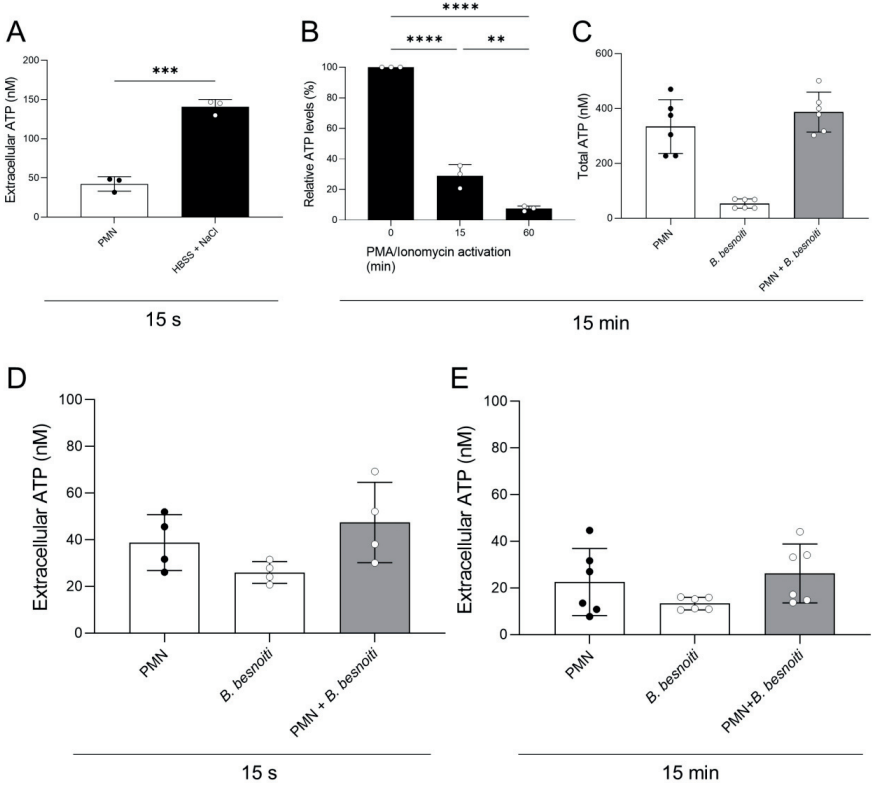

Figure 9. Total neutrophil ATP and extracellular ATP concentration in *B. besnoiti* tachyzoite-PMN co-cultures. (A) For positive control of ATP release, PMN were treated for 15 s with a hypertonic buffer (HBSS supplemented with 1 M sodium chloride). ***$p < 0.001$. (B) For positive control for neutrophil ATP consumption, PMN were stimulated with PMA/ionomycin (100 nM/5 µM) for 15 and 60 min. **$p < 0.01$; ****$p < 0.0001$. (C–E) To assess parasite-driven effects on neutrophil ATP release and consumption, bovine PMN were confronted with *B. besnoiti* tachyzoites (1:6) for 15 s and 15 min. ATP in PMN (total ATP) or supernatants (extracellular ATP) was measured by a commercial kit. All data are shown as mean ± SD; *p-values* were calculated by unpaired two-way t-test (A), or one-way ANOVA followed by Tukey´s multiple comparison (B-E) analysis (A, B, $n = 3$; D, $n = 4$; C, $n = 6$) [231].

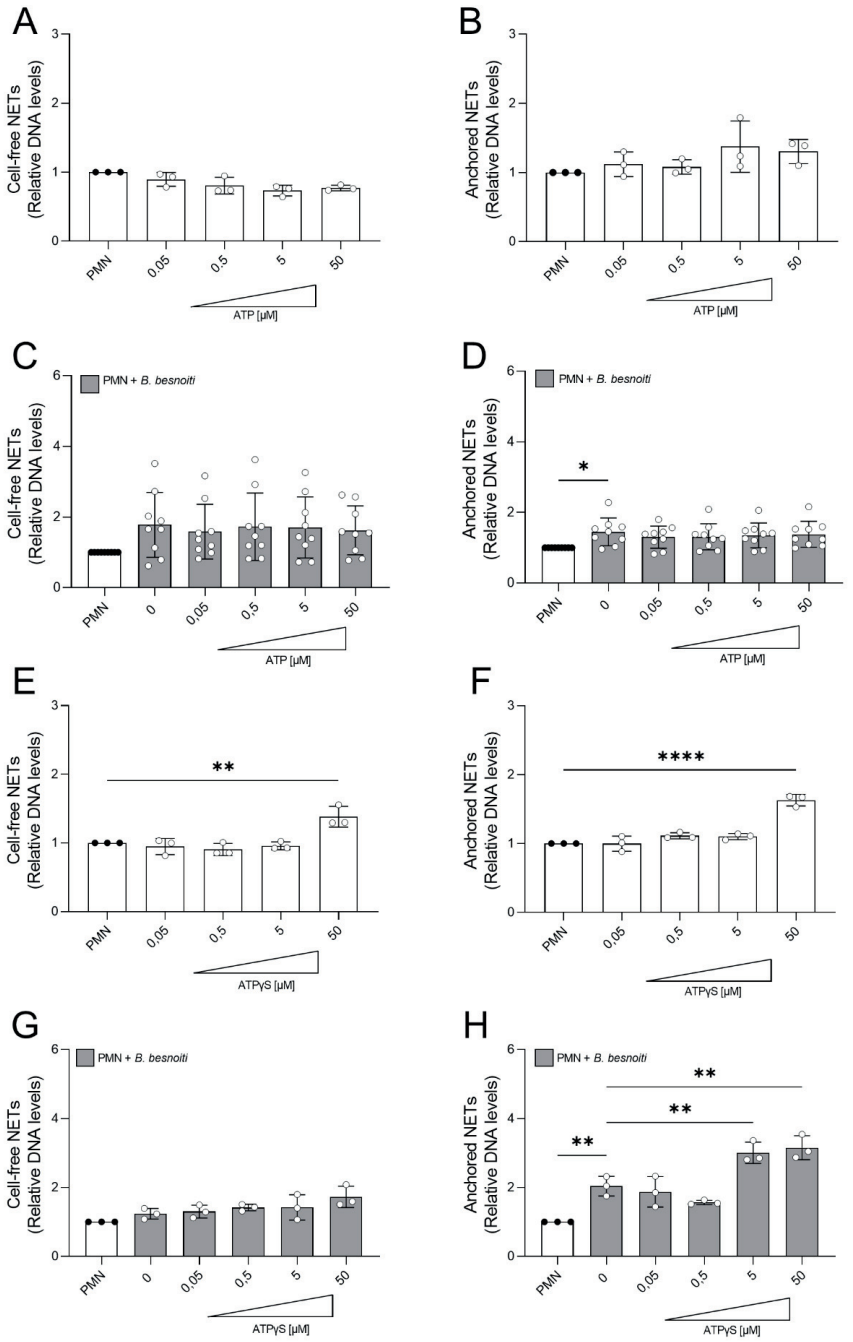
A
Cell-free NETs (Relative DNA levels)
PMN
0,05
0,5
5
50
ATP [μM]
B
Anchored NETs (Relative DNA levels)
ATP [μM]
C
PMN + B. besnoiti
Cell-free NETs (Relative DNA levels)
0
ATP [μM]
D
PMN + B. besnoiti
Anchored NETs (Relative DNA levels)
*
ATP [μM]
E
Cell-free NETs (Relative DNA levels)
**
ATPγS [μM]
F
Anchored NETs (Relative DNA levels)
****
ATPγS [μM]
G
PMN + B. besnoiti
Cell-free NETs (Relative DNA levels)
ATPγS [μM]
H
PMN + B. besnoiti
Anchored NETs (Relative DNA levels)
**
**
**
ATPγS [μM]

Figure 10. ATPγS supplementation induces NET release and boosts *B. besnoiti* tachyzoite-driven anchored NET formation. Bovine PMN were pretreated with increasing concentrations of non-modified ATP or non-hydrolyzable ATPγS (0.05-50 μM) for 10 min. Then, PMN were incubated for 4 h in plain medium (A, B, E, F) or exposed to *B. besnoiti* tachyzoites (C, D, G, H). After incubation, extracellular DNA was detected and quantified via picogreen-derived fluorescence intensities using a multi-plate reader at 480 nm excitation/520 nm emission wavelengths. All data are shown as mean ± SD; *p-values* were calculated by one-way ANOVA followed by Dunnett´s multiple comparison test. *$p < 0.05$; **$p < 0.01$; ****$p < 0.0001$. [231].

3.1.5 P_2X_1 inhibition by its antagonist NF449 blocks B. besnoiti tachyzoite-induced anchored NET formation

Since exogenous ATP seemed to play a role in NET induction, we further investigated the relevance of purinergic signaling pathways in *B. besnoiti* tachyzoite-induced NET formation. To monitor the role of different purinergic receptors, PMN were pre-treated with receptor antagonists of different P_2X (P_2X_1, P_2X_4 and P_2X_7) and P_2Y (P_2Y_1 and P_2Y_6) receptors at different concentrations and then confronted with parasite stages (Fig. 11). In antagonist-free controls, PMN confrontation with *B. besnoiti* tachyzoites resulted in a significant increase ($p < 0.05$) of anchored NET formation when compared to controls (Fig. 9B, D, H, J). In line with previous data [226], NF449 pre-treatments targeting the purinergic P_2X_1 receptor, resulted in a significant decrease of *B. besnoiti* tachyzoite-triggered anchored NETs ($p < 0.05$) when compared to non-treated PMN (Fig. 11J). However, all other treatments (pharmacological inhibition of P_2X_4, P_2X_7, P_2Y_1 and P_2Y_6 receptors) failed to affect parasite-triggered anchored or cell-free NET formation (Fig. 11A-H). Besides antagonist pre-treatments, the inhibitors were also added 40 min after *B. besnoiti* tachyzoite exposure to determine if any of the antagonist was capable to revert parasite-induced NET formation, previously described as a "point of no return" and defined as a consumption of intracellular ATP by PMN after 30-40 min of activation [237]. In this experimental setting, a selective efficacy of NF449 was confirmed since exclusively this treatments significantly decreased *B. besnoiti* tachyzoite-triggered anchored ($p < 0.01$) and cell-free ($p < 0.05$) NETs (Fig. 12C, D). The sum of these data indicated that tachyzoite-induced NET formation selectively depends on P_2X_1-mediated signaling [231].

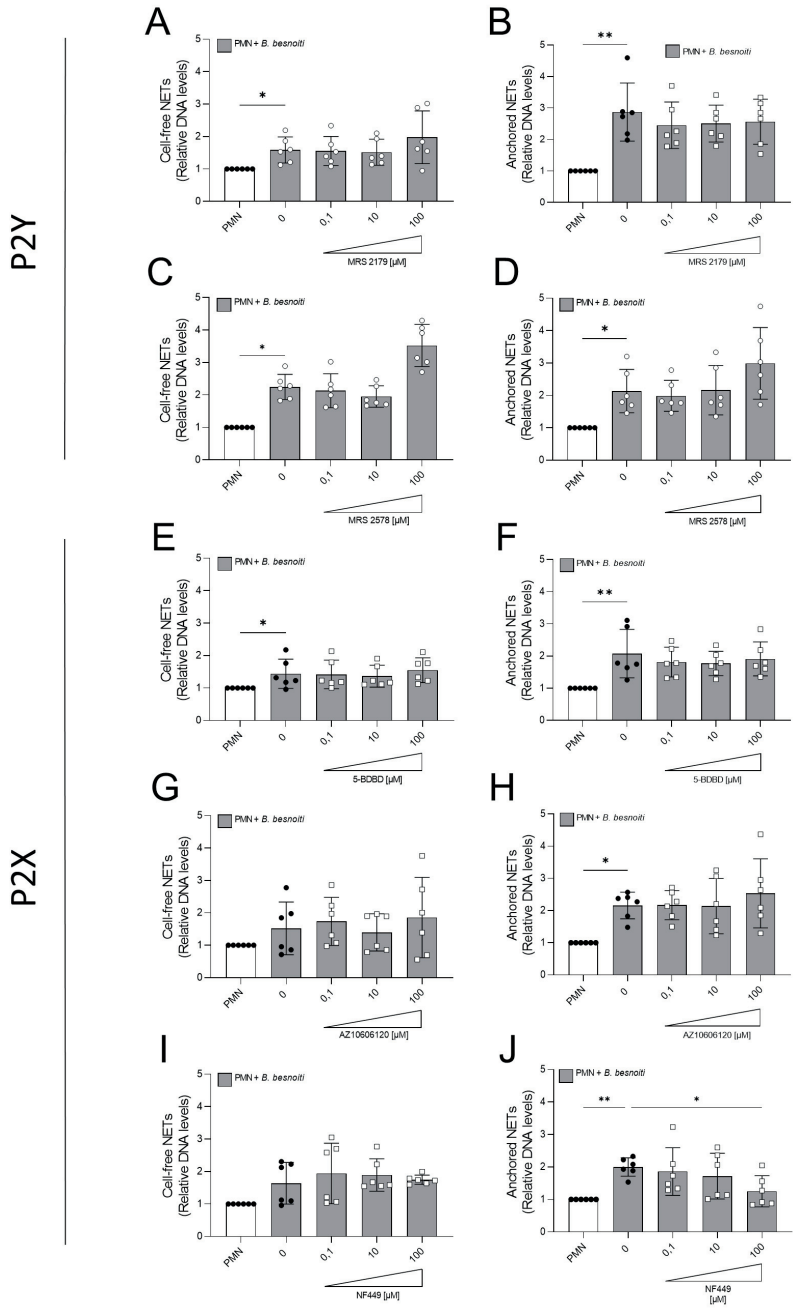
P2Y
P2X
A
B
C
D
E
F
G
H
I
J
PMN + B. besnoiti
Cell-free NETs (Relative DNA levels)
Anchored NETs (Relative DNA levels)
PMN
0
0,1
10
100
MRS 2179 [μM]
MRS 2578 [μM]
5-BDBD [μM]
AZ10606120 [μM]
NF449 [μM]

Figure 11. Effects of purinergic receptor antagonist pre-exposure treatments on *B. besnoiti*-tachyzoite driven NET formation. Bovine PMN were pre-treated for 10 min with increasing concentrations of MRS2179, MRS2578, NF449, 5-BDBD, and AZ10606120 (0.1-100 μM) targeting P_2Y_1, P_2Y_6, P_2X_1, P_2X_4, and P_2X_7 receptors, respectively, and then exposed to *B. besnoiti* tachyzoites for 4 h. Thereafter, cell-free (A, C, E, G, I) and anchored (B, D, F, H, J) NET formation was analyzed. For both NET types, extracellular DNA was detected and quantified via picogreen-derived fluorescence intensities using a multi-plate reader at 480 nm excitation/520 nm emission wavelengths. All data are shown as mean ± SD; *p-values* were calculated by Kruskal-Wallis test followed by Dunn´s multiple comparison test ($n = 6$). *$p < 0.05$; **$p < 0.01$. [231].

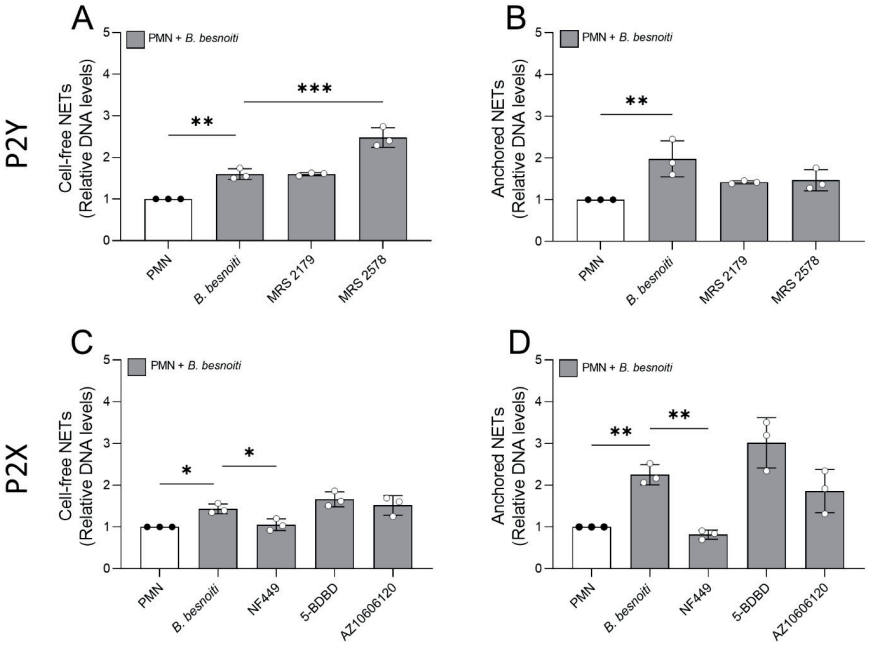

Figure 12. Effects of purinergic receptor antagonist post-exposure treatments on *B. besnoiti* tachyzoite-triggered NET formation. Bovine PMN were first exposed to *B. besnoiti* tachyzoites for 40 min and then treated with 100 μM of MRS2179, MRS2578, NF449, and 5-BDBD targeting P_2Y_1, P_2Y_6, P_2X_1, P_2X_4, and P_2X_7 receptors, respectively. After 4 h of incubation, cell-free (A, C) and anchored (B, D) NET formation was analysed. For both NET types, extracellular DNA was detected and quantified via picogreen-derived fluorescence intensities using a multi-plate reader at 480 nm excitation/520 nm emission wavelengths. All data are shown as mean ± SD; *p-values* were calculated by an ordinary one-way ANOVA with Dunnett s multiple comparison analysis. ($n = 3$). *$p < 0.05$; **$p < 0.01$; ***$p < 0.001$. [231].

3.1.6 NF449 blocks B. besnoiti tachyzoite-induced NET formation in a dose-dependent manner and without affecting cell viability

Since NF449 was the only inhibitor that consistently reduced *B. besnoiti* tachyzoite-induced NET formation, we further studied the dose dependency of this reactions in addition to eventual ATP-driven changes, but also controlled potential effects of this P_2X_1 antagonist on PMN necrosis and apoptosis by propidium iodide and Annexin V-FITC/PI staining, respectively (Fig. 13). Overall, the combination of exogenous ATP or ATPγS (50 µM) supplementation and *B. besnoiti* tachyzoite exposure did not change the consistent significant decrease ($p < 0.01$) of anchored and cell-free NET formation driven by NF449 pre-treatments (Fig. 13A, B). As revealed by propidium iodide and Annexin V-based assays, NF449 treatments (10 µM and 100 µM) had no effect on neutrophil necrosis or apoptosis, since the proportions of vital PMN remained equal (88.4% and 86.1% respectively) compared to non-treated controls (87.4%) (Fig. 13C). Analyses on NF449-related dose dependence revealed an IC_{50} of 1.27 µM for *B. besnoiti* tachyzoite-induced NET formation (Fig. 13D). In summary, NF449-mediated inhibition of *B. besnoiti* tachyzoite-induced NET formation was dose-dependent and occurred without affecting PMN viability [231].

3.1.7 B. besnoiti tachyzoite exposure induces a P2X1-dependent clustering of bovine PMN

During co-culture experiments, we noticed that the presence of *B. besnoiti* tachyzoites seemed to drive PMN clustering. To follow this impression and to study whether this finding depended on purinergic signaling, we here analyzed parasite-mediated PMN cluster formation in presence and absence of the P_2X_1 antagonist NF449 (Fig. 14). Indeed, an increase ($p < 0.05$) in PMN numbers participating in clusters was verified for *B. besnoiti* tachyzoite-confronted PMN after 4 h of incubation when compared to parasite-free controls (Fig. 14B). Notably, the number of PMN participating in clusters decreased to basal levels ($p < 0.01$) when PMN were pre-treated with the P_2X_1 inhibitor NF449 at a concentration of 100 µM (Fig. 14B), thereby confirming the critical role of purinergic signalling in the clustering process [231].

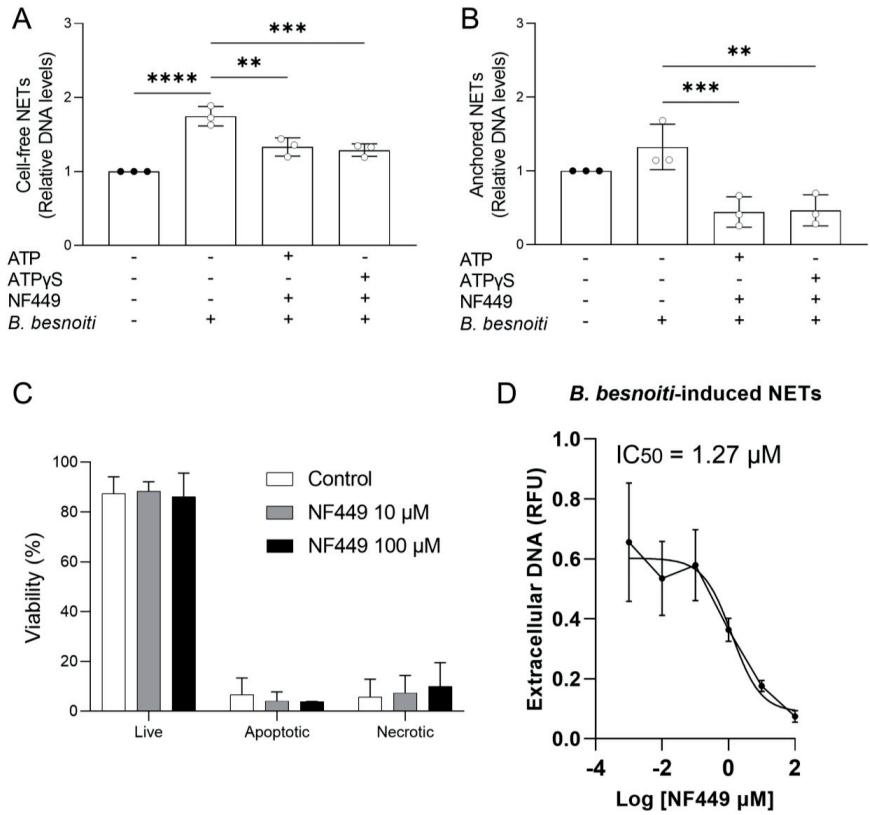

Figure 13. NF449 does not affect PMN viability and inhibits *B. besnoiti*-driven NET formation in an ATP-independent but dose-dependent manner. (A, B) Bovine PMN were pre-treated with NF449 (100 µM) in the presence or absence of ATP/ATPγS and then confronted with *B. besnoiti* tachyzoites. After 4 h of incubation, extracellular DNA was detected and quantified via picogreen-derived fluorescence intensities. (C) Annexin V-FITC and propidium iodide staining of PMN treated with NF449 for 4 h. (D) NF449-based dose-response-inhibition of *B. besnoiti* tachyzoite-induced NET formation. The IC_{50} was calculated by a nonlinear regression analysis. All data are shown as mean ± SD; *p*-values were calculated by one-way ANOVA with Dunnett´s multiple comparison analysis. (n = 3). $^{**}p < 0.01$; $^{***}p < 0.001$; $^{****}p < 0.0001$. [231].

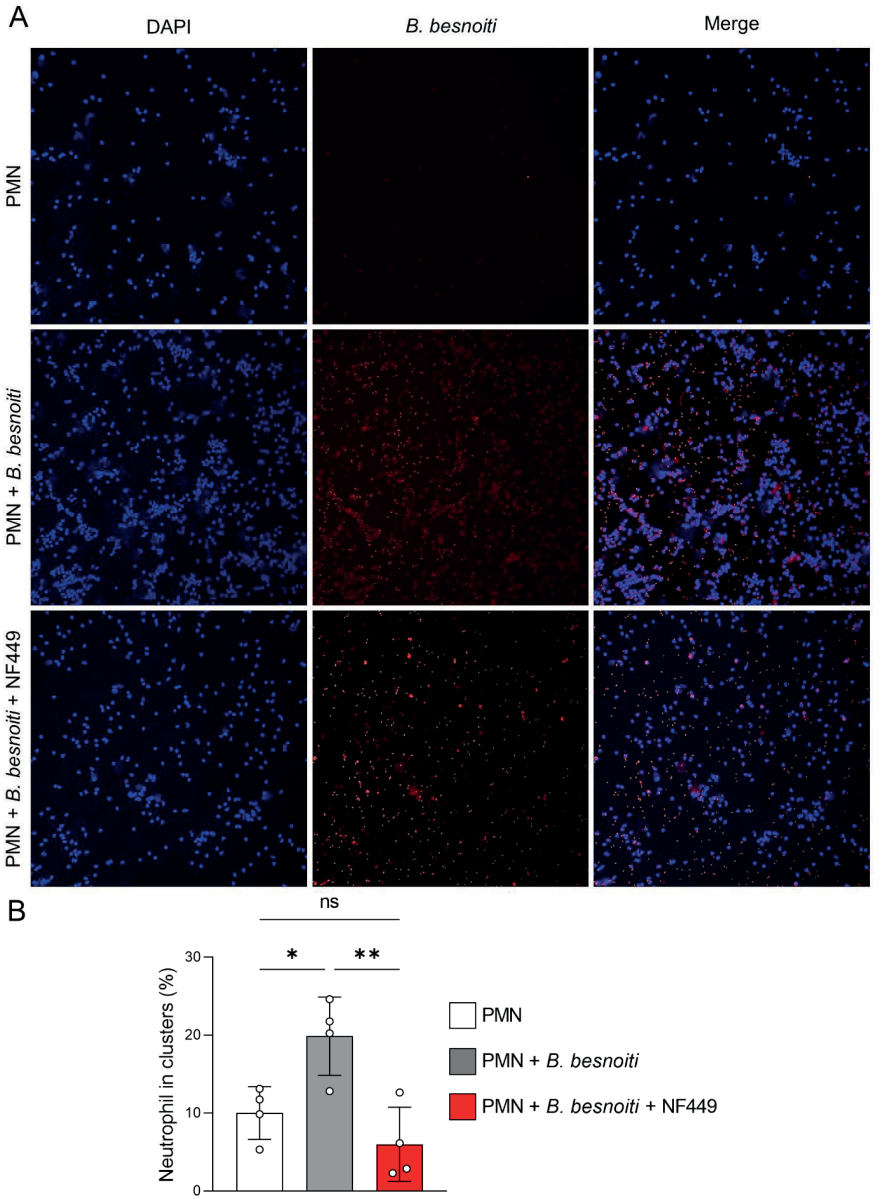

Figure 14. *B. besnoiti* tachyzoite-induced clustering of bovine PMN depends on P2X1-based purinergic signaling. PMN were co-cultured with tachyzoites for 4 h in the presence or absence of NF449 (100 μM). (A) Exemplary illustrations of tachyzoite-PMN co-cultures stained for DNA (DAPI, blue) and parasite stages (red). (B) DANA-based quantification of cluster formation. All values are presented as mean ± SD, and *p*-values were calculated using one-way ANOVA followed by Tukey s multiple comparisons. (n = 4). *$p < 0.05$; **$p < 0.01$. [231].

3.2 Chapter 2: CAMKK/AMPK pathway activation participates in early events of B. besnoiti- and T. gondii-triggered NET formation

Calcium is a key mediator of NET formation, since a rise in intracellular calcium concentrations triggers PAD4 activation, chromatin decondensation, and subsequent NET release. Calcium-related downstream signaling events include the activation of several kinases forming part of the CAMKK/AMPK pathway, and which have been implicated in NET formation. Within this cascade, CAMKK functions upstream of AMPK, whereas ULK-1 and Beclin-1 act downstream as central regulators of autophagy. Notably, AMPK activation has emerged as a pivotal regulator of PMN functions, linking metabolic sensing with effector activities, such as chemotaxis, bacterial killing, ROS generation, and autophagy. This suggests that calcium- and AMPK-driven pathways converge to coordinate neutrophil responses and parasite-triggered NET formation [181,238–240]. The current chapter aimed to investigate the role of CAMKK/AMPK pathway activation and modulation of distinct autophagic proteins (ULK-1 and Beclin-1) in *B. besnoiti* tachyzoite-exposed PMN. For a comparative approach, similar experiments were performed also performed with *T. gondii* tachyzoite-exposed PMN, considering that both parasites are closely related members of the Apicomplexa. Respective data on *B. besnoiti* and *T. gondii* have been published in Conejeros et al., 2024 and 2025, respectively.

3.2.1 PMN exposure to B. besnoiti tachyzoites induces neutrophil AMPK phosphorylation

A previous report demonstrated AMPK phosphorylation as an early event of PMN–parasite interactions since it occurred already 10 min after exposure while being sustained for up to 30 min of co-incubation of bovine PMN with *B. besnoiti* tachyzoites [62]. Here, we confirmed this observation on the level of Western blotting-based analyses of protein extracts originating from *B. besnoiti*-exposed PMN (Fig. 15A). Hence, phosphorylated AMPK (p-AMPK) but not AMPK showed a significantly enhanced expression at 30 min of co-culture (Fig. 15B, parasite-exposed PMN vs. negative control condition: $p = 0.025$). Moreover, the catalytic subunit AMPKα1 was moderately but statistically insignificantly ($p = 0.110$) upregulated in tachyzoite-exposed PMN (Fig. 16A, B). Overall, no changes were observed for the regulatory subunits AMPKβ1 and AMPKγ1 (Fig. 16A, B) [228].

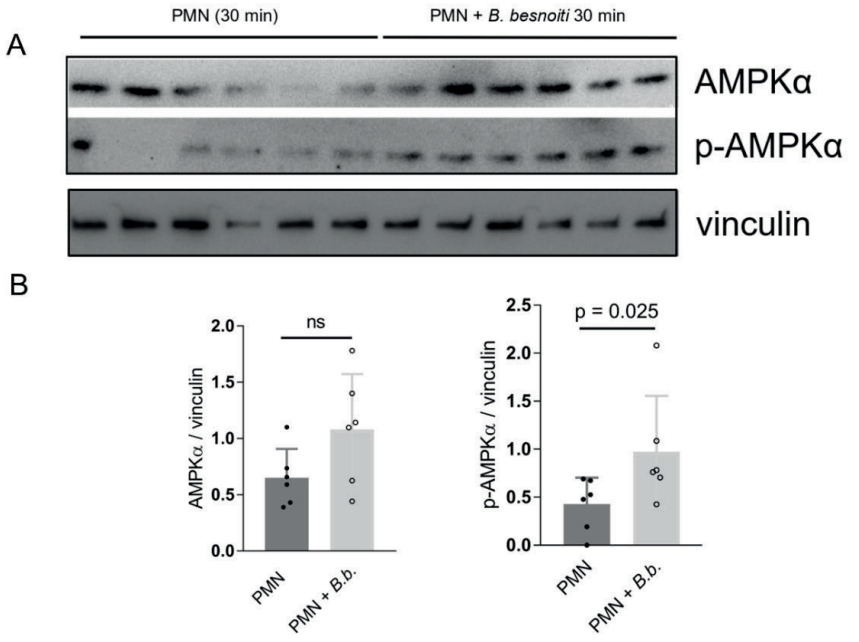

Figure 15. ***B. besnoiti*** **tachyzoite exposure induces AMPK phosphorylation in bovine PMN.** Bovine PMN were exposed to *B. besnoiti* tachyzoites at a 1:6 ratio. After 30 min of co-incubation, protein extracts were generated from PMN and tested for AMPK and p-AMPK expression by Western blotting. The expression of vinculin was used as an internal reference protein. (A) Western blot. (B) Densitometric analysis of protein bands for AMPK and p-AMPK. Bars in the graph represent mean ± SD. *p*-values were calculated by applying the Mann-Whitney test. ($n = 6$). [228].

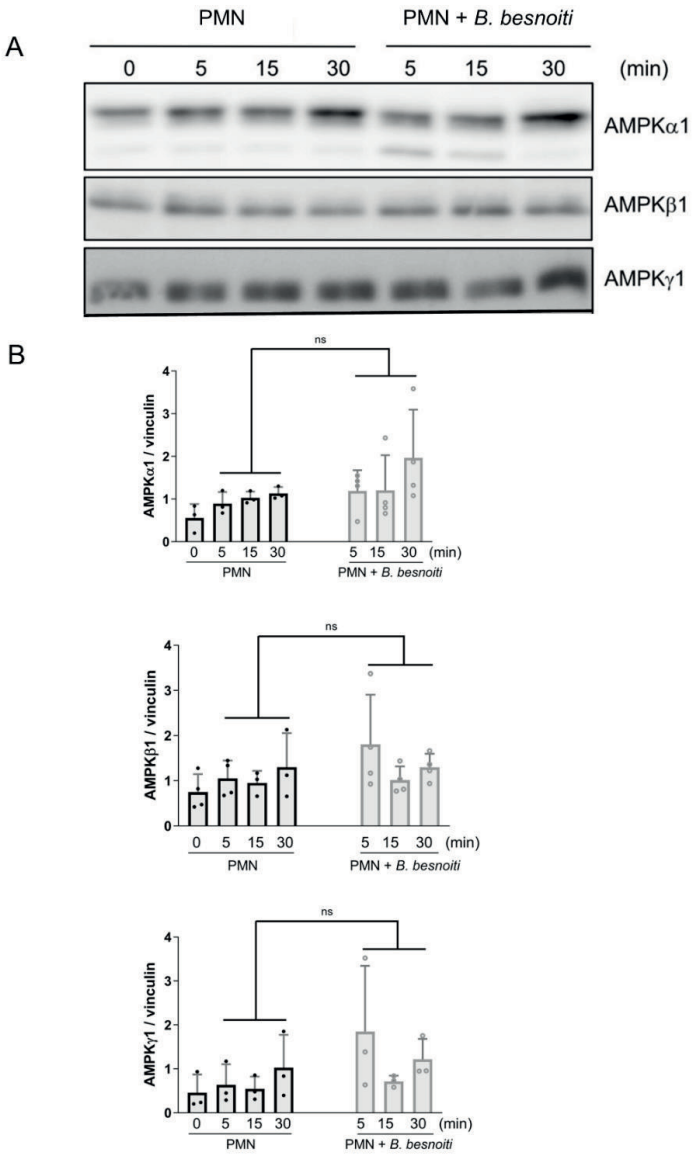

Figure 16. Analysis of the catalytic and regulatory subunits of AMPK in *B. besnoiti*-exposed bovine PMN. Bovine PMN were exposed to *B. besnoiti* tachyzoites at a 1:6 ratio. At 0–30 min of incubation, protein extracts were prepared from PMN and tested for AMPKα1, AMPKβ1, and AMPKγ1 expression by Western blotting. Vinculin was used as an internal reference protein. (A) Western blot. (B) Densitometric analysis of protein bands for AMPKα1, AMPKβ1, and AMPKγ1 at 0, 5, 15, and 30 min of PMN-tachyzoite coincubation. Bars in the graphs represent mean ± SD. *p*-values were calculated by unpaired, two-tailed *t*-tests, comparing control PMN vs. PMN incubated with *B. besnoiti* tachyzoites at each time point. ns means not significant. ($n = 4$). [228].

3.2.2 B. besnoiti tachyzoite exposure drives CAMKK upregulation and phosphorylation in PMN

Considering that AMPK activity is mainly regulated upstream by CAMKK (besides other regulators and signalling pathways), we evaluated the expression and phosphorylation status of CAMKK at 5, 15, and 30 min of PMN exposure to *B. besnoiti* tachyzoites (Fig. 17). Densitometric analysis of respective protein bands in Western blots (Fig. 17A) indicated that both non-phosphorylated (Fig. 17B) and phosphorylated (Fig. 17C) CAMKK were significantly upregulated in PMN immediately after tachyzoite encounter (from 5 min of exposure onwards; stimulated vs. control PMN at 5, 15, and 30 min: all $p < 0.05$), thereby indicating a highly sustained activation of CAMKK [228].

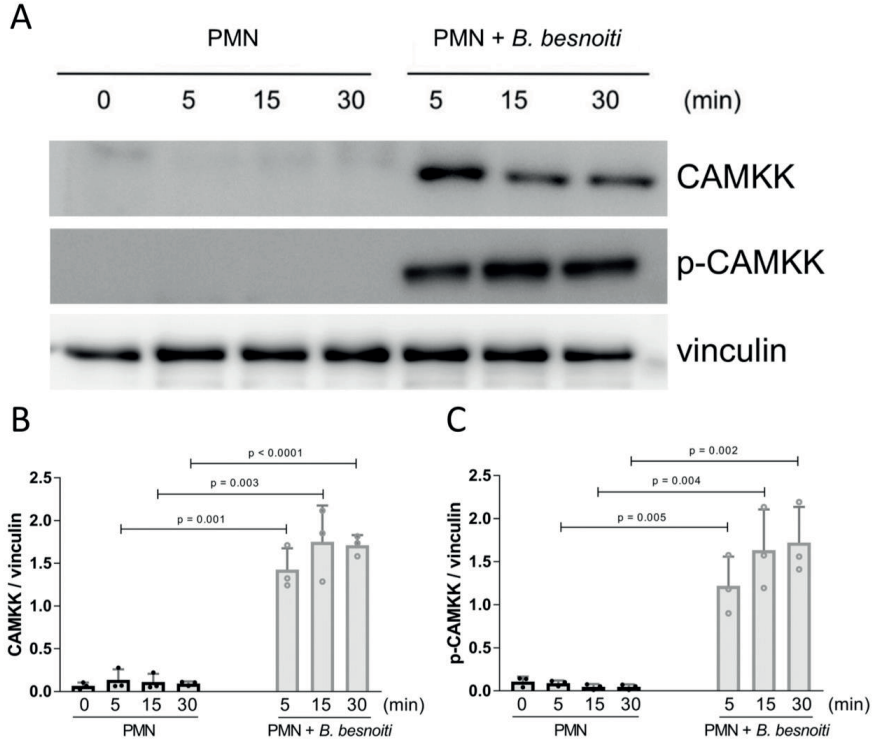

Figure 17. *B. besnoiti* tachyzoite exposure induces CAMKK expression and phosphorylation in bovine PMN. Bovine PMN were exposed to *B. besnoiti* tachyzoites at a 1:6 ratio. At 0-30 min of co-culture, protein extracts were generated from PMN and tested for CAMKK and p-CAMKK expression by Western blotting. The expression of vinculin was used as an internal reference protein. (A) Exemplary Western blot. (B-C) Densitometric analysis of protein bands for CAMKK (B) and p-CAMKK (C) at 0, 5, 15, and 30 min of PMN-tachyzoite co-culture. Bars in the graph represent mean ± SD. *p*-values were calculated by unpaired, two-tailed *t*-tests, comparing control PMN vs. PMN incubated with *B. besnoiti* tachyzoites at each time point. ($n = 3$). [228].

3.2.3 PMN exposure to T. gondii tachyzoites induces a rise in neutrophil intracellular calcium concentration in addition to AMPK and CAMKK phosphorylation

When the same experimental approach (see 3.2.2) was applied to *T. gondii*-exposed PMN, the overall responses mirrored those observed with *B. besnoiti*. After confrontation of PMN with *T. gondii*, a rapid increase in neutrophil intracellular calcium concentration $[Ca^{2+}]_i$ was observed, being represented by fluorescence changes after 5 min of co-incubation (Fig. 18A). On a statistical level, this reaction proved significant when compared to negative controls (Fig. 18A). As expected, stimulation of bovine PMN with the calcium ionophore A23187 (5 µM) caused a stronger and sustained increase in $[Ca^{2+}]_i$ (Fig. 18A), thereby proving as reliable positive control in the bovine system. Based on previous *B. besnoiti*-based data, CAMKK/AMPK phosphorylation was studied at 30 min of PMN-parasite-interaction in *T. gondii*-exposed PMN (Fig. 18B). A high variability between the biological replicates was observed. The overall effect of parasite exposure was that pAMPKα, but not total AMPKα, revealed a significantly enhanced expression after 30 min of co-culture (Fig. 18C). When we also evaluated the expression and phosphorylation status of CAMKK at 30 min of PMN exposure to *T. gondii* (Fig. 18B), densitometric analysis of respective protein bands in WB (Fig. 18D) indicated that both phosphorylated and non-phosphorylated CAMKK was upregulated in *T. gondii*-confronted PMN at 30 min of co-incubation, thereby again indicating a sustained activation of CAMKK [230].

3.2.4 ULK1 expression is upregulated in B. besnoiti tachyzoite-exposed PMN

Since PMN exposure to *B. besnoiti* tachyzoites induced LC3B-II expression in bovine PMN [62] and both parasites induced and increased p-AMPK levels in PMN after 30 min confrontation, we also studied early autophagic processes induced by tachyzoite encounter in more detail (Fig. 19). Therefore, early expression profiles of the autophagy-related molecules Beclin-1, p-Beclin-1, and ULK1 were analysed at 5, 15, and 30 min in *B. besnoiti*- and *T. gondii*-exposed PMN (Fig. 19A). Overall, only PMN confronted with *B. besnoiti* showed a selective upregulation of ULK-1 levels after 30 min of co-incubation (Fig. 19B; ULK-1 on *B. besnoiti*-exposed PMN vs. non-exposed controls: $p = 0.05$), thereby indicating that parasite exposure indeed induces autophagosome biogenesis in bovine PMN [228]. In line, the early expression profiles for ULK-1 equally showed the same trend of upregulation after 30 min of co-incubation in case of *T. gondii*-exposed PMN, however, this trend failed to reach statistical significance (Fig. 19B) [230].

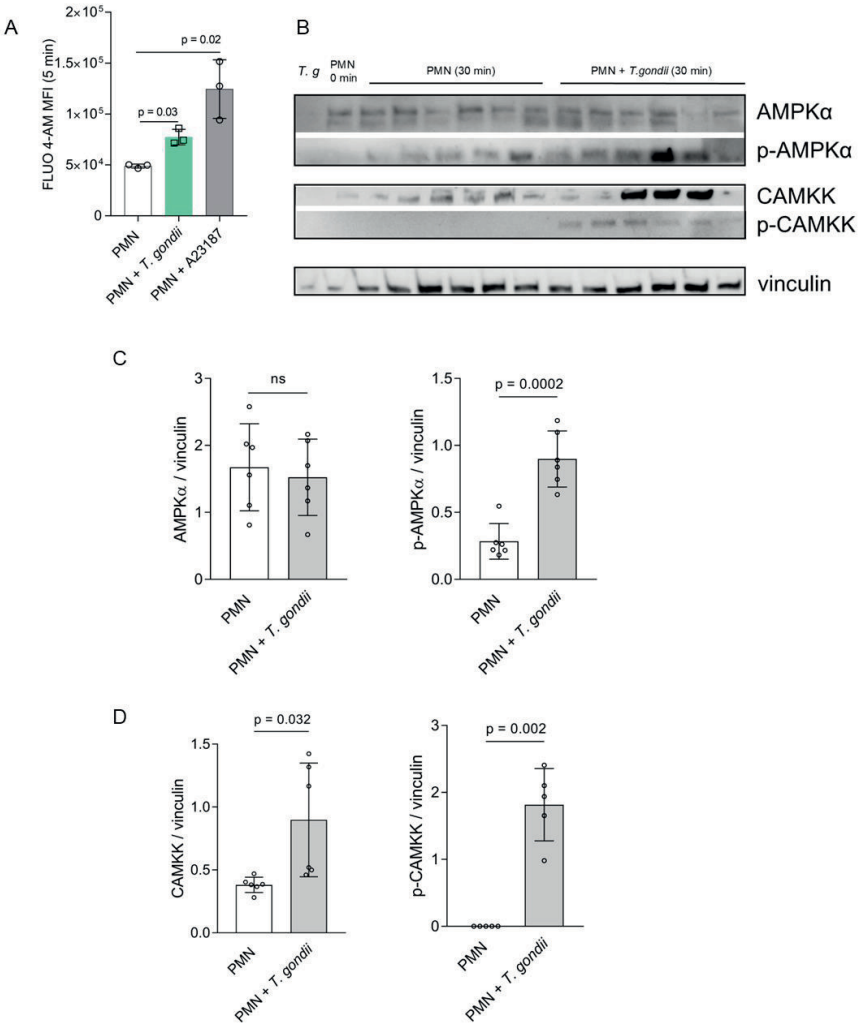

Figure 18. *T. gondii* tachyzoite exposure induces cytoplasmic calcium increase, AMPK and CAMKK phosphorylation in bovine PMN. Fluo-4 AM-loaded bovine PMN (A) (n = 3) were confronted with *T. gondii* or stimulated with the calcium ionophore A23187 for positive control. Fluo 4-AM derived fluorescence was measured by a flow cytometer and the mean of the fluorescence intensity after 5 min of co-incubation was represented as bar graph (A). Bovine PMN isolated from peripheral blood of 6 different animals (n = 6) were exposed to *T. gondii* at 1:4 PMN: *T. gondii* ratio. After 30 min of coincubation, protein extracts were generated from PMN and tested for AMPKα, p-AMPKα, CAMKK and p-CAMKK expression by Western blotting. The expression of vinculin was used as internal reference protein. (B) Representative Western blot and (C) densitometric analysis of protein bands for AMPK, p-AMPK. (D) Densitometric analysis for CAMKK and p-CAMKK. Bars in the graph represent the mean ± SD. p values were calculated by applying a Mann–Whitney test [230].

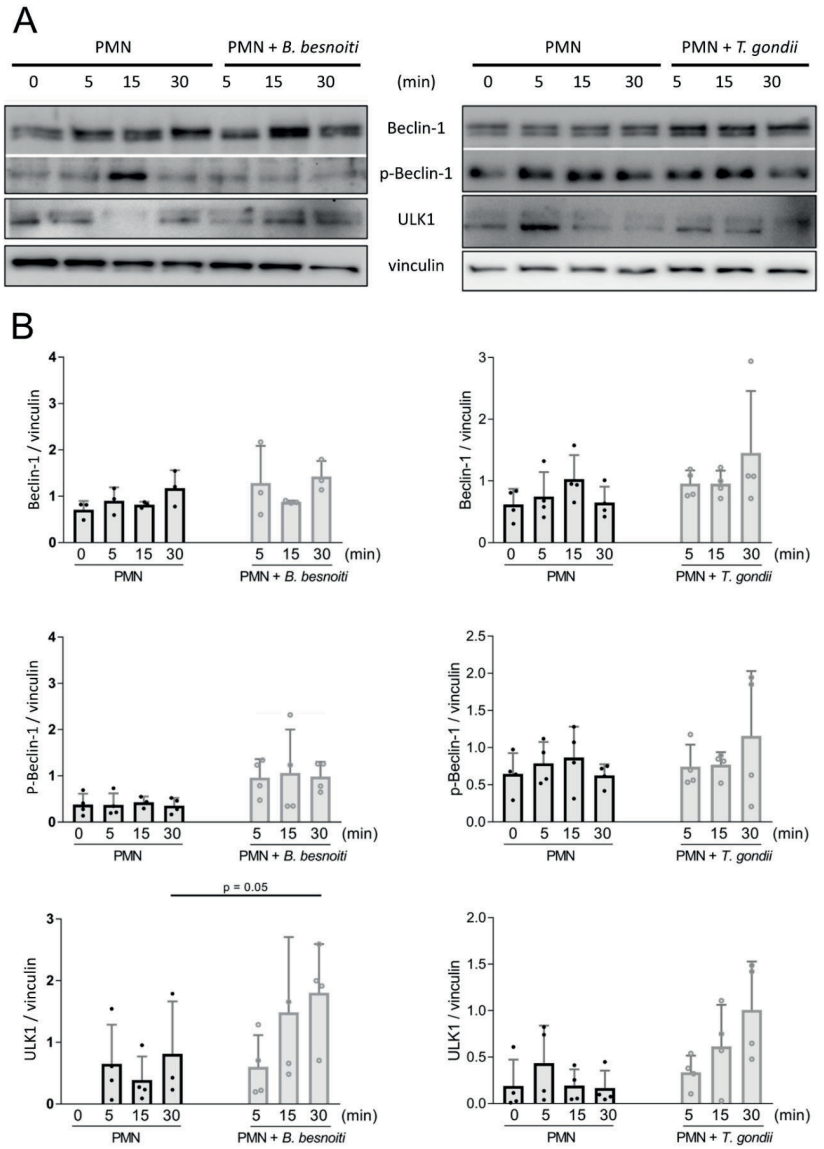

Figure 19. ***B. besnoiti*** **tachyzoite exposure induces ULK-1 expression in bovine PMN.** Bovine PMN were exposed to *B. besnoiti* or *T. gondii* tachyzoites at a 1:6 or 1:4 ratio respectively. After 0–30 min of incubation, protein extracts were generated from PMN and tested for Beclin-1, p-Beclin-1, and ULK1 expression by Western blotting. The expression of vinculin was used as an internal reference protein. (A) Western blot. (B) Densitometric analysis of protein bands for Beclin-1, p-Beclin-1, and ULK1 at 0, 5, 15, and 30 min of PMN–tachyzoite incubation. Bars in the graph represent mean ± SD. *p*-values were calculated by unpaired, two-tailed *t*-tests, comparing control PMN vs. PMN incubated with *B. besnoiti* tachyzoites at each time point. ns means not significant. ($n = 3$) [228,230].

3.2.5 AICAR treatments trigger AMPK phosphorylation in bovine PMN

So far, no data were available on the metabolic efficacy of pharmacological AMPK activators (e.g., AICAR) or inhibitors (e.g., compound C; CC) in the bovine system. Therefore, based on published compound concentrations, we first tested the principal effects of 1 mM AICAR and 10 µM CC treatments on AMPK phosphorylation in bovine PMN (Fig. 20). As expected, AICAR treatments induced AMPK phosphorylation in bovine PMN (Fig. 20A, B; treated vs. control PMN: $p = 0.05$). Moreover, 10 µM CC treatments significantly reduced both AMPKα and p-AMPKα expression in bovine PMN (Fig. 20C, D; treated vs. control PMN: $p = 0.03$). At the neutrophil functional level, AICAR treatments significantly affected neutrophil effector mechanisms by upregulating NET formation at 4 h of treatment (Fig. 20E, F), thereby once more underlining the key role of AMPK phosphorylation for effective NET formation. Moreover, CC treatments - leading to downregulation of AMPK phosphorylation - failed to affect NET formation. Importantly, neither AICAR nor CC treatments significantly affected PMN viability since the proportion of PMN experiencing apoptosis or necrosis was not changed by these treatments (Fig. 20G) [228].

3.2.6 AICAR treatments induce metabolic responses in bovine PMN but do not synergize with B. besnoiti-induced OCR and ECAR

Considering that AMPK regulates the energetic status of a cell by sensing intracellular AMP concentrations and by adapting ATP synthesis in response to current cellular needs, we furthermore evaluated the effects of AICAR treatments on oxygen consumption rates (OCR; Fig. 21A, B). OCR reflects neutrophil oxidative responses due to oxidative burst activity by assessing NADPH oxidase-related oxygen consumption, but also mirrors respiratory mitochondrial activity. Besides OCR, extracellular acidification rates (ECAR) were evaluated in AICAR-treated bovine PMN (Fig. 21C, D). In general, ECAR levels are increased when cells shift to a glycolytic state, based on the production and release of lactate as a product of glycolysis. Current analyses revealed that plain AICAR treatments induced a significant rise in both OCR and ECAR in bovine PMN (Fig. 21B, D, see the timeframe of 24–53 min). However, AICAR treatments failed to alter *B. besnoiti* tachyzoite-driven metabolic PMN responses (Fig. 21A, C, white circles) and instead maintained the metabolic active status of PMN. The effect of AICAR alone on bovine PMN was analysed after AICAR injection but before *B. besnoiti* tachyzoite supplementation (Fig. 21B, D). The AUC analyses showed that

OCR (treated vs. untreated PMN: $p = 0.0099$) and ECAR (treated vs. untreated PMN: $p = 0.0197$) were significantly increased in AICAR-treated bovine PMN [228].

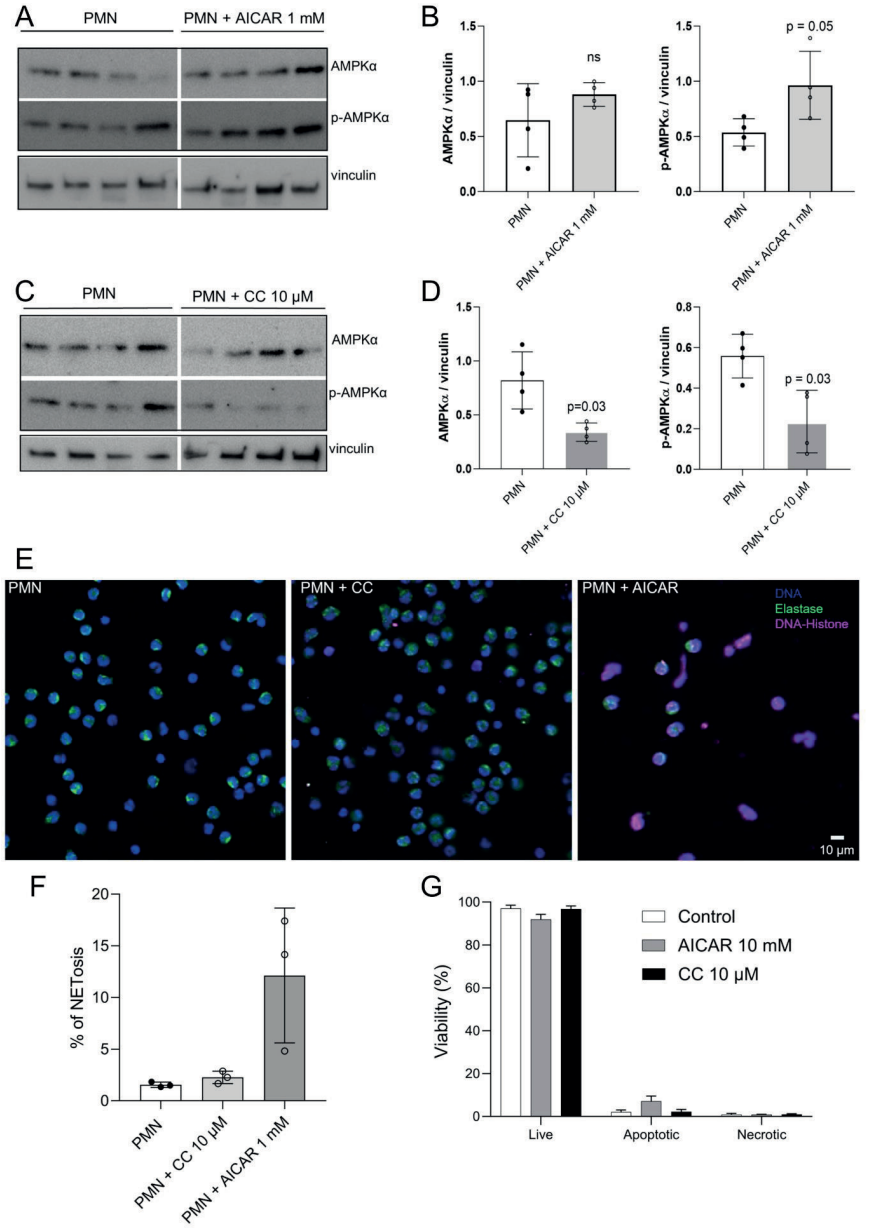

Figure 20. AICAR treatments drive AMPK phosphorylation and NET formation in bovine PMN. (A–D) Bovine PMN were treated with AICAR (10 mM) or CC (10 µM) for 30 min. Thereafter, protein extracts were generated from PMN and tested for AMPKα and p-AMPKα expression by Western blotting. The expression of vinculin was used as an internal reference protein. (A, C) Western blot of AICAR-treated (A) or CC-treated (C) PMN. (B, D) Densitometric analysis of protein bands for AMPKα and p-AMPKα at 30 min of AICAR (B) or CC (D) treatments. Bars in the graph represents mean ± SD. *p*-values were calculated by applying the Mann–Whitney test. (E, F) Immunofluorescence images showing DNA (DAPI, blue), neutrophil elastase (NE, green), and DNA-histone complexes (magenta) in AICAR-treated bovine PMN (E). The percentage of NET-releasing PMN was calculated by a semi-automatic quantification method via image analysis (Image J, Fiji version) and is represented as a bar graph, showing mean ± SD (F). Viability of AICAR- and CC-treated bovine PMN, as evaluated by flow cytometry based on Annexin-V and propidium-iodide-positive staining. The percentages of live, apoptotic, and necrotic PMN are presented in the bar graphs (G). Bars in the graph represent mean ± SD. (n = 4). [228].

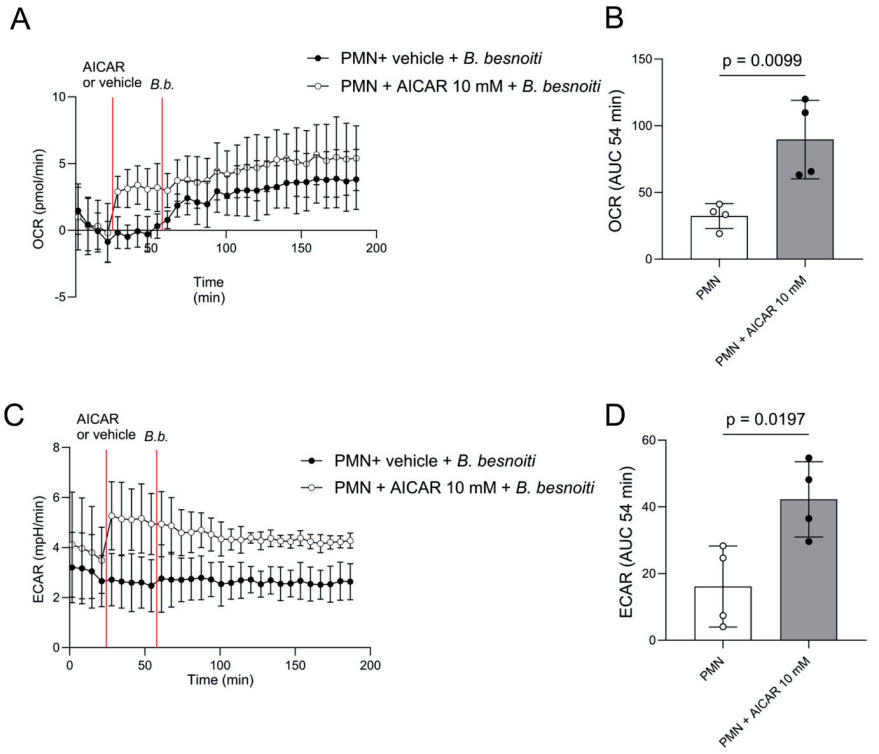

Figure 21. AICAR treatments induce oxygen consumption (OCR) and extracellular acidification (ECAR) rates in bovine PMN. Bovine PMN were pretreated with AICAR or vehicle and then exposed to *B. besnoiti* tachyzoites at a 1:6 ratio at 54 min. The effects of 10 mM AICAR treatments on tachyzoite-induced PMN responses were evaluated by Seahorse technology. AICAR treatments (white circles registry) induced both OCR (A, B) and ECAR (C, D), but failed to change *B. besnoiti*-induced OCR (B, D). The AUC of the registries after the baseline and before *B. besnoiti* tachyzoite supplementation was calculated to evaluate the effect of AICAR alone on OCR and ECAR. The bars represent mean ± SD. *p*-values were calculated by the Mann-Whitney test. (n = 4). [228].

3.2.7 Pharmacological AMPK activation enhances B. besnoiti and T. gondii tachyzoite-induced NET formation

To further confirm the role of AMPK in the process of early NET formation, we assessed additive effect of AICAR pre-treatments on *B. besnoiti* and *T. gondii* tachyzoite-driven NET formation (Fig. 22A, C und B, D, respectively). Therefore, bovine PMN were either exposed to tachyzoites or additionally treated with AICAR. NET formation was evaluated by immunofluorescence and posterior image analyses using a semi-automatic method for NET quantification (Fig. 22C, D) [234]. Current data showed that AICAR treatments had additive effects on tachyzoite-induced NETosis since NET formation was significantly enhanced by additional AICAR supplementation when compared to tachyzoite exposure alone (Fig. 22C, D) and to non-exposed bovine PMN [228,230].

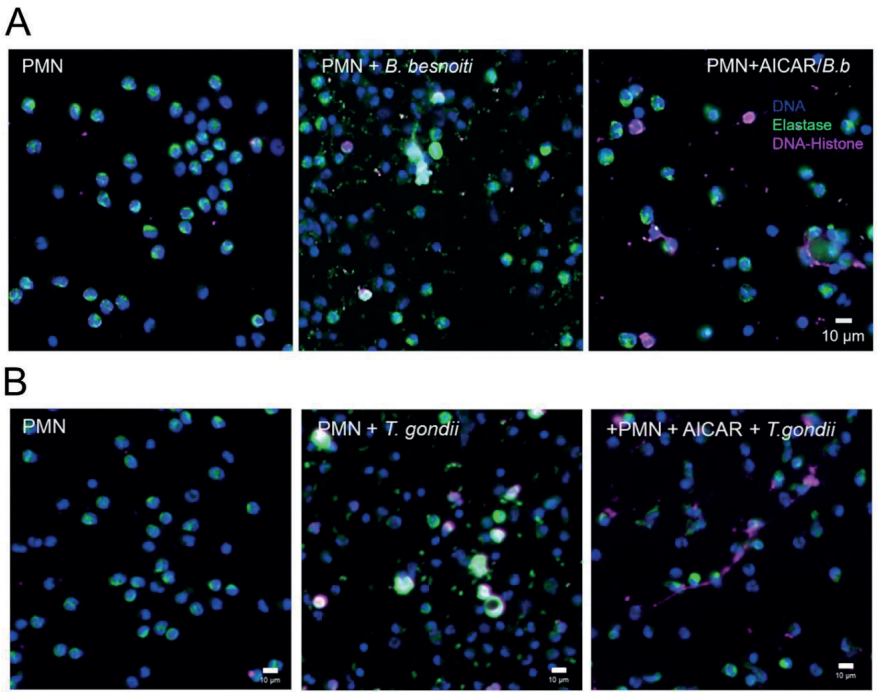

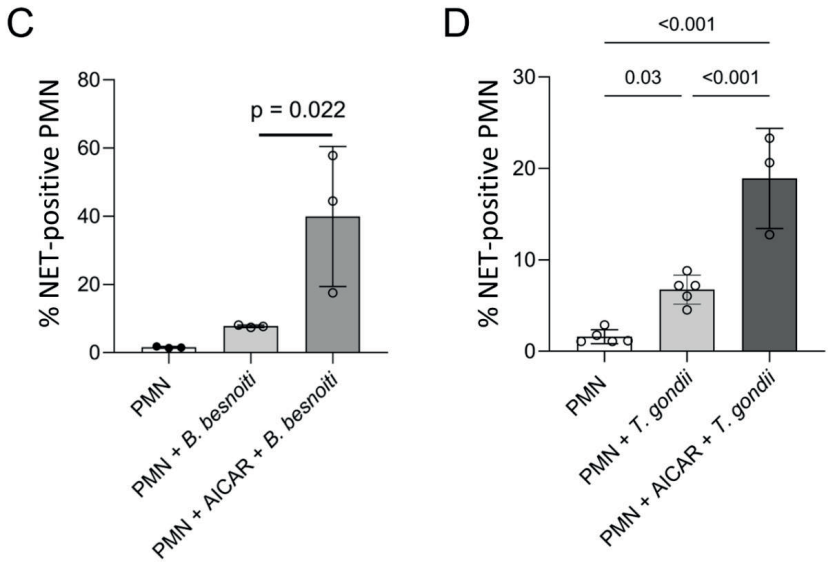

Figure 22. AICAR treatments enhance *B. besnoiti* and *T. gondii* tachyzoite-induced NET formation. Here, 2.5×10^5 bovine PMN were pretreated with 1 mM of AICAR or plain medium for 30 min before exposure for 4 h to *B. besnoiti* or *T. gondii* tachyzoites. (A, B) Fixed samples were immunostained for NE (green) and DNA-histone complex (magenta). DNA was stained with DAPI. (C, D) The percentage of NET-releasing cells was determined by a semi-automatic quantification method via image analysis (Image J, Fiji version). Bars in the graph represent mean ± SD. *p*-values were calculated by applying the Kruskal-Wallis test. ($n = 3$) [228,230].

3.2.8 T. gondii tachyzoite-induced DNA release depends on MAPK- and SOCE-related pathways

To further expand and complement the results on the relevance of the AMPK pathway in *T. gondii*-exposed PMN, we also evaluated the effects of chemical inhibitors targeting related signaling pathways (Fig. 23). UO126, an inhibitor of MEK1/2 in the MAPK pathway, blocks the downstream phosphorylation and activation of ERK1/2. LY294002, a PI3K inhibitor, inhibits akt activation. 2-Aminoethoxydiphenyl borate (2-APB), an inhibitor of store-operated calcium entry (SOCE), acts on IP3 receptor and blocks calcium channels in the plasma membrane that are essential for Ca^{2+} influx after ER store depletion. Current data confirmed that *T. gondii* exposure indeed induces DNA release from bovine PMN and that this DNA release is dependent on both, the MAPK pathway and SOCE (Fig. 23). Moreover, we confirmed DNA as the main component of *T. gondii*-induced NETs by DNAse I treatments, which significantly diminished extracellular DNA levels (Fig. 23; PMN + *T. gondii* vs PMN + *T. gondii* + DNAse I) [230].

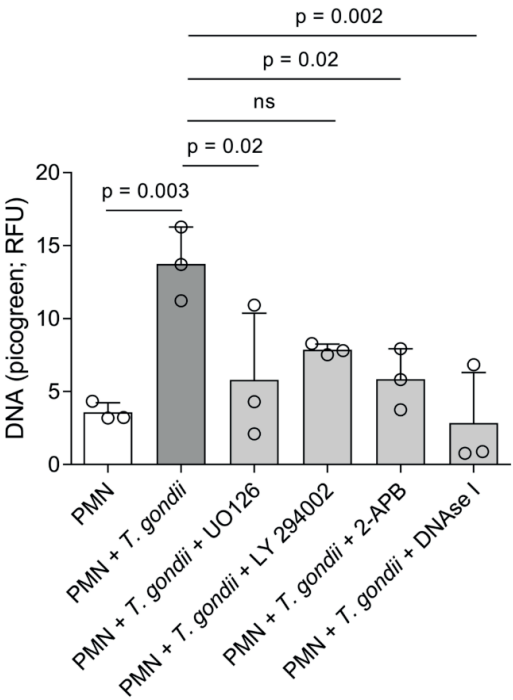

Figure 23. ***Toxoplasma gondii*****-induced DNA release in bovine PMN depends on ERK- and SOCE-related signaling pathways.** Bovine PMN (n = 3) were pre-treated for 30 min with UO126 (50 μM), LY294002 (1 μM) or 2-APB (50 μM) before the addition of *T. gondii* stages (1:4 PMN: tachyzoites ratio). After 4 h of co-incubation, the Picogreen-derived fluorescence, corresponding to extracellular DNA amount, was determined in a plate reader. DNAse I (90 U) was added after the 4 h of incubation in the corresponding experiments to confirm the DNA nature of the emitted fluorescence. Bars represent the mean ± SD. p-values were calculated by applying an ANOVA test followed by a Dunnet multiple comparison test [230].

3.3 Chapter 3: PMN responses to EVs released by B. besnoiti tachyzoites and B. besnoiti-infected host cells

EVs are nano-sized membrane-bound structures released by various cell types and parasites, serving as mediators of intercellular communication. Reciprocal EV-driven interactions between PMN and endothelial cells promote PMN extravasation to infection sites, while EVs also influence PMN effector functions, including NET formation [141,185]. In addition, parasite-derived EVs can transfer virulence and resistance factors and modulate host immune responses, thereby contributing to immune evasion [141,183–186,194]. Therefore, the aim of this chapter was to determine effects of EVs of differential cell origin on both host cell and PMN functions. Related data have been published in Espinosa et al., 2024.

3.3.1 Isolation and characterization of EVs

EVs were isolated by size exclusion chromatography (SEC) from non-infected BUVEC, *B. besnoiti*-infected BUVEC, non-stimulated PMN, zymosan-stimulated PMN, tachyzoite-exposed PMN and *B. besnoiti* tachyzoites using qEV/70 nm Original (IZON) columns, which are optimized for both high recovery of EVs (70-1000 nm optimum recovery range) and low lipoprotein overlap. EV numbers and sizes from pooled fractions were assessed by Nano-Flow cytometry. EV-specific markers were detected by Western blotting and EV morphology was illustrated by TEM (Fig. 24). In all cases, EVs peaked in size around 60-80 nm (Fig. 24A). Overall, mean EV sizes of 73.47 ± 33 nm from control BUVEC, 77.82 ± 32.6 nm from *B. besnoiti*-infected BUVEC, 74.96 ± 18.52 nm from PMN, 72.84 ± 17.34 nm from *B. besnoiti*-confronted PMN, 75.58 ± 21.43 nm from zymosan-stimulated PMN, and 71.51 ± 22-91 nm from *B. besnoiti* tachyzoites were detected (Fig. 24B). Consequently, current particle sizes fitted well to literature data describing a general size of 30-120 nm for small EVs [241]. The mean concentration of particles per cell after 24 h incubation showed comparable EV secretion from BUVECs, regardless of infection (Fig. 24C). In contrast, EV secretion experienced a 3-fold increment when PMN were exposed for 4 hours to *B. besnoiti* tachyzoites in comparison to plain PMN or zymosan-stimulated PMN (Fig. 24D). Western blot analyses confirmed the EV nature of the particles since the samples proved positive for CD9 and showed weak signals for CD81 (besides vinculin as loading control), both representing typical EV markers (Fig. 24E). TEM analyses illustrated for the first time *B. besnoiti* tachyzoite-derived and *B. besnoiti*-infected BUVEC-derived EVs by confirming the typical EV morphology (Fig. 24F) [229].

3.3.2 Exposure of PMN to EVs from different cellular sources does not affect neutrophil oxidative and glycolytic responses

To explore if exposure of unprimed PMN to EVs of different cellular sources changed their energetic status and oxidative responses, we here analysed the neutrophil metabolic parameters of oxygen consumption (OCR) and extracellular acidification rates (ECAR) via Seahorse analytics (Fig. 25). Overall, encounter with EVs neither affected oxidative nor glycolytic responses of bovine PMN, irrespective of the EV source (Fig. 25) [229].

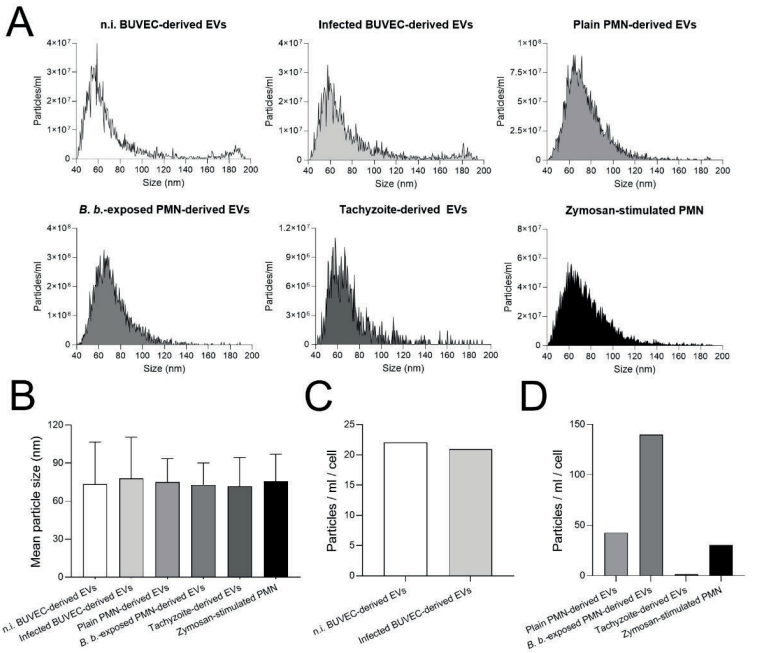
A
n.i. BUVEC-derived EVs
Infected BUVEC-derived EVs
Plain PMN-derived EVs
B. b.-exposed PMN-derived EVs
Tachyzoite-derived EVs
Zymosan-stimulated PMN
Particles/ml
Size (nm)
B
Mean particle size (nm)
C
Particles / ml / cell
D
Particles / ml / cell
n.i. BUVEC-derived EVs
Infected BUVEC-derived EVs
Plain PMN-derived EVs
B. b.-exposed PMN-derived EVs
Tachyzoite-derived EVs
Zymosan-stimulated PMN

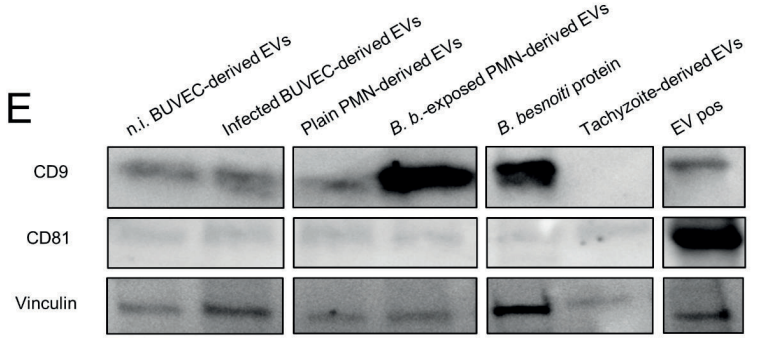
E
n.i. BUVEC-derived EVs
Infected BUVEC-derived EVs
Plain PMN-derived EVs
B. b.-exposed PMN-derived EVs
B. besnoiti protein
Tachyzoite-derived EVs
EV pos
CD9
CD81
Vinculin

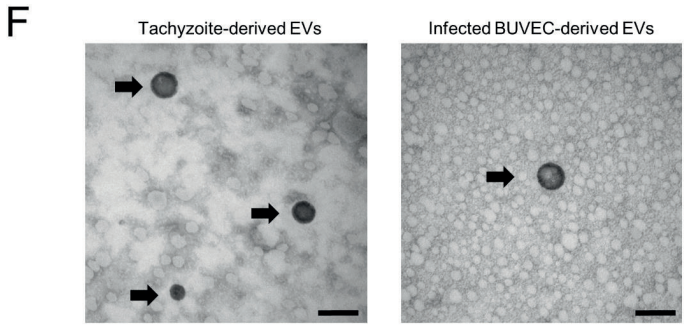
F
Tachyzoite-derived EVs
Infected BUVEC-derived EVs

Figure 24. Characterization of BUVEC-, PMN- and *B. besnoiti* tachyzoite-derived EVs. Extracellular vesicles (EVs) were isolated from non-infected BUVEC (n.i. BUVEC), *B. besnoiti*-infected BUVEC (Infected BUVEC), non-exposed PMN (Plain PMN), *B. besnoiti* tachyzoite-exposed PMN (*B. b.*-exposed PMN) and from plain *B. besnoiti* tachyzoites (Tachyzoite). (A) Exemplary histograms on EV size distribution, (B) particle concentration and (C, D) particle release per cell as assessed by Nano-Flow cytometry. Zymosan-stimulated PMN served as positive control for PMN-derived EV production. Mean particle diameters of EVs showed values around 70 nm. (E) Western blot analysis of BUVEC-, PMN- and *B. besnoiti* tachyzoite-derived EV samples probed with anti-CD9, anti-CD81 and anti-vinculin antibodies. Commercially available human EV-derived proteins (EV pos) and *B. besnoiti* protein extract were used as controls. (F) *B. besnoiti* tachyzoite-derived and infected BUVEC-derived EVs were studied by TEM (black arrows) and showed a typical EV morphology (scale bars indicate 100 nm) [229].

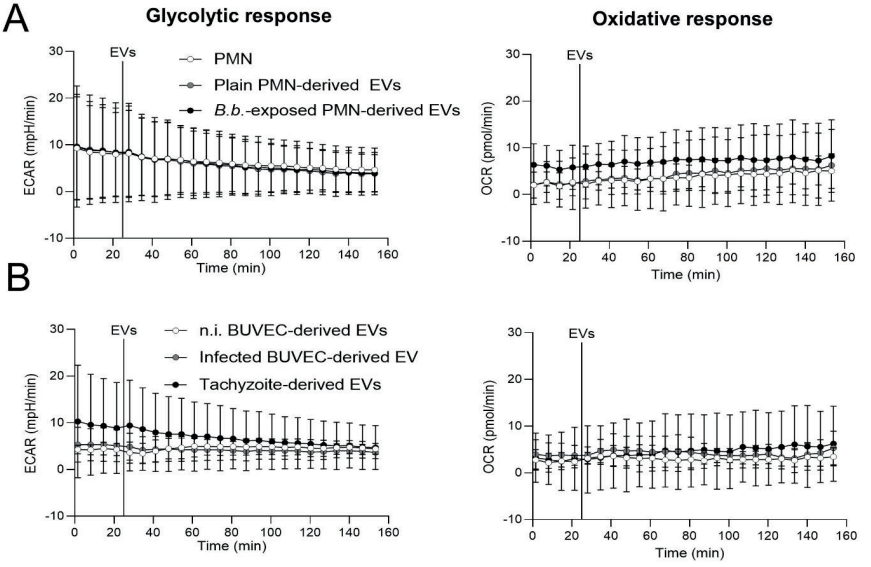

Figure 25. Exposure to EVs does not affect oxidative and glycolytic responses in bovine PMN. In absence of CO_2, PMN were incubated in XF RPMI media for 45 min. Four basal measurements were performed and then PMN-derived EVs (A) or BUVEC-derived EVs (B) were supplemented to bovine PMN at the time point indicated by a vertical line. OCR and ECAR values were obtained by Seahorse technology and plotted over time (n = 3 for each condition). All data are shown as mean ± SD [229]

3.3.3 Exposure of PMN to BUVEC- and B. besnoiti tachyzoite-derived EVs induce extracellular DNA release in a ROS-independent manner

To address if EV exposure has an impact on neutrophil effector mechanisms, we here first focused on NET formation. Bovine PMN were exposed to EVs derived from non-infected BUVEC, *B. besnoiti*-infected BUVEC, non-stimulated PMN, tachyzoite-exposed PMN and *B. besnoiti* tachyzoites (Fig. 26). Extracellular DNA quantification based on picogreen-derived fluorescence intensities was performed at 4 hours of incubation, thereby rather reflecting a late phase of NET formation. Relative DNA level analysis showed a significant increase of extracellular DNA release only for PMN stimulated with EVs derived from BUVEC ($p < 0.001$) and from *B. besnoiti* tachyzoites ($p < 0.05$) when compared to medium controls (Fig. 26A). In the former case, EV-driven NET formation revealed independent of the infection status of BUVEC since EVs from non-infected and *B. besnoiti*-infected BUVEC equally induced NET formation. In contrast, PMN-derived EVs failed to induce extracellular DNA release, irrespective of PMN stimulation (Fig. 26A). Therefore, we focused further experimentation on BUVEC- and *B. besnoiti* tachyzoite-derived EVs. To confirm typical characteristics of NET formation, classical NET markers (NE and histone-DNA) were visualized by immunostaining (Fig. 26B), applying a semi-automated image analysis for NET quantification (Fig. 26C). Here, the presence of extracellular DNA concomitant with histones and NE was confirmed for NET structures from PMN stimulated with BUVEC- and tachyzoite-derived EVs at 4 h (Fig. 26B). Further analysis revealed an increase in the percentage of PMN extruding NETs in case of tachyzoite-derived EVs (11.41 ± 4.38%), *B. besnoiti*-infected BUVEC-derived EVs (18.8 ± 5.62%), non-infected BUVEC-derived EVs (11.49 ± 5.16%), and *B. besnoiti* tachyzoite-derived EVs (12.68 ± 5.14%) in comparison with controls (6.48 ± 0.98%) (Fig. 26C). To study, if extracellular DNA release coincided with neutrophil ROS production, total ROS production was measured in PMN stimulated with BUVEC- and tachyzoite-derived EVs (Fig. 26D, E). However, current data revealed that EVs from all tested sources failed to affect PMN-derived total ROS production (Fig. 26E). In contrast, stimulation of PMN with zymosan, serving as positive control for ROS synthesis, indeed triggered significant ROS production [229].

3.3.4 PMN take up EVs from different cellular sources

To study PMN-EV-interactions on the level of EV internalization, bovine PMN were co-cultured for 6 hours with far red-labelled EVs derived from non-infected BUVEC, *B. besnoiti*-infected BUVEC and *B. besnoiti* tachyzoite (Fig. 27). PMN-mediated EV uptake was assessed by confocal microscopy (Fig. 27A) illustrating a rather globular staining within the PMN cytoplasm, most likely reflecting an endosomal localization of internalized EVs, as also described in literature [242] (Fig. 27B). Semi-automated microscopic quantification revealed a significant increase in PMN-derived far red signals upon EV encounter (Fig. 27C). Thus, almost equal fractions of PMN with far red signals were detected in case of EVs from tachyzoites (7.43 ± 1.01%, $p = 0.0011$), *B. besnoiti*-infected BUVEC (7.58 ± 1.18%, $p = 0.0009$) and non-infected BUVEC (6.70 ± 2.17%, $p = 0.0026$) (Fig. 27C) [229].

3.3.5 EV exposure to PMN selectively induces the release of IL-1β and IL-6 but not of CXCL8

Since EVs are well-documented for their role in intercellular communication, we here explored their capacity to induce inflammatory responses in PMN and BUVEC by assessing the release of IL-1β, IL-6 and CXCL8. These pro-inflammatory molecules were quantified via commercially available ELISAs in supernatants from both PMN and BUVEC being exposed to EVs from BUVEC and *B. besnoiti* tachyzoites (Fig. 28). At 4 and 24 hours of exposure for PMN and BUVEC, respectively, only trace amounts of IL-1β, IL-6 and CXCL8 were detected in supernatants of PMN (Fig. 28A, C, D) and BUVEC (Fig. 28B, D, F). Nevertheless, neutrophil-derived IL-1β and IL-6 release was significantly increased after PMN exposure to EVs derived from *B. besnoiti*-infected BUVEC ($p = <0.0001$ and $p = <0.0001$, respectively, Fig. 28C, E). In contrast, EVs failed to induce CXCL8 secretion in PMN (Fig. 28A). BUVEC stimulation with EVs of different origin all failed to affect endothelial IL-1β, IL-6 and CXCL8 release (Fig. 28B, D, F). Interestingly, PMN showed differential cytokine secretion depending on the stimuli initially used for positive controls. Thus, LPS (1 µg/ml) induced an increase in IL-1β secretion whilst stimulation with PMA/ionomycin (100 nM/5 µM) enhanced IL-6 release. Furthermore, LPS (0.01 µg/ml) functioned as a positive stimulus for BUVEC by inducing an enhanced secretion of both IL-1β and IL-6 [229].

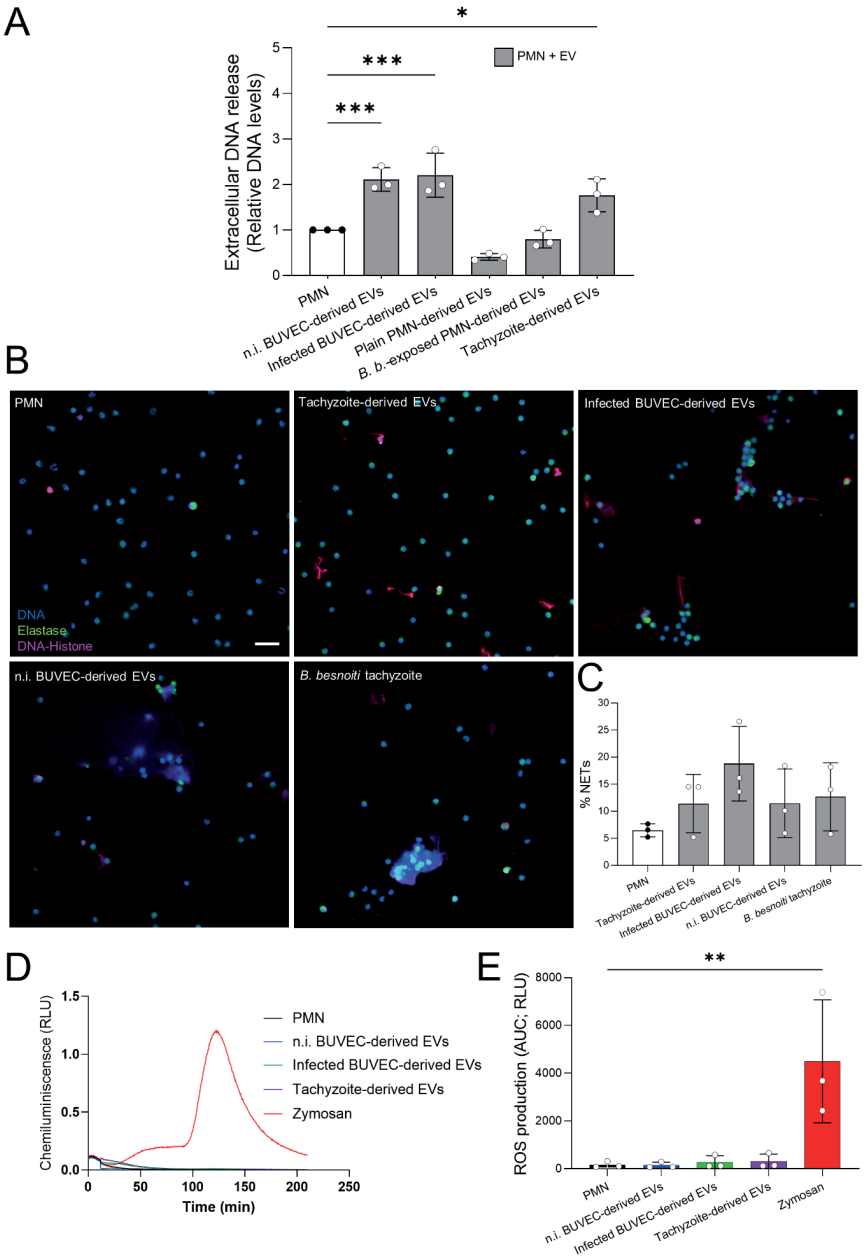

Figure 26. Exposure of bovine PMN to BUVEC- and *B. besnoiti* tachyzoite-derived EVs induced NET formation in a ROS-independent manner. (A) Bovine PMN were stimulated with EVs derived from non-infected BUVEC (n.i. BUVEC), *B. besnoiti*-infected BUVEC (Infected BUVEC), unstimulated PMN (Plain

PMN), *B. besnoiti* tachyzoite-exposed PMN (*B. b.*-exposed PMN) and from plain *B. besnoiti* tachyzoites (Tachyzoite) for 4 h After incubation, extracellular DNA was quantified via picogreen-derived fluorescence intensities. All data are shown as mean ± SD; *p*-values were calculated by one-way ANOVA followed by Dunnett´s multiple comparison test. *$p < 0.05$; **$p < 0.01$; ***$p < 0.001$. (B) Exemplary immunofluorescence images showing DNA (blue), NE (green) and DNA-histone complexes (magenta) in EVs-exposed PMN. (C) The percentage of NET-releasing PMN was calculated via image analysis (Image J, Fiji version); bars represent mean ± SD. (D, E). Representative kinetic and total ROS production of EV-exposed PMN, evaluated by luminol-based assays. Zymosan served as positive control. ($n = 3$). Scale bar = 30 µm [229].

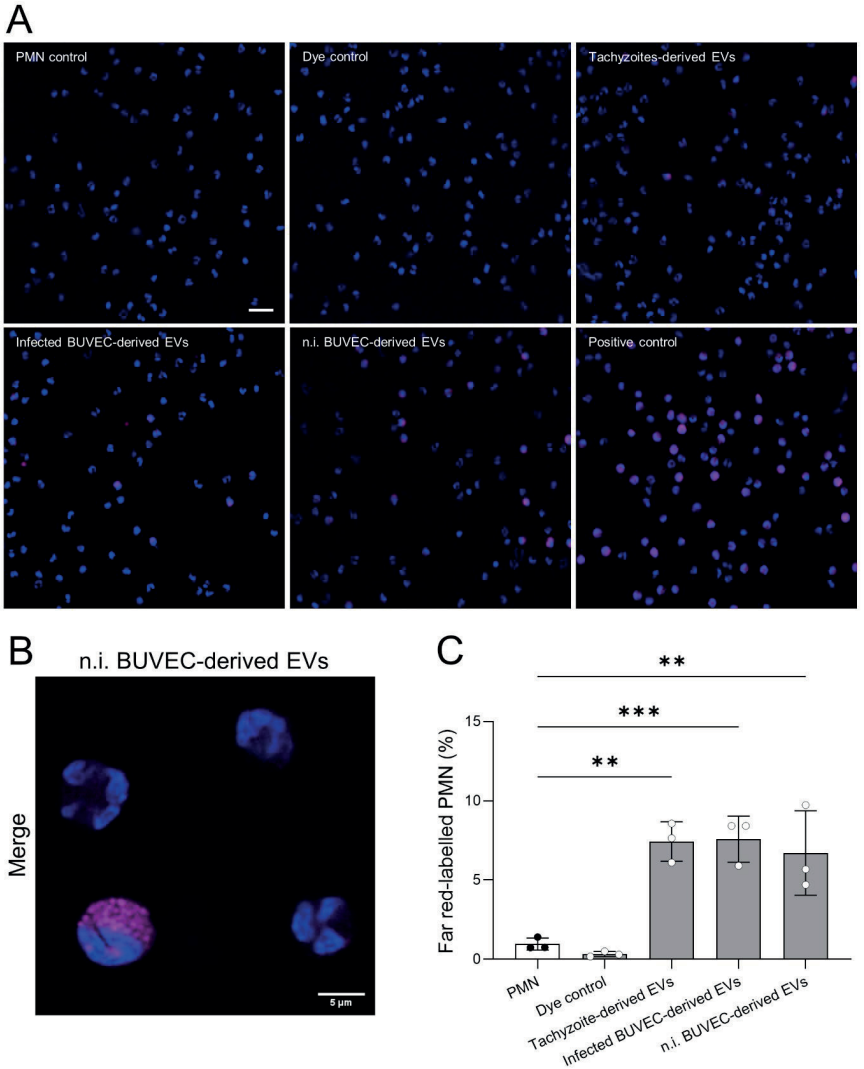

Figure 27. PMN-mediated uptake of far red-labeled EVs. Bovine PMN were exposed to far red-labelled EVs for 6 h, fixed and mounted with fluoromount G (DAPI). (A, B) Representative microscopic images depict PMN (nuclei, blue) with internalized EVs (magenta). (C) Semi-automated quantitative analysis of EV internalization showing that PMN equally internalized EVs from all cellular sources. All data are shown as mean ± SD; p-values

were calculated by one-way ANOVA followed by Dunnett´s multiple comparison test. **$p < 0.01$; ***$p < 0.001$. Scale bar in A = 20 µm. ($n = 3$) [229].

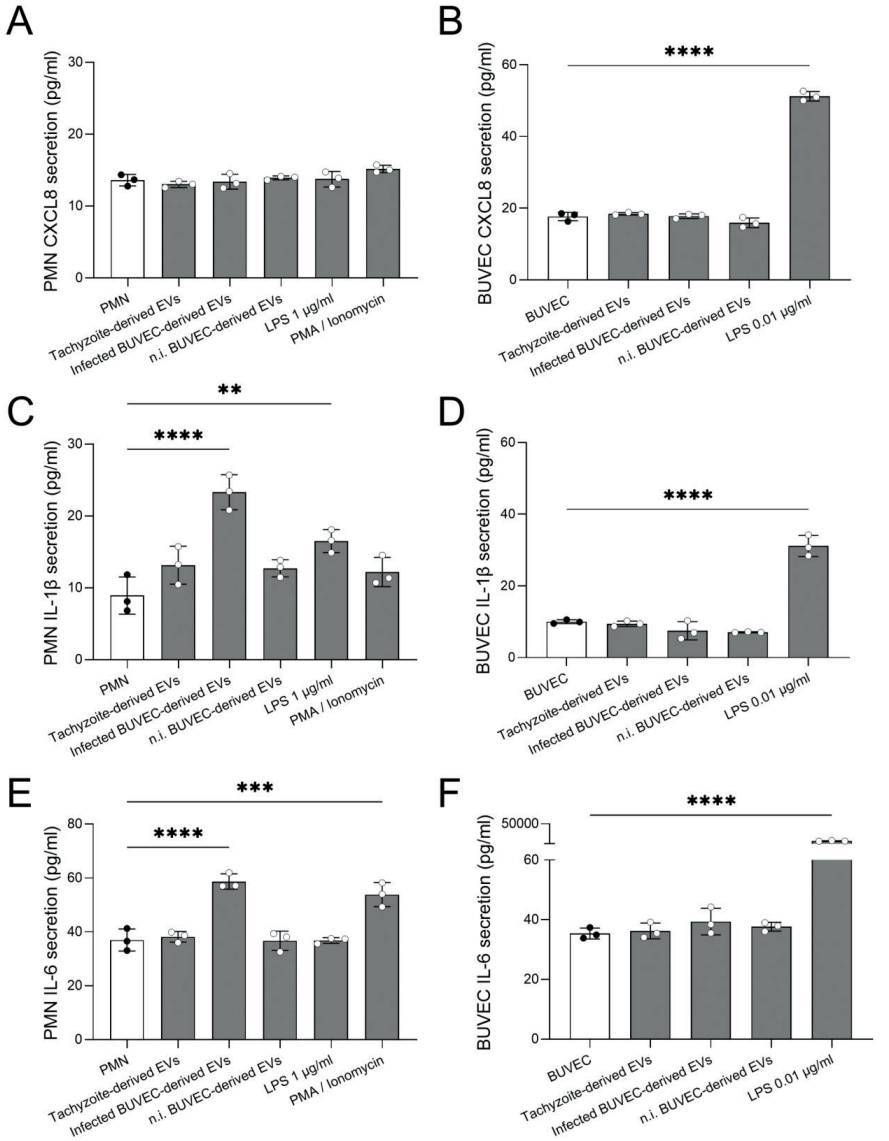

Figure 28. Selected EV exposure induced IL-1b and IL-6 release in bovine PMN. Bovine PMN or BUVEC were exposed to EVs from different cellular sources for 4 h (PMN) and 24 h (BUVEC). Thereafter, CXCL8 (A, B), IL-1b (C, D), and IL-6 (E, F) was quantified via commercially available ELISAs in co-culture-derived supernatants. Stimulation with LPS and PMA/ionomycin was used for positive controls. All data are shown as mean ± SD; p-values were calculated by one-way ANOVA followed by Dunnett´s multiple comparison test. (n = 3). **p < 0.01; *** p < 0.001; **** p < 0.0001 [229].

4. DISCUSSION

With the present study, novel data were added on the role of: i) ATP and purinergic receptor signaling [231], ii) CAMKK/AMPK signalling [228,230], and iii) EVs from differential cellular origin [229], in *B. besnoiti* (and *T. gondii*) tachyzoite-induced bovine PMN activation. Since the discovery of NETs in 2004 [129], there is accumulating evidence that NET formation represents a conserved mechanism among multiple kingdoms [243–245]. Referring to protozoan parasites, NET formation is induced by both extra- and intracellular parasites, such as *T. b. brucei*, *T. gondii, E. bovis, C. parvum, N. caninum*, and *B. besnoiti* [62,130,162,165,166,201,217,221,225,226,246–248].

Meanwhile, several aspects of *B. besnoiti*-driven NET formation have been elucidated: Hence, *B. besnoiti* tachyzoites induce bovine NET formation in a time- and dose-dependent manner; it is accompanied by increased NE and MPO activities in addition to enhanced ROS production [224]. In the case of vital tachyzoites, NETs did not kill these stages but impaired their capacity to infect endothelial host cells, an effect that was restored by DNAse treatment [224]. Notably, primary bovine monocytes also formed extracellular traps (METs) when exposed to *B. besnoiti* tachyzoites, thereby emphasizing the general capacity of these parasitic stages to induce this innate effector mechanism [249]. Moreover, under physiological flow conditions, PMN induced damage of *B. besnoiti*-infected endothelium, an effect which was attributed to NET formation and to the presence of histone 2A (H2A) as one of the main NET components [227]. Notably, *B. besnoiti*-infected endothelium induced NETs as well [62]. Furthermore, *B. besnoiti*-driven NET formation proved stage-independent since bradyzoites, recovered from skin cysts of infected animals, also induced NETs [225]. Moreover, metabolic requirements of *B. besnoiti*-induced NET formation were shown to mainly rely on pyruvate- and lactate-mediated catabolic pathways and ATP availability [226]. In addition, *B. besnoiti* tachyzoites induced both NET formation and LC3B-associated autophagosome formation in parallel, statistically being correlated with one another [62]. However, pharmacological intervention with rapamycin or wortmannin did not alter these responses, and isolated NETs did not trigger autophagy, indicating that these processes eventually occur independently [62]. The finding of early AMPKα phosphorylation upon tachyzoite exposure in bovine PMN further supports a parallel activation of autophagy and NET formation [62].

Since several molecular aspects of *B. besnoiti* tachyzoite-driven NET formation are still not entirely elucidated and due to the importance of *B. besnoiti* infection in cattle, we here intended

to fill some further gaps by adding new findings to the fundamental understanding of the parasite-driven NETotic process.

4.1 Chapter 1: B. besnoiti-induced PMN clustering and NET formation depend on P_2X_1 purinergic receptor signalling

PMN are considered as highly glycolytic cells and glycolysis is active when PMN produce ROS or perform phagocytosis [250,251]. Recently, both gluconeogenesis and glycogenesis were demonstrated as critical for the neutrophil lifespan and function, indicating a complex and context-dependent PMN catabolism to fulfill killing functions [252]. In general, PMN-derived oxidative responses (here: OCR) are mainly derived from NOX-based ROS production, with little or no mitochondrial contribution [253,254]. In the present study, the early activation of bovine PMN seemed to be related to ROS production without the involvement of glycolysis. Thus, PMN oxidative activity increased at 5-10 min post *B. besnoiti* tachyzoite exposure, as detected by a continuous increment of OCR values most likely reflecting PMN oxidative burst. This is in line with previous observations using DCFH-DA to measure *B. besnoiti* tachyzoite-induced ROS in PMN [224]. These data, even though measured by different techniques, confirmed a consistent role of ROS production, accompanied by oxygen consumption in parasite-induced NETosis as also driven by *T. gondii* [246], *E. bovis* [158], and trypomastigote stages of *T. b. brucei* [166]. Overall, *B. besnoiti* tachyzoite-induced oxygen consumption was not influenced by the addition of exogenous ATP or ATPγS, thereby denying a priming effect of ATP. Intriguingly, *B. besnoiti* tachyzoite-induced NET formation was recently proven as mitochondrial ATP synthase-dependent since it was significantly dampened by oligomycin treatments [226], thereby indicating a potential later relevance (i. e., after 30 min of confrontation) of the mitochondrial activity or mitochondrial ROS to sustain *B. besnoiti* tachyzoite-induced NET formation. Given that ECAR enhancement mirrors the extracellular accumulation of lactate [254], the current lack of tachyzoite-driven ECAR increment may indicate that immediate bovine PMN reactions to parasite stages may not rely on glycolytic responses. On the other hand, ATP/ATPγS supplementation led to an acute (within a few minutes) increase in neutrophil ECAR. However, when referring to later effector phases by analyzing NET formation after 6 h of co-culture, metabolic signatures of *B. besnoiti* heat-inactivated tachyzoite-exposed bovine PMN showed a significant increase in glucose and serine consumption and glutamate release in addition to a decrease in glutamine release during NET formation, thereby suggesting a switch in parasite-driven metabolic

responses towards glycolysis [226]. These differences may rely on the use of heat-inactivated tachyzoites, the presence of cytochalasin to block phagocytosis - likely altering PMN catabolism - and on the later time point compared to current data (40 min vs 6 h), highlighting the time- and context-dependent nature of PMN responses upon activation [252]. In line, recent findings on PMN-specific immunometabolism revealed that this innate "differentiated" cell type can indeed selectively induce different metabolic pathways after activation, depending on the effector mechanism to be performed (e.g., chemotaxis, ROS production, NET formation or degranulation) [255]. Overall, in the case of NET formation, there is a consensus that glycolysis seems to be the main neutrophil mechanism of energy generation. However, referring to *B. besnoiti* tachyzoite-driven NETosis, the blockage of glycolysis via FDG treatments did not directly affect NET formation [226]. Nevertheless, a key role of pyruvate- and lactate-mediated metabolic pathways for effective tachyzoite-driven NET formation was demonstrated since chemical inhibition of lactate release via oxamate and dichloroacetate and blockage of pyruvate dehydrogenase, α-ketoglutarate dehydrogenase, and transketolase via oxythiamine significantly dampened *B. besnoiti* tachyzoite-driven NET formation [226]. Comparable NET-related findings were reported for the closely related apicomplexan parasite *E. bovis*. Here, *E. bovis*-triggered NET formation was also not affected by FDG treatments, but by oxamate, oligomycin, and MCT inhibitors [158]. Altogether, these data may indicate a pivotal role of secondary metabolites of the carbohydrate catabolism rather than of glycolysis itself in apicomplexan parasite-induced NET formation at times later than 40 min of activation [158,226,231].

In general, ATP is either synthesized by mitochondrial respiration or by glycolysis. Importantly, ATP not only represents the key energy source but also actively participates in the activation of PMN effector functions via purinergic signaling. During differential pathological conditions like inflammation or ischemia, several cell types release cellular ATP as a danger and "find me" signal fueling inside-out signaling mechanisms that regulate the activation and function of PMN. Under physiological conditions, the released ATP boosts PMN effector functions like chemotaxis, degranulation, phagocytosis, and NET formation via autocrine feedback mechanisms which involve ATP and adenosine receptors [150,256]. These purinergic signaling mechanisms regulate calcium influx and additional downstream signaling pathways that are required for proper PMN functionality. Overall, a complex network of metabolic pathways regulates ATP release and purinergic signaling mechanisms. This network involves mitochondria which produce ATP fueling purinergic signaling in an autocrine or

paracrine manner. Thus, mitochondria represent the link between metabolic and calcium signaling events and the purinergic signaling mechanisms that regulate immune cell functions. In line, pre-treatments of bovine PMN with oligomycin (blocking mitochondrial ATP synthase) entirely abolished *B. besnoiti* tachyzoite-induced cell-free NET formation, thereby underlining the relevant role of mitochondrial ATP production and purinergic signaling for effective parasite-driven NET formation [226]. To study the paracrine effects of ATP, we here quantified both extracellular and total ATP concentrations in cultures of *B. besnoiti* tachyzoite-confronted PMN. In supernatants of unstimulated control PMN, an extracellular ATP concentration ([ATP]) of 37.3 nM and 22.6 nM was detected after 15 s and 15 min, respectively. Moreover, a total cellular [ATP] of 334.2 nM (334 fmol/cell) was measured in untreated bovine PMN. In human PMN, the reported intracellular [ATP] is 1.9 fmol/cell [250]. In contrast, under physiological conditions, extracellular [ATP] is typically low (< 1 µM) [257,258]. Whilst current data on extracellular [ATP] match typical basal concentrations, current total cellular [ATP] values seemed rather high; however detailed reference data for bovine PMN are currently missing in literature. Interestingly, recent data showed that PMN express Cx43 and Panx1 hemi-channels mediating ATP release linked to autocrine purinergic signaling which finally regulates PMN chemotaxis [150]. In this context, supplementation of exogenous non-hydrolyzable ATP (ATPγS), but not of non-modified ATP, significantly induced cell-free and anchored NET formation in the current work. Moreover, ATPγS supplementation enhanced anchored NET formation in *B. besnoiti* tachyzoite-exposed PMN. In general, ATP levels of the extracellular environment are tightly controlled and eventually lowered by conversion via different cell types that express plasma membrane ectonucleotidases, such as nucleoside triphosphate diphosphohydrolase 1 (CD39, converts ATP/ADP to AMP) and ecto-5′-nucleotidase (CD73, converts AMP to ADO). Notably, CD39 and CD73 are both expressed in PMN [259]. Thus, these ectonucleotidase activities of bovine PMN may explain both the current failure of non-modified ATP supplementation to induce NETs and the capacity of ATPγS (which cannot be hydrolyzed by ectonucleotidases) to successfully trigger this effector mechanism [231].

Recent studies have highlighted the critical role of autocrine purinergic signaling in different PMN-derived effector mechanisms. Two main classes of membrane receptors mediate the effects of extracellular ATP: metabotropic G protein-coupled P_2Y receptors and ionotropic P_2X receptors acting as ligand-gated non-selective cation channels. For P_2Y receptors, eight subtypes ($P_2Y_{1/2/4/6/11/12/13/14}$) are known, while for P_2X receptors, seven subtypes ($P_2X_{1–7}$)

were recorded [149,259]. Based on data from mRNA, protein, and functional assays, PMN were reported to express P_2X_1, P_2X_7, P_2Y_2, and P_2Y_{14}, as well as all four ADO receptors [150]. In this context, Panx1 hemi-channels rapidly release ATP during PMN chemotaxis from pseudopod protrusions, amplifying chemotactic signals through activation of P_2Y_2-mediated mTOR signaling at the leading edge [260–262]. Furthermore, stimulation with LPS enhanced phagocytosis of *Escherichia coli* in human PMN, and these effects were abolished when the P_2X_1 purinergic receptor was blocked [263]. Moreover, an antagonist of P_2Y_6 suppressed monosodium urate crystal-induced neutrophil oxidative burst [154,264] and aggregated NET formation [264]. In the current dissertation, the effects of inhibit different P_2X and P_2Y receptor (P_2Y_1, P_2Y_6, P_2X_1, P_2X_4, and P_2X_7) on tachyzoite-driven NET formation were explored. We showed that exclusively pre-treatments of PMN with the P_2X_1 antagonist NF449 resulted in a significant reduction of parasite-induced anchored NET formation whilst all other antagonists failed to affect NET formation. Similar results were obtained when applying post-exposure treatments. The NF449-related data in principle confirmed recent findings of Zhou et al. (2020) stating the relevance of P_2X_1-mediated purinergic signaling in *B. besnoiti* tachyzoite-mediated NET formation. We here furthermore proved that NF449 treatments neither induced apoptotic nor necrotic PMN cell death and elucidated dose-dependent effects of NF449 by estimating an IC_{50} of 1.27 µM. Given that NF449 treatments also inhibited NET formation induced by other protozoan parasites like *T. b. brucei* [166] and *C. parvum* [162], a conserved P_2X_1-related mechanism in parasite-driven NET formation may be proposed. As an additional and interesting finding, P_2X_1-mediated signaling also seemed involved in *B. besnoiti* tachyzoite-mediated clustering of bovine PMN. Hence, during PMN-tachyzoite-co-cultures, we consistently observed that PMN tend to form clusters, which most probably result from chemotactic and migratory actions. Notably, pre-treatments of PMN with NF449 significantly diminished the number of PMN forming clusters. Therefore, the current work adds new data on the role of P_2X_1-mediated purinergic signaling in parasite-PMN interactions and expands the relevance of this specific receptor to further PMN-derived effector mechanisms besides NET formation [231].

4.2 Chapter 2: The CAMKK/AMPK pathway activation participate in early events of B. besnoiti and T. gondii tachyzoite-triggered NET formation in PMN

The intracellular calcium concentration ($[Ca^{2+}]_i$) controls several bovine PMN functions like ROS production, degranulation and NETosis [265,266]. In the current study, exposure of bovine PMN to *T. gondii* tachyzoites indeed induced a rapid increase in $[Ca^{2+}]_i$ in PMN, which was later accompanied by an activation of both CAMKK and AMPK, with the former being commonly reported as Ca^{2+}-dependent. Hence, CAMKK is able to activate AMPK in response to a rise in $[Ca^{2+}]_i$, independent of the AMP/ATP ratio [267]. One of the underlying main mechanisms that mediates a transient, fast rise in $[Ca^{2+}]_i$ in PMN, is the so-called store-operated calcium entry (SOCE). SOCE, in turn, is well-documented to control ROS production, chemotaxis, degranulation and NET formation [265,268,269]. The blockage of *T. gondii* tachyzoite-induced DNA release by the SOCE inhibitor 2-APB is in line with former data on parasite-driven NET formation using stages of the related parasites *E. bovis* [265] and *C. parvum* [270], thereby indicating a conserved role of SOCE in protozoa-induced NETosis [230].

One of the targets of free cytosolic Ca^{2+} is the CAMK family of enzymes. In PMN, CAMK activities have been associated with neutrophil development and maturation [271], superoxide production [272], phagocytosis, migration, and adhesion. When referring to the AMPK-related signaling pathway, CAMKK is a prominent enzyme located upstream of AMPK phosphorylation. CAMKK in PMN is activated by a $[Ca^{2+}]_i$ rise, by IL-8 [273], fMLP and platelet activating factor (PAF) but not by phorbol 12-myristate-13-acetate (PMA) [274] and regulates functions via an ERK-MAP kinase-dependent mechanism [273]. It is expressed in human PMN and participates in the regulation of neutrophil respiratory burst and chemoattractant-induced PMN migration [275]. However, there is almost no information on CAMKK expression or phosphorylation in bovine neutrophils. One report studied CAMKK responses at the transcriptomic level in PMN of cows experiencing subclinical hypocalcemia and found that calcium binding- and calcium-signaling-related proteins showed decreased expression in this scenario [276]. Current data showed that both CAMKK expression and phosphorylation were highly upregulated in bovine PMN (≥ 6-fold increase) after exposure to *B. besnoiti* tachyzoites. Considering that this response was uniform in all PMN donors, occurred in a fast manner, as early as 5 min post-interaction as shown in *B. besnoiti*-exposed PMN, and remained sustained over 30 min, it was most probably linked to and consistent with

the parasite-driven AMPK activation [228,230]. In a comparative approach, this observation was confirmed for another coccidian parasite by increased levels of CAMKK and p-CAMKK present in *T. gondii*-exposed PMN after 30 min of confrontation [228,230].

AMPKα is a metabolic master regulator in eukaryotes with a high impact on several important cellular mechanisms. AMPKα activation is initiated by changes in the metabolic status, mainly resulting from the inhibition of ATP generation during hypoxia, glucose deprivation, or increased ATP consumption [172]. Previous observations in PMN showed AMPK activation to diminish PMA-mediated ROS production in human PMN [176], but to enhance PMN chemotaxis, bacterial killing, MMP-8 secretion, and phagocytosis [174,277]. In the bovine system, neutrophil AMPK is activated by β-hydroxybutyrate and hydroxycarboxylic acid receptor 2 (HCA2) agonists [278]. Moreover, AMPK proved related to increased autophagy in estrogen (17β-estradiol, E2)-treated PMN in low-glucose (2.5 mM) settings, leading to increased LC3, ATG5, and Beclin-1 expression [279]. Furthermore, AMPK induction promoted autophagy by directly activating ULK1 - which is an enzyme downstream of mTOR - during autophagosome formation [280]. In line, bovine PMN exposure to *B. besnoiti* and *T. gondii* tachyzoites was shown to induce AMPK phosphorylation after 30 min of PMN-tachyzoite-co-culture and, as previously reported, a positive correlation with LC3B expression was observed in *B. besnoiti*-exposed PMN [62].

In the current work, expression profiles of specific AMPK subunits and downstream autophagy-related proteins, such as Beclin-1 and ULK-1, were studied. The current data showed that exposure of PMN to *B. besnoiti* tachyzoites indeed induced AMPKα activation in a time-dependent manner, occurring as early as 5 min after exposure resulting in a sustained activation. During the first 30 min of interaction, there were no changes in the regulatory subunits AMPKβ and AMPKγ. However, one limitation of the current study is that we did not include the AMPKα2 subunit, which was also demonstrated to be upregulated in activated PMN, especially in a hypoxia-related inflammation context [281]. Interestingly, AMPK is also involved in fluorine-induced ROS and NETs in carps, an effect that is inhibited by compound C [282], indicating that AMPK-controlled NET release is an ancient and conserved mechanism [228].

Autophagy is a physiological process, which maintains homeostasis or normal cell function by protein degradation and turnover of destroyed cell organelles for new cell formation, especially in response to cellular stress [283]. Furthermore, autophagy plays a pivotal role in regulating

early innate leukocyte-associated effector mechanisms against pathogens, such as phagocytosis [284], cytokine secretion [285], and NET formation [239]. Inflammatory inducers of autophagy include PAMPs, TLRs, TLR adaptors, ROS, NOD-like receptors, and AMPK [62,239,284]. In this regard, AMPK-related signaling plays a key role in NET formation via the regulation of autophagy pathways [62,181,239]. AMPK promotes autophagy, amongst other signaling cascades, by directly activating the pre-initiation complex ULK1 via phosphorylation [286]. In the current work, *B. besnoiti* tachyzoite exposure to bovine PMN induced a modest but statistically significant neutrophil ULK-1 upregulation, thereby temporally coinciding with AMPK activation. Interestingly, *T. gondii*-exposed PMN equally showed an upregulation trend for ULK-1, which failed to reach statistical significance. In principle, current results indicated that autophagy-related activation occurs more pronounced in *B. besnoiti* tachzoite-confronted bovine PMN than in case of *T. gondii* stages. However, it remains currently entirely unclear, which specific parasite-derived factors may trigger these differences on autophagy-dependent mechanisms [228,230]. In contrast to ULK-1, no changes were observed for Beclin-1 protein expression, indicating that, eventually, a Beclin-1-independent autophagy pathway operates in *B. besnoiti* and *T. gondii* tachzoite-exposed PMN. Since ULK-1 but not Beclin-1 was shown to be involved in phagocytosis-related autophagy, current data may indicate a similar mechanism to be driven by *B. besnoiti* tachyzoite exposure [62,287]. Thus, these responses seem directly linked and complementary, which is in line with a previous report on the presence of increased numbers of LC3B-positive autophagosomes in *B. besnoiti*-exposed PMN [62]. Since LC3B induction was also reported to be associated with enhanced phagocytosis [288], both effector mechanisms are most probably related and interconnected in *B. besnoiti*-exposed PMN [228].

As mentioned above, AMPK and related signaling is involved in differential neutrophil effector mechanism activation. Hence, it was reported that treatments with a pharmacological AMPK activator (AICAR) improved bacterial killing and phagocytosis [174] but inhibited PMN apoptosis [289]. In literature, compound C is used as an AMPK inhibitor, but considered as unspecific. In bone marrow-derived neutrophil-like cells, compound C inhibited chemotaxis in a dose-dependent manner [174]. In human PMN, compound C blocked the MMP-8 release induced by conditioned media from monocytes infected with *Mycobacterium tuberculosis* [277]. To our knowledge, the current work includes the first report on the use of compound C for bovine PMN treatments, showing an inhibition of both AMPK and p-AMPK protein expression, without affecting the viability of PMN. Unexpectedly, compound C

treatments failed to significantly affect NET formation in the current work [228]. To further study the role of AMPK activity in *B. besnoiti*-induced PMN activation, we showed that AICAR treatments indeed worked in the bovine system and promoted AMPK phosphorylation in bovine PMN. This is coherent with data in human PMN [176]. In addition, we here demonstrated that plain AICAR treatments induced NET formation and triggered both mitochondrial and glycolytic responses in bovine PMN. Moreover, AICAR induced moderate oxidative responses in PMN, which may support the idea of NOX-dependent NET formation for the bovine system. In contrast to current data, AICAR treatments reduced PMN-derived ROS production in response to PMA stimulation and failed to induce H_2O_2 production in the human system, even though this effect proved dependent on the incubation time [176]. Considering that no additional mitochondrial or NADPHOX inhibitors were used in current experiments, it remains unclear if current AICAR-driven oxidative responses in bovine PMN correspond to NADPHOX-related ROS production or to mitochondrial activities. Moreover, it remains to be elucidated if these differences indeed mirror host species-specific reactions, especially since it is well documented that bovine PMN differ significantly from human PMN in their ROS-based responses to general stimulants [290]. In this regard, the differences and similarities of both host systems were recently reviewed [86] and call for more detailed analyses in the bovine system [228].

Furthermore, current AICAR treatments resulted in additive effects referring to *B. besnoiti* tachyzoite-driven NET formation. This result was confirmed in a comparative approach by PMN treatments of *T. gondii*-exposed PMN with AICAR showing the same effects in NET formation. In contrast to above mentioned findings, AICAR treatments led to diminished ROS production in PMA-activated human PMN, suggesting an overall stimulus-dependent response. In the human system, *T. gondii* -induced NET formation showed to be ROS- and glycolysis-dependent with the participation of gasdermin D and NE [246]. Interestingly, the percentage of PMN performing NETosis in response to parasite encounter was higher (approximately 20%) in human neutrophils [246] than in bovine ones (10%), indicating host species-specific effects, besides the potential impact of differential experimental settings [228,230].

In order to place the AMPK-related findings into a broader signaling framework, we included additional inhibitors targeting pathways with known relevance in immune cell activation. Referring to the inhibition of *T. gondii*-driven extracellular DNA release by treatments with both the SOCE inhibitor 2-APB and the MAPK pathway inhibitor UO126, current findings are

in line with observations on bovine PMN confronted with other coccidian stages, such as *E. bovis* sporozoites and *N. caninum* tachyzoites [165,214]. The observed lack of effect by the PI3K inhibitor LY294002 may be due to the small sample size. Thus, more biological replicates or microscopic analyses of NET formation are necessary to propose more precise conclusions. Altogether, these results suggest a conserved nature of these canonical activation pathways in bovine PMN driven by encounter with different apicomplexan parasites species and stages. Notably, another protozoan but non-related parasite, *Leishmania donovani*, induces autophagy in human PMN, depending on ROS production, AMPK activation and PI3K/Akt and ERK/MAPK signaling pathways [205]. The authors were able to demonstrate that augmented autophagy was a prerequisite for the subsequent macrophage-mediated uptake of infected PMN, thus promoting *L. donovani* infection [205,291].

Altogether, current findings highlighted the complex interplay between protozoan parasites and host-dependent innate immune responses. Overall, current data are consistent with the hypothesis that *B. besnoiti* and *T. gondii* encounter activates bovine PMN via a CAMKK-/AMPK-/ /NETosis-dependent mechanism [228,230]

4.3 Chapter 3: Bovine PMN responses to EVs released by B. besnoiti tachyzoites and B. besnoiti-infected host cells

In the field of parasitology, EVs have come into interest based on their principle ability to mediate communication between cells, but also between parasites and cells [292]. EVs contain proteins, RNA/DNA, lipids and metabolites and EV-derived molecules were shown to be involved in drug resistance, cell growth regulation and immune cell modulation [196]. EVs are of a complex nature, therefore a plethora of protocols and guidelines on their isolation and characterization exist using differential centrifugation/ultracentrifugation, affinity-based capture (such as antibody-coated magnetic beads or resins), ultrafiltration, size-exclusion chromatography and Nano-Flow cytometry, amongst others [293,294]. In the current work, we used differential centrifugation at low-speed to eliminate high molecular contaminants, ultrafiltration to eliminate proteins and to enrich EVs and size-exclusion chromatography to purify and recover EVs. The latter process was performed with the help of an automated collector (IZON), thereby achieving an improved reproducibility, speed and simplicity of EV isolation. In the current work, EVs from different cellular sources (BUVEC, PMN, tachyzoites) and stimulation status (unstimulated vs tachyzoite-exposed or -infected) were isolated. EV

characterization was performed following MISEV 2018 guidelines [294], considering the parameters EV size, concentration, membrane protein biomarkers and morphology. Overall, particles from all cellular sources showed a mean size of 70 nm, thereby fitting well to size ranges described for small EVs in literature (30-150 nm; [186,295]. For further characterization, all EV samples were tested for the presence of the tetraspanins CD9 and CD81 used as EV markers. Western blot analyses proved BUVEC- and PMN-derived EVs as positive for both CD9 and CD81 proteins. Moreover, the expected size and morphology of EVs from selected sources were verified by TEM, thereby illustrating for the first time *B. besnoiti* tachyzoite-derived EVs. Taken together, these results confirmed that the particles isolated from BUVEC-, PMN- and *B. besnoiti* tachyzoite-derived supernatants were indeed EVs in terms of size, morphology, and protein components [229].

Host-parasite-communication via EVs has extensively been analyzed in the last decade [184–186,193,195,196,198]. In general, pathogen encounter seems to foster EV release by effector cells. Thus, infections with *Plasmodium* stimulated EV release from endothelial cells, platelets, and red blood cells (RBCs). In agreement, exposure of PMN to *B. besnoiti* tachyzoites led to a rise in neutrophil EV release in the current work. Interestingly, enhanced EV levels correlated with severe illness both in rodent malaria model and in malaria patients since EVs originating from parasite-infected RBCs activated the innate immune response via pro- and anti-inflammatory cytokines in *P. falciparum* and *P. berghei* infections [296,297]. These EVs may also play a role in vascular activation and dysfunction, thereby facilitating parasite sequestration and associated pathology [296,297]. Moreover, *Cryptosporidium parvum* infection of human cells lines (H69 and 603B cells) induced an increment of luminal EV release from biliary and intestinal epithelium. These EVs carried antimicrobial peptides from epithelial cell origin (e.g., beta-defensin 2), aiding to decrease sporozoite viability and infectivity both *in vitro* and *ex vivo* [298]. In general, the extent of EV production and/or nature of content may vary depending on the cell type and activation status. In line with current results denying any infection-driven increase of endothelial EV release, treatments of HUVEC with TNF-α did not affect the production, size or morphology of EVs [299]. In a another study, unstimulated human PMN secreted lower EV quantities than PMN exposed to different classes of physiological stimuli, such as fMLP, LPS and TNF-α [300]. Given that GM-CSF and IFNγ failed to induce EV release, stimuli-specific reactions were suggested [300].

After having confirmed EV numbers and characteristics, EVs from BUVEC, PMN and *B. besnoiti* tachyzoites were here studied for their effects on glycolytic and oxidative responses, NET formation, ROS production and chemokine/cytokine secretion in unstimulated PMN. Unexpectedly, current findings revealed that EVs from all cellular sources failed to affect neutrophil metabolic (glycolytic and oxidative) responses and ROS production. However, we here aimed to characterize immediate reactions of resting bovine PMN and therefore worked with non-activated cells. In line, EVs from both unstimulated human PMN and opsonized particle-activated PMN failed to affect ROS production in resting PMN [190,301]. By contrast, EV treatments decreased ROS production in PMA-pre-activated PMN [190]. In contrast to current data, EVs derived from human PMN stimulated with another protozoa (*Entamoeba histolytica)* triggered a significant increase of neutrophil ROS production [301]. However, when PMN were pre-stimulated with PMA or *E. histolytica* trophozoites and then exposed to EVs from unstimulated or *E. histolytica*-stimulated PMN, a significant decrease or no change in ROS production was observed, respectively [301]. The sum of these data indicates that several factors like the pre-stimulus status of donor or receiver PMN and the type of stimulus highly matter in EV-mediated PMN reactions. Current data showed that resting bovine PMN failed to respond to EVs of different cellular sources on the level of ROS or metabolic changes. In addition, stimulation of PMN with EVs from both *B. besnoiti*-exposed PMN and unstimulated PMN also failed to significantly drive extracellular DNA release. Nevertheless, in case of NET formation, exposure of resting PMN to EV samples showed a differential reaction pattern compared to ROS-related responses. Here, BUVEC- and tachyzoite-derived EVs indeed fostered NET release. The fact, that PMN-derived EVs failed to drive NET formation in the current experimental setting is in line with former data on *E. histolytica*, stating that unstimulated PMN-derived EVs and EVs from parasite-stimulated PMN did not induce NET formation in resting PMN [301], thereby highlighting again the importance of the neutrophil priming state.

Of note, endothelial cells are well-known as effective producers of EVs, thereby communicating with all kinds of cells [183,299,302]. In the current work, BUVEC-derived EVs triggered NET formation in resting bovine PMN, independent of the infection status of BUVEC, but being accompanied by a lack of ROS production, thereby indicating NOX-independent NET formation. NOX-independent NET formation was recently described to be triggered by an increase in calcium and mitochondrial ROS, activating PAD4 and histone citrullination, concomitant with ERK1/2 and JNK pathway activation [128]. In that context, EVs were described to carry miRNAs and other signaling molecules, which are able to activate

the JNK and ERK1/2 signaling pathway [303–305]. Furthermore, EVs may also transport trace amounts of ROS from their progenitor cell [301]. However, the potential mechanisms being involved in NOX-independent NET formation triggered by BUVEC- and *B. besnoiti* tachyzoite-derived EVs await further investigation [229].

EVs participate in immune signaling due to their capacity to transport both pro-inflammatory and anti-inflammatory cytokines to designated target cells, in addition to their ability to induce cytokine secretion in recipient cells [306]. Current data showed that bovine PMN upregulated IL-1β and IL-6 secretion in a stimulus-dependent manner since exclusively EVs from *B. besnoiti*-infected BUVEC fostered the release of these cytokines. Meanwhile, BUVEC failed to react by IL-1β, IL-6 or CXCL8 release after exposure to EVs, independent of the cellular source. Referring to PMN, this finding correlates with data on other innate immune cells like macrophages, monocytes or dendritic cells. Hence, *T. gondii*-derived EVs were shown to drive resting macrophage activation by inducing IL-12, TNFα and INFγ secretion [307]. Moreover, *Leishmania donovani* promastigote-derived EVs modulated the cytokine response of monocytes by enhancing IL-10 expression but suppressing TNFα synthesis, while EV-exposed monocyte-derived dendritic cells (DCs) showed diminished levels of IL-10, IL-12p70, TNFα [308]. Moreover, *in vivo* administration of EVs from *T. gondii* antigen-stimulated DCs led to an increased release of Th1 cytokines (including IL-2 and IFN-γ) with concurrent diminishment of Th2 cytokines (e.g., IL-4, IL-5, and IL-10) [309]. Furthermore, IL-6 deficient mice were found more susceptible to *T. gondii* infection, allowing for increased parasite growth [310]. Additionally, *T. gondii* is able to suppress IL-1β production from human PMN as an evasion mechanism of host defense [311]. These reports indicated that IL-1β and IL-6 mediate host protection against parasites infection, activating inflammatory responses. It is important to highlight that this EV-cytokine-communication is bidirectional. Hence, neutrophil EV production can also be induced by CXCL8 and TNF-α [312]. Of note, several host molecules and proinflamatory cytokines induce or boost NET formation [127,313]. Hence, both macrophage-derived and plasmacytoid dendritic cells (pDCs)-derived type I IFNs promote NET release [127]. Additionally, proinflammatory cytokines, such as tumor necrosis factor (TNF), IL-1β, and IL-12, which are secreted by leukocytes during inflammation, have been shown to enhance NET formation [127]. Furthermore, patients with systemic inflammatory response syndrome possess higher plasma levels of IL-8, IL-1β, and TNF-α, which induce NET formation in PMN from healthy individuals [314]. These findings underscore the critical role of cytokines in modulating NET formation, particularly in inflammatory conditions [229].

To fulfill their function in cell-to-cell communication, EVs interact with target cells through receptor-ligand binding mechanisms or by internalization via different endocytic mechanisms, which include clathrin-dependent endocytosis and clathrin-independent routes like caveolin-mediated uptake, macropinocytosis, phagocytosis, and lipid raft-mediated internalization [315]. Therefore, we here tested if EVs from the different cellular sources are taken up by resting bovine PMN. Indeed, confocal microscopy confirmed that BUVEC- and *B. besnoiti* tachyzoite-derived far red-labeled EVs were internalized by PMN resulting in a globular cytoplasmic localization in exposed PMN, suggesting EVs were internalized by endocytic mechanisms. As expected, PMN-derived EV uptake occurred irrespective of the EV source. In principle, these data match with findings on human PMN or other innate immune cell types. Thus, *E. histolytica*-derived EVs fused with neutrophil cell membranes and were internalized into the cytoplasm by human PMN [301]. Moreover, cytoplasmic internalization of immature DC-derived EVs was described for unstimulated DCs [316] and *T. gondii*-derived EVs were taken up into the cytoplasm of RAW264.7 macrophages [307].

To summarize, we here showed that bovine PMN enhanced their EV production when being confronted to *B. besnoiti* stages. Bovine PMN showed no ROS production or glycolytic/oxidative responses when being exposed to EVs from differential cellular origin. Importantly, NET formation and neutrophil IL-1β/IL-6 secretion were upregulated by *B. besnoiti* infected-endothelium- and *B. besnoiti* tachyzoite-derived EVs [229] indicating a potential role of EVs in innate intercellular or parasite-driven communication.

5. ZUSAMMENFASSUNG

Studien der letzten Jahre haben unser Verständnis der bovinen neutrophilen Reaktionen auf *Besnoitia besnoiti*, einen apikomplexen Parasiten und Erreger der wiederaufkommenden Rinderkrankheit Bovine Besnoitiose, wesentlich, jedoch nicht abschließend erweitert. Im Mittelpunkt der vorliegenden Arbeit stand die Aufklärung bestimmter molekularer Mechanismen, die der Bildung neutrophiler extrazellulärer Fallen (NETs), einer zentralen Abwehrstrategie des angeborenen Immunsystems, zugrunde liegen. Entsprechend wurde zum einen die Rolle der purinergen Signalübertragung analysiert und gezeigt, dass Tachyzoiten von *B. besnoiti* eine starke NETs-Bildung in bovinen polymorphkernigen neutrophile Granulozyten (PMN) induzieren, ohne allerdings die intra- oder extrazellulären ATP-Konzentrationen zu verändern. Dennoch führte die extrazelluläre Zugabe von ATPγS, einem nicht-hydrolysierbaren ATP-Analogon, zu einer signifikanten Verstärkung der NETs-Freisetzung – insbesondere von verankerten NETs –, während natives ATP keinen solchen Effekt zeigte. Dieser Prozess erwies sich als abhängig vom purinergen Rezeptor P2X1, da der spezifische Antagonist NF449 (IC_{50} = 1,27 µM) sowohl die NET-Bildung als auch die auffällige PMN-Clusterbildung nach Tachyzoitenexposition hemmte. Im Gegensatz dazu hatte die pharmakologische Blockade anderer purinerger Rezeptoren (P2Y2, P2Y6, P2X4, P2X7) keinen Einfluss auf die parasiten-induzierte NETose, was auf eine selektive Rolle des P2X1-Rezeptors hinwies. Weiterführende Stoffwechselanalysen mittels Seahorse-Technologie zeigten eine erhöhte Sauerstoffverbrauchsrate (OCR) in PMN nach Exposition gegenüber Tachyzoiten, während ATPγS die extrazelluläre Ansäuerungsrate (ECAR) steigerte, was auf eine mitochondriale Beteiligung bzw. metabolische Anpassung während der frühen Phase der NETose hindeutet.

Eine zweite Studie ergänzte die oben genannten Befunde, indem sie sich auf die Calcium/Calmodulin-abhängige Proteinkinase-Kinase 2 (CAMKK)/AMPK-Signalkaskade und deren Verbindung zur Autophagie konzentrierte. Die Exposition boviner PMN gegenüber *B. besnoiti*- und *Toxoplasma gondii*-Tachyzoiten führte innerhalb von 30 Minuten zu einer schnellen Phosphorylierung von AMPK, was auch durch Behandlungen mit dem AMPK-Aktivator AICAR nachgeahmt wurde. Im Hinblick auf die Signaltransduktion korrelierte die AMPK-Phosphorylierung mit der Aktivierung des Upstream-Regulators CAMKK in *B. besnoiti*- und *T. gondii*-exponierten PMN sowie mit der Hochregulierung des autophagieassoziierten Proteins ULK-1 (aber nicht Beclin-1) im Fall von *B. besnoiti*-exponierten PMN, was auf eine selektive autophagische Signatur hinweist.

Bemerkenswerterweise führten AICAR-Behandlungen allein zu einer verstärkten NETs-Bildung, ohne die Lebensfähigkeit der PMN zu beeinträchtigen. In *B. besnoiti*-exponierten PMN zeigten AICAR-Kombinationsbehandlungen jedoch keinen Einfluss auf die oxidative Antwort. Darüber hinaus induzierten AICAR-Kombinationsbehandlungen additive Effekte auf die durch Tachyzoiten ausgelöste NETs-Bildung. Im Fall von *T. gondii* war diese NETs-Reaktion zusätzlich abhängig von MAPK- und Store-operated calcium entry (SOCE)-Signalwegen, was durch eine verminderte DNA-Freisetzung nach Inhibition von MAPK und SOCE bestätigt wurde. Diese Ergebnisse deuten darauf hin, dass Autophagie und AMPK-Signale parallele, ROS-unabhängige Signalwege darstellen, die die durch *B. besnoiti* induzierte NETs-Bildung unterstützen.

Eine dritte Untersuchungsreihe widmete sich der Rolle extrazellulärer Vesikel (EVs) als potenzielle Modulatoren neutrophiler Reaktionen. Für die Experimente wurden EVs unterschiedlicher Quellen analysiert. Entsprechend wurden EVs aus Überständen von *B. besnoiti*-Tachyzoiten, von *B. besnoiti*-infizierten und nicht-infizierten bovinen Nabelvenen-Endothelzellen (BUVEC) sowie von Tachyzoiten-exponierten PMN gewonnen. Ihre Identität wurde über Nano-Flow-Zytometrie, die Detektion der EV-Marker CD9 und CD81 sowie durch Transmissionselektronenmikroskopie bestätigt. Die Exposition boviner PMN mit diesen EVs, insbesondere jenen von Tachyzoiten und infizierten BUVEC, führte zu einer signifikanten NET-Freisetzung. Mikroskopisch konnte diese durch die Anwesenheit extrazellulärer DNA-Strukturen mit Histonen und neutrophiler Elastase – typische Merkmale klassischer NETs – bestätigt werden. Interessanterweise induzierten EVs von PMN selbst keine NETose, und keiner der EV-Typen veränderte das metabolische Profil (oxidative und glykolytische Reaktionen) oder die ROS-Produktion der exponierten Zellen, wie durch Seahorse-Analysen bzw. Chemilumineszenz-Assays gezeigt wurde. Dies weist auf einen NADPH-Oxidase (NOX)-unabhängigen Mechanismus der EV-induzierten NET-Bildung hin. Darüber hinaus zeigten Zytokinanalysen (IL-6 und IL-1β), dass EVs von *B. besnoiti*-infizierten BUVECs selektiv die Sekretion von IL-1β und IL-6 in PMN erhöhten, ohne die Produktion von CXCL8 zu beeinflussen und lieferten darüber einen Hinweis auf eine gezielte, zellursprungsabhängige Entzündungsantwort.

6. SUMMARY

Recent studies have collectively advanced our understanding of bovine neutrophil responses against tachyzoite stages of *Besnoitia besnoiti*, an apicomplexan parasite responsible for the re-emerging cattle disease bovine besnoitiosis. A central focus of the current work was to fill some gaps on the molecular mechanisms underlying the parasite-driven formation of neutrophil extracellular traps (NETs), a key innate effector mechanism. Therefore, in a first investigation, the role of neutrophil purinergic signalling was studied, revealing that *B. besnoiti* tachyzoites significantly induce NET formation without altering intracellular or extracellular ATP concentrations in bovine PMN. Despite this finding, extracellular supplementation with ATPγS, a non-hydrolyzable ATP analog, significantly enhanced NET release - specifically anchored NETs - whilst native ATP failed to do so. This response depended on the P2X1 purinergic receptor since treatments with the specific antagonist NF449 (IC_{50} = 1.27 µM) inhibited both NET formation and PMN clustering triggered by tachyzoite exposure. In contrast, pharmacological blockade of other purinergic receptors (P2Y2, P2Y6, P2X4, P2X7) did not affect NET formation, thereby highlighting a selective role for the P2X1 puringergic receptor in *B. besnoiti* tachyzoite-driven NET formation. Metabolic assays using Seahorse technology further revealed increased oxygen consumption rates (OCR) in tachyzoite-exposed PMN, while ATPγS treatment led to enhanced extracellular acidification rates (ECAR), suggesting mitochondrial involvement and metabolic adaptation during the early steps of the NETotic process.

A second study complemented above-mentioned findings by focusing on the calcium/calmodulin-dependent protein kinase kinase 2 (CAMKK)/AMPK signalling axis and its link to autophagy. *B. besnoiti* and *Toxoplasma gondii* tachyzoite exposure induced rapid phosphorylation of AMPK in bovine PMN within 30 minutes, a response mirrored by the AMPK activator AICAR. Referring to signalling pathways, AMPK phosphorylation correlated with an activation of the upstream regulator CAMKK in both *B. besnoiti* and *T. gondii*-exposed PMN and upregulation of the downstream autophagy-related protein ULK-1 (but not Beclin-1) in the case of *B. besnoiti*-exposed PMN, indicating a selective autophagic signature. Notably, AICAR treatments alone led to enhanced NET formation without compromising PMN viability. However, in *B. besnoiti* tachyzoite-exposed PMN, AICAR co-treatments failed to affect oxidative response. Moreover, AICAR co-treatments induced additive effects on tachyzoite-induced NET formation. In the case of *T. gondii*, this NET formation response further depended on MAPK and store-operated calcium entry (SOCE) pathways, as shown by

reduced DNA release upon MAPK- and SOCE inhibition. These findings suggest that autophagy and AMPK signaling signify parallel, ROS-independent pathways involved in the support of *B. besnoiti*-driven NET formation.

A third line of investigation explored the role of extracellular vesicles (EVs) as potential modulators of *B. besnoiti*-driven bovine neutrophil responses. To obtain EVs from differential sources, EVs were isolated from *B. besnoiti* tachyzoites, infected and non-infected bovine umbilical vein endothelial cells (BUVEC), and tachyzoite-exposed PMN. Their identity was confirmed via nano-flow cytometry, by EV markers like CD9 and CD81, and morphologically by transmission electron microscopy. When bovine PMN were exposed to differential EVs, particularly those derived from tachyzoites and infected BUVECs induced a significant NET release. This was validated microscopically by the presence of extracellular DNA structures adorned with histones and neutrophil elastase - hallmarks of classical NETs. Interestingly, PMN-derived EVs failed to trigger NET formation. Moreover, none of the different EV types drove changes in the neutrophil metabolic profile (oxidative and glycolytic responses) or ROS production in exposed bovine neutrophils, as assessed by Seahorse analysis and chemiluminescence assays, respectively. These findings indicated a NADPH oxidase (NOX)-independent mechanism of EV-induced NET formation. Furthermore, cytokine analyses revealed that EVs from infected BUVECs selectively induced IL-1β and IL-6 secretion in PMN, without influencing CXCL8 production, thereby pointing towards a tailored inflammatory response modulated by EVs of distinct cellular origin.

7. REFERENCES

1. Álvarez-García, G., Frey, C. F., Mora, L. M. O. & Schares, G. A century of bovine besnoitiosis: an unknown disease re-emerging in Europe. *Trends in Parasitology* **29**, 407–415 (2013).
2. Anastácio, C. *et al.* Impact of Endemic Besnoitiosis on the Performance of a Dairy Cattle Herd. *Animals* **12**, 1291 (2022).
3. Gazzonis, A. L., Ferre, I. & Alvarez Garcia, G. Bovine Besnoitiosis. in *Encyclopedia of Livestock Medicine for Large Animal and Poultry Production* (ed. Simões, J.) 1–12 (Springer Nature Switzerland, Cham, 2025). doi:10.1007/978-3-031-52133-1_9-1.
4. Malatji, M. P., Tembe, D. & Mukaratirwa, S. An update on epidemiology and clinical aspects of besnoitiosis in livestock and wildlife in sub-Saharan Africa: A systematic review. *Parasite Epidemiology and Control* **21**, e00284 (2023).
5. Cortes, H., Leitão, A., Gottstein, B. & Hemphill, A. A review on bovine besnoitiosis: a disease with economic impact in herd health management, caused by. *Parasitology* **141**, 1406–1417 (2014).
6. Gutiérrez-Expósito, D. *et al.* Clinical and Serological Dynamics of Besnoitia besnoiti Infection in Three Endemically Infected Beef Cattle Herds. *Transboundary and Emerging Diseases* **64**, 538–546 (2017).
7. Rodríguez-Espinosa, O., Rojas-Espinosa, O., Moreno-Altamirano, M. M. B., López-Villegas, E. O. & Sánchez-García, F. J. Metabolic requirements for neutrophil extracellular traps formation. *Immunology* **145**, 213–224 (2015).
8. Dubey, J. P., Wilpe, E. van, Blignaut, D. J. C., Schares, G. & Williams, J. H. Development of Early Tissue Cysts and Associated Pathology of Besnoitia besnoiti in a Naturally Infected Bull (Bos taurus) from South Africa. *para* **99**, 459–466 (2013).

9. Jacquiet, P., Liénard, E. & Franc, M. Bovine besnoitiosis: Epidemiological and clinical aspects. *Veterinary Parasitology* **174**, 30–36 (2010).

10. Authority, E. F. S. Bovine Besnoitiosis: An emerging disease in Europe. *EFSA Journal* **8**, 1499 (2010).

11. Besnoit, C. & Robin, V. Sarcosporidiose cutanée chez une vache. *Revue Vétérinaire* **37(11)**, 649–663 (1912).

12. Franco, E. E. & Borges, I. Sur la sarcosporidiose Bovine. *Arquivos do Instituto Bacteriologico Câmara Pestana* **4**, 269-289. (1916).

13. Bigalke, R. D. Besnoitiosis and Globidiosis. in *Diseases of Cattle in the Tropics: Economic and Zoonotic Relevance* (eds Ristic, M. & McIntyre, I.) 429–442 (Springer Netherlands, Dordrecht, 1981). doi:10.1007/978-94-015-6895-1_34.

14. Chatikobo, P., Choga, T., Ncube, C. & Mutambara, J. Participatory diagnosis and prioritization of constraints to cattle production in some smallholder farming areas of Zimbabwe. *Preventive Veterinary Medicine* **109**, 327–333 (2013).

15. Álvarez-García, G., García-Lunar, P., Gutiérrez-Expósito, D., Shkap, V. & Ortega-Mora, L. M. Dynamics of *Besnoitia besnoiti* infection in cattle. *Parasitology* **141**, 1419–1435 (2014).

16. Castillo, J. A., Marcén, J. M., Ortega Mora, L. M. & Álvarez García, G. La besnoitiosis bovina, presentada como una enfermedad emergente europea. *Albéitar (España)* https://agris.fao.org/search/en/providers/122599/records/64724a51e17b74d2224f8fd8 (2009).

17. Cortes, H., Ferreira, M. L., Vidal, R., Serra, P. & Caeiro, V. Contribuição para o estudo da besnoitiose bovina em Portugal. *Contribution to the knowledge of bovine besnoitiosis in Portugal* https://dspace.uevora.pt/rdpc/handle/10174/1947 (2003).

18. Schares, G. *et al.* First in vitro isolation of Besnoitia besnoiti from chronically infected cattle in Germany. *Vet. Parasitol.* **163**, 315–322 (2009).
19. Basso, W. *et al.* Bovine besnoitiosis in Switzerland: Imported cases and local transmission. *Veterinary Parasitology* **198**, 265–273 (2013).
20. Cortes, H. C. E. *et al.* Isolation of Besnoitia besnoiti from infected cattle in Portugal. *Veterinary Parasitology* **141**, 226–233 (2006).
21. Delooz, L., Evrard, J., Mpouam, S. E. & Saegerman, C. Emergence of Besnoitia besnoiti in Belgium. *Pathogens* **10**, 1529 (2021).
22. Gutiérrez-Expósito, D. *et al.* Prevalence of *Besnoitia besnoiti* infection in beef cattle from the Spanish Pyrenees. *The Veterinary Journal* **200**, 468–470 (2014).
23. Hornok, S., Fedák, A., Baska, F., Hofmann-Lehmann, R. & Basso, W. Bovine besnoitiosis emerging in Central-Eastern Europe, Hungary. *Parasit Vectors* **7**, 20 (2014).
24. Neve, V. C. *et al.* Investigation of an Autochthonous Outbreak of Bovine Besnoitiosis in Northwestern Sicily. *Pathogens* **11**, 122 (2022).
25. Rhodes, V., Hayes, C. J., Sánchez-Miguel, C., O'Donovan, J. & Ryan, E. G. An investigation into bovine besnoitiosis (Besnoitia besnoiti) in an Irish pedigree Aberdeen Angus herd. *Veterinary Record Case Reports* **10**, e379 (2022).
26. Ryan, E. G. *et al.* Bovine besnoitiosis (Besnoitia besnoiti) in an Irish dairy herd. *Veterinary Record* **178**, 608–608 (2016).
27. Tinkler, S. H., Villa, L., Manfredi, M. T., Walshe, N. & Jahns, H. First report of Besnoitia bennetti in Irish donkeys: an emerging parasitic disease in Europe. *Ir Vet J* **77**, 2 (2024).
28. Olias, P., Schade, B. & Mehlhorn, H. Molecular pathology, taxonomy and epidemiology of Besnoitia species (Protozoa: Sarcocystidae). *Infection, Genetics and Evolution* **11**, 1564–1576 (2011).

29. Villa, L. *et al.* Bovine besnoitiosis in an endemically infected dairy cattle herd in Italy: serological and clinical observations, risk factors, and effects on reproductive and productive performances. *Parasitol Res* **118**, 3459–3468 (2019).

30. Coelho, J., Domingues, J., Waap, H. & Stilwell, G. Epidemiological characteristics of bovine besnoitiosis (Besnoitia besnoiti) in a beef cattle farm: a cross-sectional serological assessment. *Frontiers in Veterinary Science* **10**, (2023).

31. Gazzonis, A. L. *et al.* Serological dynamics and risk factors of Besnoitia besnoiti infection in breeding bulls from an endemically infected purebred beef herd. *Parasitol Res* **116**, 1383–1393 (2017).

32. Liénard, E. *et al.* A longitudinal study of Besnoitia besnoiti infections and seasonal abundance of Stomoxys calcitrans in a dairy cattle farm of southwest France. *Veterinary Parasitology* **177**, 20–27 (2011).

33. Álvarez-García, G. *et al.* Seroprevalence of *Besnoitia besnoiti* infection and associated risk factors in cattle from an endemic region in Europe. *The Veterinary Journal* **200**, 328–331 (2014).

34. Gollnick, N. S., Scharr, J. C., Schares, G. & Langenmayer, M. C. Natural Besnoitia besnoiti infections in cattle: chronology of disease progression. *BMC Vet Res* **11**, 35 (2015).

35. González-Barrio, D. *et al.* Identification of molecular biomarkers associated with disease progression in the testis of bulls infected with Besnoitia besnoiti. *Vet Res* **52**, 106 (2021).

36. Grau-Roma, L. *et al.* Pathological findings in genital organs of bulls naturally infected with Besnoitia besnoiti. *Parasitol Res* **119**, 2257–2262 (2020).

37. Langenmayer, M. C., Scharr, J. C., Sauter-Louis, C., Schares, G. & Gollnick, N. S. Natural Besnoitia besnoiti infections in cattle: hematological alterations and changes in serum chemistry and enzyme activities. *BMC Vet Res* **11**, 32 (2015).

38. Diezma-Díaz, C. *et al.* A model for chronic bovine besnoitiosis: Parasite stage and inoculation route are key factors. *Transboundary and Emerging Diseases* **67**, 234–249 (2020).

39. Gutiérrez-Expósito, D., Ferre, I., Ortega-Mora, L. M. & Álvarez-García, G. Advances in the diagnosis of bovine besnoitiosis: current options and applications for control. *International Journal for Parasitology* **47**, 737–751 (2017).

40. Jacinto, J. *et al.* Bovine besnoitiosis: Assessment of the diagnostic accuracy of three different tests using a Bayesian latent class model approach and clinical characterization of the disease. *Preventive Veterinary Medicine* **235**, 106415 (2025).

41. Schares, G. *et al.* Novel tools for the diagnosis and differentiation of acute and chronic bovine besnoitiosis. *International Journal for Parasitology* **43**, 143–154 (2013).

42. Schares, G. *et al.* First highly sensitive and specific competitive ELISA for detection of bovine besnoitiosis with potential as a multi-species test. *International Journal for Parasitology* **50**, 389–401 (2020).

43. Diezma-Díaz, C. *et al.* The route of *Besnoitia besnoiti* tachyzoites inoculation does not influence the clinical outcome of the infection in calves. *Veterinary Parasitology* **267**, 21–25 (2019).

44. Diezma-Díaz, C. *et al.* Added value of IgM detection and low avidity index as markers of acute bovine besnoitiosis. *Veterinary Parasitology* **277**, 109012 (2020).

45. Schares, G. *et al.* Naturally acquired bovine besnoitiosis: Differential distribution of parasites in the skin of chronically infected cattle. *Veterinary Parasitology* **216**, 101–107 (2016).

46. García-Lunar, P., Ortega-Mora, L. M., Schares, G., Diezma-Díaz, C. & Álvarez-García, G. A new lyophilized tachyzoite based ELISA to diagnose Besnoitia spp. infection in

bovids and wild ruminants improves specificity. *Veterinary Parasitology* **244**, 176–182 (2017).

47. García-Lunar, P. *et al.* An Inter-Laboratory Comparative Study of Serological Tools Employed in the Diagnosis of *Besnoitia besnoiti* Infection in Bovines: Bovine Besnoitiosis: Comparative Study of Serological Tests. *Transbound Emerg Dis* **60**, 59–68 (2013).

48. García-Lunar, P., Moré, G., Campero, L., Ortega-Mora, L. M. & Álvarez-García, G. Anti-*Neospora caninum* and anti-*Sarcocystis* spp. specific antibodies cross-react with *Besnoitia besnoiti* and influence the serological diagnosis of bovine besnoitiosis. *Veterinary Parasitology* **214**, 49–54 (2015).

49. Schares, G. *et al.* Validation of a commercial version of a competitive enzyme linked immunosorbent assay for the detection of antibodies to Besnoitia besnoiti. *Parasites Vectors* **15**, 455 (2022).

50. Jiménez-Meléndez, A. *et al.* In vitro efficacy of bumped kinase inhibitors against *Besnoitia besnoiti* tachyzoites. *International Journal for Parasitology* **47**, 811–821 (2017).

51. Jiménez-Meléndez, A. *et al.* Repurposing of commercially available anti-coccidials identifies diclazuril and decoquinate as potential therapeutic candidates against Besnoitia besnoiti infection. *Vet Parasitol* **261**, 77–85 (2018).

52. Cortes, H. C. E. *et al. In vitro* efficacy of nitro- and bromo-thiazolyl-salicylamide compounds (thiazolides) against *Besnoitia besnoiti* infection in Vero cells. *Parasitology* **134**, 975–985 (2007).

53. Cortes, H. C. E., Muller, N., Boykin, D., Stephens, C. E. & Hemphill, A. In vitro effects of arylimidamides against Besnoitia besnoiti infection in Vero cells. *Parasitology* **138**, 583–592 (2011).

54. Müller, J., Manser, V. & Hemphill, A. In vitro treatment of Besnoitia besnoiti with the naphto-quinone buparvaquone results in marked inhibition of tachyzoite proliferation, mitochondrial alterations and rapid adaptation of tachyzoites to increased drug concentrations. *Parasitology* **146**, 112–120 (2019).

55. Eberhard, N. *et al.* Activities of Endochin-Like Quinolones Against in vitro Cultured Besnoitia besnoiti Tachyzoites. *Front. Vet. Sci.* **7**, (2020).

56. Ellis, J. T. *et al.* Molecular Phylogeny of *Besnoitia* and the Genetic Relationships Among *Besnoitia* of Cattle, Wildebeest and Goats. *Protist* **151**, 329–336 (2000).

57. Mehlhorn, H. Besnoitia. in *Parasitic Protozoa of Farm Animals and Pets* (eds Florin-Christensen, M. & Schnittger, L.) 169–185 (Springer International Publishing, Cham, 2018). doi:10.1007/978-3-319-70132-5_7.

58. Dubey, J. P., Shkap, V., Pipano, E., Fish, L. & Fritz, D. L. Ultrastructure of Besnoitia besnoiti Tissue Cysts and Bradyzoites. *Journal of Eukaryotic Microbiology* **50**, 240–244 (2003).

59. Arrabal, J. P. *et al.* A putative new *Besnoitia* species in the southern black-eared opossum *Didelphis aurita*. *International Journal for Parasitology: Parasites and Wildlife* **25**, 100998 (2024).

60. Reis, Y. *et al.* Microtubule cytoskeleton behavior in the initial steps of host cell invasion by *Besnoitia besnoiti*. *FEBS Letters* **580**, 4673–4682 (2006).

61. Velásquez, Z. D. *et al.* Besnoitia besnoiti–driven endothelial host cell cycle alteration. *Parasitol Res* **119**, 2563–2577 (2020).

62. Zhou, E. *et al.* Simultaneous and Positively Correlated NET Formation and Autophagy in Besnoitia besnoiti Tachyzoite-Exposed Bovine Polymorphonuclear Neutrophils. *Front Immunol* **10**, 1131 (2019).

63. Wiedemann, K. R. *et al.* Mass Spectrometry Imaging of Lipid and Metabolite Distributions in Cysts of Besnoitia besnoiti-Infected Bovine Skin. *J. Am. Soc. Mass Spectrom.* **36**, 1017–1026 (2025).

64. Fernández-García, A. *et al.* Identification of Besnoitia besnoiti proteins that showed differences in abundance between tachyzoite and bradyzoite stages by difference gel electrophoresis. *Parasitology* **140**, 999–1008 (2013).

65. Ramakrishnan, C. *et al.* Dissection of Besnoitia besnoiti intermediate host life cycle stages: From morphology to gene expression. *PLOS Pathogens* **18**, e1010955 (2022).

66. Bohne, W., Heesemann, J. & Gross, U. Reduced replication of Toxoplasma gondii is necessary for induction of bradyzoite-specific antigens: a possible role for nitric oxide in triggering stage conversion. *Infection and Immunity* **62**, 1761–1767 (1994).

67. Tomavo, S. & Boothroyd, J. C. Interconnection between organellar functions, development and drug resistance in the protozoan parasite, *Toxoplasma gondii*. *International Journal for Parasitology* **25**, 1293–1299 (1995).

68. Fox, B. A., Gigley, J. P. & Bzik, D. J. *Toxoplasma gondii* lacks the enzymes required for de novo arginine biosynthesis and arginine starvation triggers cyst formation. *International Journal for Parasitology* **34**, 323–331 (2004).

69. Bohne, W., Heesemann, J. & Gross, U. Induction of bradyzoite-specific Toxoplasma gondii antigens in gamma interferon-treated mouse macrophages. *Infection and Immunity* **61**, 1141–1145 (1993).

70. Soete, M., Camus, D. & Dubrametz, J. F. Experimental Induction of Bradyzoite-Specific Antigen Expression and Cyst Formation by the RH Strain of *Toxoplasma gondii in Vitro*. *Experimental Parasitology* **78**, 361–370 (1994).

71. Ihara, F. & Nishikawa, Y. Starvation of low-density lipoprotein-derived cholesterol induces bradyzoite conversion in Toxoplasma gondii. *Parasites Vectors* **7**, 248 (2014).

72. Weiss, L. M. *et al.* A Cell Culture System for Study of the Development of Toxoplasma gondii Bradyzoites. *Journal of Eukaryotic Microbiology* **42**, 150–157 (1995).

73. Bohne, W. & Roos, D. S. Stage-specific expression of a selectable marker in *Toxoplasma gondii* permits selective inhibition of either tachyzoites or bradyzoites. *Molecular and Biochemical Parasitology* **88**, 115–126 (1997).

74. Cerutti, A., Blanchard, N. & Besteiro, S. The Bradyzoite: A Key Developmental Stage for the Persistence and Pathogenesis of Toxoplasmosis. *Pathogens* **9**, 234 (2020).

75. Eaton, M. S., Weiss, L. M. & Kim, K. Cyclic nucleotide kinases and tachyzoite–bradyzoite transition in *Toxoplasma gondii*. *International Journal for Parasitology* **36**, 107–114 (2006).

76. Sugi, T. *et al.* Toxoplasma gondii Cyclic AMP-Dependent Protein Kinase Subunit 3 Is Involved in the Switch from Tachyzoite to Bradyzoite Development. *mBio* **7**, 10.1128/mbio.00755-16 (2016).

77. Augusto, L., Wek, R. C. & Sullivan Jr, W. J. Host sensing and signal transduction during Toxoplasma stage conversion. *Molecular Microbiology* **115**, 839–848 (2021).

78. Diesing, L. *et al.* Besnoitia besnoiti: Studies on the definitive host and experimental infections in cattle. *Parasitol Res* **75**, 114–117 (1988).

79. Basso, W., Schares, G., Gollnick, N. S., Rütten, M. & Deplazes, P. Exploring the life cycle of Besnoitia besnoiti—Experimental infection of putative definitive and intermediate host species. *Veterinary Parasitology* **178**, 223–234 (2011).

80. Millán, J. *et al.* Large-scale serosurvey of *Besnoitia besnoiti* in free-living carnivores in Spain. *Veterinary Parasitology* **190**, 241–245 (2012).

81. Bigalke, R. D. Preliminary observations on the mechanical transmission of cyst organisms of Besnoitia besnoiti (Marotel, 1912) from a chronically infected bull to rabbits by

Glossina brevipalpis Newstead , 1910. *Journal of the South African Veterinary Association* **31**, 37–44 (1960).

82. Esteban-Gil, A. *et al.* No detection of Besnoitia besnoiti DNA in the semen of chronically infected bulls. *Parasitol Res* **113**, 2355–2362 (2014).
83. Medzhitov, R. & Janeway, C. Innate Immunity. *New England Journal of Medicine* **343**, 338–344 (2000).
84. Amersfoort, J., Eelen, G. & Carmeliet, P. Immunomodulation by endothelial cells — partnering up with the immune system? *Nat Rev Immunol* **22**, 576–588 (2022).
85. Kellie, S. & Al-Mansour, Z. Chapter Four - Overview of the Immune System. in *Micro and Nanotechnology in Vaccine Development* (eds Skwarczynski, M. & Toth, I.) 63–81 (William Andrew Publishing, 2017). doi:10.1016/B978-0-323-39981-4.00004-X.
86. Bassel, L. L. & Caswell, J. L. Bovine neutrophils in health and disease. *Cell Tissue Res* **371**, 617–637 (2018).
87. Farschtschi, S., Mattes, M. & Pfaffl, M. W. Advantages and Challenges of Differential Immune Cell Count Determination in Blood and Milk for Monitoring the Health and Well-Being of Dairy Cows. *Vet Sci* **9**, 255 (2022).
88. George, J. W., Snipes, J. & Lane, V. M. Comparison of bovine hematology reference intervals from 1957 to 2006. *Vet Clin Pathol* **39**, 138–148 (2010).
89. Jain, N. C., Paape, M. J. & Miller, R. H. Use of flow cytometry for determination of differential leukocyte counts in bovine blood. https://doi.org/10.2460/ajvr.1991.52.04.630 (1991) doi:10.2460/ajvr.1991.52.04.630.
90. Burn, G. L., Foti, A., Marsman, G., Patel, D. F. & Zychlinsky, A. The Neutrophil. *Immunity* **54**, 1377–1391 (2021).
91. Liew, P. X. & Kubes, P. The Neutrophil's Role During Health and Disease. *Physiological Reviews* **99**, 1223–1248 (2019).

92. Ng, L. G., Liu, Z., Kwok, I. & Ginhoux, F. Origin and Heterogeneity of Tissue Myeloid Cells: A Focus on GMP-Derived Monocytes and Neutrophils. *Annu Rev Immunol* **41**, 375–404 (2023).

93. Lawrence, S. M., Corriden, R. & Nizet, V. The Ontogeny of a Neutrophil: Mechanisms of Granulopoiesis and Homeostasis. *Microbiology and Molecular Biology Reviews* **82**, 10.1128/mmbr.00057-17 (2018).

94. Ng, L. G., Ostuni, R. & Hidalgo, A. Heterogeneity of neutrophils. *Nat Rev Immunol* **19**, 255–265 (2019).

95. Scapini, P., Marini, O., Tecchio, C. & Cassatella, M. A. Human neutrophils in the saga of cellular heterogeneity: insights and open questions. *Immunol Rev* **273**, 48–60 (2016).

96. Adrover, J. M., Nicolás-Ávila, J. A. & Hidalgo, A. Aging: A Temporal Dimension for Neutrophils. *Trends Immunol* **37**, 334–345 (2016).

97. Adrover, J. M. *et al.* A Neutrophil Timer Coordinates Immune Defense and Vascular Protection. *Immunity* **50**, 390-402.e10 (2019).

98. Ella, K., Csépányi-Kömi, R. & Káldi, K. Circadian regulation of human peripheral neutrophils. *Brain, Behavior, and Immunity* **57**, 209–221 (2016).

99. Amulic, B., Cazalet, C., Hayes, G. L., Metzler, K. D. & Zychlinsky, A. Neutrophil Function: From Mechanisms to Disease. *Annual Review of Immunology* **30**, 459–489 (2012).

100. Filippi, M.-D. Neutrophil transendothelial migration: updates and new perspectives. *Blood* **133**, 2149–2158 (2019).

101. Hickey, M. J. & Kubes, P. Intravascular immunity: the host–pathogen encounter in blood vessels. *Nat Rev Immunol* **9**, 364–375 (2009).

102. Ley, K., Laudanna, C., Cybulsky, M. I. & Nourshargh, S. Getting to the site of inflammation: the leukocyte adhesion cascade updated. *Nat Rev Immunol* **7**, 678–689 (2007).

103. Sadik, C. D., Kim, N. D. & Luster, A. D. Neutrophils cascading their way to inflammation. *Trends in Immunology* **32**, 452–460 (2011).

104. Faurschou, M. & Borregaard, N. Neutrophil granules and secretory vesicles in inflammation. *Microbes and Infection* **5**, 1317–1327 (2003).

105. Segal, A. W. & Shatwell, K. P. The NADPH Oxidase of Phagocytic Leukocytes. *Annals of the New York Academy of Sciences* **832**, 215–222 (1997).

106. Valenta, H., Erard, M., Dupré-Crochet, S. & Nüβe, O. The NADPH Oxidase and the Phagosome. in *Molecular and Cellular Biology of Phagocytosis* (ed. Hallett, M. B.) 153–177 (Springer International Publishing, Cham, 2020). doi:10.1007/978-3-030-40406-2_9.

107. Borregaard, N. Neutrophils, from Marrow to Microbes. *Immunity* **33**, 657–670 (2010).

108. Lacy, P. The role of Rho GTPases and SNAREs in mediator release from granulocytes. *Pharmacology & Therapeutics* **107**, 358–376 (2005).

109. Metzler, K. D. *et al.* Myeloperoxidase is required for neutrophil extracellular trap formation: implications for innate immunity. *Blood* **117**, 953–959 (2011).

110. Papayannopoulos, V. Neutrophil extracellular traps in immunity and disease. *Nat Rev Immunol* **18**, 134–147 (2018).

111. Lacy, P. Mechanisms of Degranulation in Neutrophils. *All Asth Clin Immun* **2**, 98 (2006).

112. Othman, A., Sekheri, M. & Filep, J. G. Roles of neutrophil granule proteins in orchestrating inflammation and immunity. *The FEBS Journal* **289**, 3932–3953 (2022).

113. Belambri, S. A. *et al.* NADPH oxidase activation in neutrophils: Role of the phosphorylation of its subunits. *European Journal of Clinical Investigation* **48**, e12951 (2018).

114. Nunes, P., Demaurex, N. & Dinauer, M. C. Regulation of the NADPH Oxidase and Associated Ion Fluxes During Phagocytosis. *Traffic* **14**, 1118–1131 (2013).

115. Sumimoto, H. Structure, regulation and evolution of Nox-family NADPH oxidases that produce reactive oxygen species. *The FEBS Journal* **275**, 3249–3277 (2008).

116. Winterbourn, C. C., Kettle, A. J. & Hampton, M. B. Reactive Oxygen Species and Neutrophil Function. *Annual Review of Biochemistry* **85**, 765–792 (2016).

117. Ulfig, A. & Leichert, L. I. The effects of neutrophil-generated hypochlorous acid and other hypohalous acids on host and pathogens. *Cell. Mol. Life Sci.* **78**, 385–414 (2021).

118. Naish, E. *et al.* The formation and function of the neutrophil phagosome. *Immunological Reviews* **314**, 158–180 (2023).

119. Nordenfelt, P. & Tapper, H. Phagosome dynamics during phagocytosis by neutrophils. *Journal of Leukocyte Biology* **90**, 271–284 (2011).

120. Uribe-Querol, E. & Rosales, C. Phagocytosis. in *Encyclopedia of Infection and Immunity* (ed. Rezaei, N.) 99–109 (Elsevier, Oxford, 2022). doi:10.1016/B978-0-12-818731-9.00049-5.

121. Freeman, S. A. & Grinstein, S. Phagocytosis: receptors, signal integration, and the cytoskeleton. *Immunological Reviews* **262**, 193–215 (2014).

122. Rosales, C. & Uribe-Querol, E. Phagocytosis: A Fundamental Process in Immunity. *BioMed Research International* **2017**, 9042851 (2017).

123. Niedergang, F. & Grinstein, S. How to build a phagosome: new concepts for an old process. *Current Opinion in Cell Biology* **50**, 57–63 (2018).

124. Branzk, N. *et al.* Neutrophils sense microbe size and selectively release neutrophil extracellular traps in response to large pathogens. *Nat Immunol* **15**, 1017–1025 (2014).

125. Manfredi, A. A., Ramirez, G. A., Rovere-Querini, P. & Maugeri, N. The Neutrophil's Choice: Phagocytose vs Make Neutrophil Extracellular Traps. *Front. Immunol.* **9**, (2018).

126. Warnatsch, A. *et al.* Reactive Oxygen Species Localization Programs Inflammation to Clear Microbes of Different Size. *Immunity* **46**, 421–432 (2017).

127. Poli, V. & Zanoni, I. Neutrophil intrinsic and extrinsic regulation of NETosis in health and disease. *Trends in Microbiology* **31**, 280–293 (2023).

128. Ravindran, M., Khan, M. A. & Palaniyar, N. Neutrophil Extracellular Trap Formation: Physiology, Pathology, and Pharmacology. *Biomolecules* **9**, 365 (2019).

129. Brinkmann, V. *et al.* Neutrophil Extracellular Traps Kill Bacteria. *Science* **303**, 1532–1535 (2004).

130. Abi Abdallah, D. S. *et al.* Toxoplasma gondii Triggers Release of Human and Mouse Neutrophil Extracellular Traps. *Infect Immun* **80**, 768–777 (2012).

131. Saitoh, T. *et al.* Neutrophil Extracellular Traps Mediate a Host Defense Response to Human Immunodeficiency Virus-1. *Cell Host & Microbe* **12**, 109–116 (2012).

132. Urban, C. F., Reichard, U., Brinkmann, V. & Zychlinsky, A. Neutrophil extracellular traps capture and kill Candida albicans yeast and hyphal forms. *Cellular Microbiology* **8**, 668–676 (2006).

133. Pinegin, B., Vorobjeva, N., Pashenkov, M. & Chernyak, B. The role of mitochondrial ROS in antibacterial immunity. *Journal of Cellular Physiology* **233**, 3745–3754 (2018).

134. Douda, D. N., Khan, M. A., Grasemann, H. & Palaniyar, N. SK3 channel and mitochondrial ROS mediate NADPH oxidase-independent NETosis induced by calcium influx. *Proc. Natl. Acad. Sci. U.S.A.* **112**, 2817–2822 (2015).

135. Lood, C. *et al.* Neutrophil extracellular traps enriched in oxidized mitochondrial DNA are interferogenic and contribute to lupus-like disease. *Nat Med* **22**, 146–153 (2016).

136. Malawista, S. & De Boisfleury Chevance, A. The cytokineplast: purified, stable, and functional motile machinery from human blood polymorphonuclear leukocytes. *Journal of Cell Biology* **95**, 960–973 (1982).

137. Pilsczek, F. H. *et al.* A Novel Mechanism of Rapid Nuclear Neutrophil Extracellular Trap Formation in Response to Staphylococcus aureus. *The Journal of Immunology* **185**, 7413–7425 (2010).

138. Yipp, B. G. *et al.* Infection-induced NETosis is a dynamic process involving neutrophil multitasking in vivo. *Nat Med* **18**, 1386–1393 (2012).

139. Yipp, B. G. & Kubes, P. NETosis: how vital is it? *Blood* **122**, 2784–2794 (2013).

140. Yousefi, S. *et al.* Untangling "NETosis" from NETs. *Eur. J. Immunol.* **49**, 221–227 (2019).

141. Pfister, H. Neutrophil Extracellular Traps and Neutrophil-Derived Extracellular Vesicles: Common Players in Neutrophil Effector Functions. *Diagnostics* **12**, 1715 (2022).

142. Takeuchi, O. & Akira, S. Pattern Recognition Receptors and Inflammation. *Cell* **140**, 805–820 (2010).

143. Metzler, K. D., Goosmann, C., Lubojemska, A., Zychlinsky, A. & Papayannopoulos, V. A Myeloperoxidase-Containing Complex Regulates Neutrophil Elastase Release and Actin Dynamics during NETosis. *Cell Reports* **8**, 883–896 (2014).

144. Papayannopoulos, V., Metzler, K. D., Hakkim, A. & Zychlinsky, A. Neutrophil elastase and myeloperoxidase regulate the formation of neutrophil extracellular traps. *Journal of Cell Biology* **191**, 677–691 (2010).

145. Vorobjeva, N. V. & Chernyak, B. V. NADPH Oxidase Modulates Ca2+-Dependent Formation of Neutrophil Extracellular Traps. *Moscow Univ. Biol.Sci. Bull.* **75**, 104–109 (2020).

146. Chen, W. A. & Boskovic, D. S. Neutrophil Extracellular DNA Traps in Response to Infection or Inflammation, and the Roles of Platelet Interactions. *International Journal of Molecular Sciences* **25**, 3025 (2024).

147. Huang, J., Hong, W., Wan, M. & Zheng, L. Molecular mechanisms and therapeutic target of NETosis in diseases. *MedComm* **3**, e162 (2022).

148. Schoen, J. *et al.* Neutrophils' Extracellular Trap Mechanisms: From Physiology to Pathology. *International Journal of Molecular Sciences* **23**, 12855 (2022).

149. Junger, W. G. Purinergic regulation of neutrophil chemotaxis. *Cell. Mol. Life Sci.* **65**, 2528–2540 (2008).

150. Wang, X. & Chen, D. Purinergic Regulation of Neutrophil Function. *Front. Immunol.* **9**, (2018).

151. Antonioli, L., Pacher, P., Vizi, E. S. & Haskó, G. CD39 and CD73 in immunity and inflammation. *Trends in Molecular Medicine* **19**, 355–367 (2013).

152. Baron, L. *et al.* The NLRP3 inflammasome is activated by nanoparticles through ATP, ADP and adenosine. *Cell Death Dis* **6**, e1629–e1629 (2015).

153. Burnstock, G. & Knight, G. E. Cellular Distribution and Functions of P2 Receptor Subtypes in Different Systems. in *International Review of Cytology* vol. 240 31–304 (Elsevier, 2004).

154. Chen, Y. *et al.* Purinergic signaling: a fundamental mechanism in neutrophil activation. *Sci Signal* **3**, ra45 (2010).

155. Fredholm, B. B., IJzerman, A. P., Jacobson, K. A., Klotz, K. N. & Linden, J. International Union of Pharmacology. XXV. Nomenclature and classification of adenosine receptors. *Pharmacol Rev* **53**, 527–552 (2001).

156. Eltzschig, H. K., Sitkovsky, M. V. & Robson, S. C. Purinergic Signaling during Inflammation. *New England Journal of Medicine* **367**, 2322–2333 (2012).

157. Xu, K. *et al.* Adenosine from a biologic source regulates neutrophil extracellular traps (NETs). *Journal of Leukocyte Biology* **105**, 1225–1234 (2019).

158. Conejeros, I. *et al.* Glycolysis, monocarboxylate transport, and purinergic signaling are key events in Eimeria bovis-induced NETosis. *Front. Immunol.* **13**, (2022).

159. Di Virgilio, F., Ceruti, S., Bramanti, P. & Abbracchio, M. P. Purinergic signalling in inflammation of the central nervous system. *Trends in Neurosciences* **32**, 79–87 (2009).

160. Fredholm, B. B. Adenosine, an endogenous distress signal, modulates tissue damage and repair. *Cell Death Differ* **14**, 1315–1323 (2007).

161. Fuller, S. J., Stokes, L., Skarratt, K. K., Gu, B. J. & Wiley, J. S. Genetics of the P2X7 receptor and human disease. *Purinergic Signalling* **5**, 257–262 (2009).

162. Hasheminasab, S. S. *et al.* ATP Purinergic Receptor P2X1-Dependent Suicidal NETosis Induced by Cryptosporidium parvum under Physioxia Conditions. *Biology* **11**, 442 (2022).

163. Haskó, G., Linden, J., Cronstein, B. & Pacher, P. Adenosine receptors: therapeutic aspects for inflammatory and immune diseases. *Nat Rev Drug Discov* **7**, 759–770 (2008).

164. Qu, Y. *et al.* P2X7 Receptor-Stimulated Secretion of MHC Class II-Containing Exosomes Requires the ASC/NLRP3 Inflammasome but Is Independent of Caspase-1. *J Immunol* **182**, 5052–5062 (2009).

165. Villagra-Blanco, R. *et al.* Bovine Polymorphonuclear Neutrophils Cast Neutrophil Extracellular Traps against the Abortive Parasite Neospora caninum. *Front. Immunol.* **8**, (2017).

166. Grob, D. *et al.* Trypanosoma brucei brucei Induces Polymorphonuclear Neutrophil Activation and Neutrophil Extracellular Traps Release. *Front. Immunol.* **11**, (2020).

167. Garcia, D. & Shaw, R. J. AMPK: Mechanisms of Cellular Energy Sensing and Restoration of Metabolic Balance. *Molecular Cell* **66**, 789–800 (2017).

168. Kurumbail, R. G. & Calabrese, M. F. Structure and Regulation of AMPK. in *AMP-activated Protein Kinase* (eds Cordero, M. D. & Viollet, B.) 3–22 (Springer International Publishing, Cham, 2016). doi:10.1007/978-3-319-43589-3_1.

169. Shaw, R. J. *et al.* The tumor suppressor LKB1 kinase directly activates AMP-activated kinase and regulates apoptosis in response to energy stress. *Proceedings of the National Academy of Sciences* **101**, 3329–3335 (2004).

170. Woods, A. *et al.* Ca2+/calmodulin-dependent protein kinase kinase-β acts upstream of AMP-activated protein kinase in mammalian cells. *Cell Metabolism* **2**, 21–33 (2005).

171. Kim, J., Yang, G., Kim, Y., Kim, J. & Ha, J. AMPK activators: mechanisms of action and physiological activities. *Exp Mol Med* **48**, e224 (2016).

172. Zhao, X. *et al.* Activation of AMPK attenuates neutrophil proinflammatory activity and decreases the severity of acute lung injury. *Am J Physiol Lung Cell Mol Physiol* **295**, L497-504 (2008).

173. Hardie, D. G. Minireview: the AMP-activated protein kinase cascade: the key sensor of cellular energy status. *Endocrinology* **144**, 5179–5183 (2003).

174. Park, D. W. *et al.* Activation of AMPK enhances neutrophil chemotaxis and bacterial killing. *Mol Med* **19**, 387–398 (2013).

175. Bae, H.-B. *et al.* AMP-activated protein kinase enhances the phagocytic ability of macrophages and neutrophils. *FASEB J* **25**, 4358–4368 (2011).

176. Alba, G. *et al.* Stimulators of AMP-activated protein kinase inhibit the respiratory burst in human neutrophils. *FEBS Lett* **573**, 219–225 (2004).

177. Skendros, P., Mitroulis, I. & Ritis, K. Autophagy in Neutrophils: From Granulopoiesis to Neutrophil Extracellular Traps. *Front. Cell Dev. Biol.* **6**, 109 (2018).

178. Sil, P., Muse, G. & Martinez, J. A ravenous defense: canonical and non-canonical autophagy in immunity. *Current Opinion in Immunology* **50**, 21–31 (2018).

179. Laplante, M. & Sabatini, D. M. mTOR Signaling in Growth Control and Disease. *Cell* **149**, 274–293 (2012).

180. Lin, M. G. & Hurley, J. H. Structure and function of the ULK1 complex in autophagy. *Current Opinion in Cell Biology* **39**, 61–68 (2016).

181. Park, S. Y. *et al.* Autophagy Primes Neutrophils for Neutrophil Extracellular Trap Formation during Sepsis. *Am J Respir Crit Care Med* **196**, 577–589 (2017).

182. Remijsen, Q. *et al.* Neutrophil extracellular trap cell death requires both autophagy and superoxide generation. *Cell Res* **21**, 290–304 (2011).

183. Mathiesen, A. *et al.* Endothelial Extracellular Vesicles: From Keepers of Health to Messengers of Disease. *International Journal of Molecular Sciences* **22**, 4640 (2021).

184. Szempruch, A. J., Dennison, L., Kieft, R., Harrington, J. M. & Hajduk, S. L. Sending a message: extracellular vesicles of pathogenic protozoan parasites. *Nat Rev Microbiol* **14**, 669–675 (2016).

185. Varikuti, S. *et al.* The role of vascular endothelium and exosomes in human protozoan parasitic diseases. *Vessel plus* **4**, (2020).

186. Wu, Z. *et al.* Extracellular Vesicle-Mediated Communication Within Host-Parasite Interactions. *Frontiers in Immunology* **9**, (2019).

187. Zhang, Y., Liu, Y., Liu, H. & Tang, W. H. Exosomes: biogenesis, biologic function and clinical potential. *Cell & Bioscience* **9**, 19 (2019).

188. Zhang, Y. *et al.* Exosome: A Review of Its Classification, Isolation Techniques, Storage, Diagnostic and Targeted Therapy Applications. *Int J Nanomedicine* **15**, 6917–6934 (2020).

189. Tian, T., Wang, Y., Wang, H., Zhu, Z. & Xiao, Z. Visualizing of the cellular uptake and intracellular trafficking of exosomes by live-cell microscopy. *Journal of Cellular Biochemistry* **111**, 488–496 (2010).

190. Kolonics, F. *et al.* Neutrophils produce proinflammatory or anti-inflammatory extracellular vesicles depending on the environmental conditions. *J Leukoc Biol* **109**, 793–806 (2021).

191. Timár, C. I. *et al.* Antibacterial effect of microvesicles released from human neutrophilic granulocytes. *Blood* **121**, 510–518 (2013).

192. Sung, P.-S., Huang, T.-F. & Hsieh, S.-L. Extracellular vesicles from CLEC2-activated platelets enhance dengue virus-induced lethality via CLEC5A/TLR2. *Nat Commun* **10**, 2402 (2019).

193. Carrera-Bravo, C., Koh, E. Y. & Tan, K. S. W. The roles of parasite-derived extracellular vesicles in disease and host-parasite communication. *Parasitology International* **83**, 102373 (2021).

194. Khosravi, M., Mirsamadi, E. S., Mirjalali, H. & Zali, M. R. Isolation and Functions of Extracellular Vesicles Derived from Parasites: The Promise of a New Era in Immunotherapy, Vaccination, and Diagnosis. *International Journal of Nanomedicine* **15**, 2957–2969 (2020).

195. Marcilla, A. *et al.* Extracellular vesicles in parasitic diseases. *J Extracell Vesicles* **3**, 10.3402/jev.v3.25040 (2014).

196. Marti, M. & Johnson, P. J. Emerging roles for extracellular vesicles in parasitic infections. *Current Opinion in Microbiology* **32**, 66–70 (2016).

197. Montaner, S. *et al.* The Role of Extracellular Vesicles in Modulating the Host Immune Response during Parasitic Infections. *Front. Immunol.* **5**, (2014).

198. Sharma, M., Lozano-Amado, D., Chowdhury, D. & Singh, U. Extracellular Vesicles and Their Impact on the Biology of Protozoan Parasites. *Tropical Medicine and Infectious Disease* **8**, 448 (2023).

199. Masebo, N. T., Bolcato, M., Jacinto, J., Gentile, A. & Militerno, G. GENITAL TRACT INVOLVEMENTS IN A BULL AFFECTED BY BOVINE BESNOITIOSIS. *Large Animal Review* **28**, 161–164 (2022).

200. Maksimov, P., Hermosilla, C., Kleinertz, S., Hirzmann, J. & Taubert, A. Besnoitia besnoiti infections activate primary bovine endothelial cells and promote PMN adhesion and NET formation under physiological flow condition. *Parasitol Res* **115**, 1991–2001 (2016).

201. Díaz-Godínez, C. & Carrero, J. C. The state of art of neutrophil extracellular traps in protozoan and helminthic infections. *Bioscience Reports* **39**, BSR20180916 (2019).

202. Zhang, J., Sun, Y. & Zheng, J. The State of Art of Extracellular Traps in Protozoan Infections (Review). *Front. Immunol.* **12**, (2021).

203. Uribe-Querol, E. & Rosales, C. Neutrophils versus Protozoan Parasites: Plasmodium, Trichomonas, Leishmania, Trypanosoma, and Entameoba. *Microorganisms* **12**, 827 (2024).

204. Rochael, N. C. *et al.* Classical ROS-dependent and early/rapid ROS-independent release of Neutrophil Extracellular Traps triggered by Leishmania parasites. *Sci Rep* **5**, 18302 (2015).

205. DeSouza-Vieira, T. *et al.* Neutrophil extracellular traps release induced by Leishmania: role of PI3Kγ, ERK, PI3Kσ, PKC, and [Ca2+]. *Journal of Leukocyte Biology* **100**, 801–810 (2016).

206. Sousa-Rocha, D. *et al.* Trypanosoma cruzi and Its Soluble Antigens Induce NET Release by Stimulating Toll-Like Receptors. *PLOS ONE* **10**, e0139569 (2015).

207. Ogier-Denis, E., Mkaddem, S. B. & Vandewalle, A. NOX enzymes and Toll-like receptor signaling. *Semin Immunopathol* **30**, 291–300 (2008).

208. Heiner, I., Eisfeld, J. & Lückhoff, A. Role and regulation of TRP channels in neutrophil granulocytes. *Cell Calcium* **33**, 533–540 (2003).

209. Villalta, F. & Kierszenbaum, F. Effects of human colony-stimulating factor on the uptake and destruction of a pathogenic parasite (Trypanosoma cruzi) by human neutrophils. *J Immunol* **137**, 1703–1707 (1986).

210. Sanderson, C. J. & Souza, W. de. A morphological study of the interaction between Trypanosoma Cruzi and rat eosinophils, neutrophils and macrophages In Vitro. *J Cell Sci* **37**, 275–286 (1979).

211. Villalta, F. & Kierszenbaum, F. Role of polymorphonuclear cells in Chagas' disease. I. Uptake and mechanisms of destruction of intracellular (amastigote) forms of Trypanosoma cruzi by human neutrophils. *J Immunol* **131**, 1504–1510 (1983).

212. de Andrade, M. F. *et al.* Involvement of neutrophils in Chagas disease pathology. *Parasite Immunology* **40**, e12593 (2018).

213. Behrendt, J. H., Ruiz, A., Zahner, H., Taubert, A. & Hermosilla, C. Neutrophil extracellular trap formation as innate immune reactions against the apicomplexan parasite Eimeria bovis. *Veterinary Immunology and Immunopathology* **133**, 1–8 (2010).

214. Muñoz-Caro, T. *et al.* Eimeria bovis-triggered neutrophil extracellular trap formation is CD11b-, ERK 1/2-, p38 MAP kinase- and SOCE-dependent. *Vet Res* **46**, 23 (2015).

215. Muñoz-Caro, T., Machado Ribeiro da Silva, L., Rentería-Solis, Z., Taubert, A. & Hermosilla, C. Neutrophil extracellular traps in the intestinal mucosa of Eimeria-infected animals. *Asian Pacific Journal of Tropical Biomedicine* **6**, 301–307 (2016).

216. Villagra-Blanco, R. *et al.* Bottlenose dolphins (*Tursiops truncatus*) do also cast neutrophil extracellular traps against the apicomplexan parasite *Neospora caninum*. *International Journal for Parasitology: Parasites and Wildlife* **6**, 287–294 (2017).

217. Wei, Z. *et al.* Canine Neutrophil Extracellular Traps Release Induced by the Apicomplexan Parasite Neospora caninum In Vitro. *Front. Immunol.* **7**, (2016).

218. Wei, Z. *et al.* Toxoplasma gondii Triggers Neutrophil Extracellular Traps Release in Dogs. *Front. Cell. Infect. Microbiol.* **10**, (2020).

219. Jin, Z. *et al.* Toxoplasma gondii-induced neutrophil extracellular traps are relevant to glycolysis, TLR2, and TLR4 MAPK signaling pathway in goats. *Parasitol Res* **123**, 34 (2023).

220. Macedo, I. S. *et al.* Human neutrophil extracellular traps do not impair in vitro Toxoplasma gondii infection. *Front. Immunol.* **14**, (2023).

221. Muñoz-Caro, T., Lendner, M., Daugschies, A., Hermosilla, C. & Taubert, A. NADPH oxidase, MPO, NE, ERK1/2, p38 MAPK and Ca2+ influx are essential for *Cryptosporidium parvum*-induced NET formation. *Developmental & Comparative Immunology* **52**, 245–254 (2015).

222. Grabbe, M. *et al.* Cryptosporidium parvum-induced neutrophil extracellular traps in neonatal calves is a stage-independent process. *Front. Vet. Sci.* **10**, 1256726 (2023).

223. Knackstedt, S. L. *et al.* Neutrophil extracellular traps drive inflammatory pathogenesis in malaria. *Science Immunology* **4**, eaaw0336 (2019).

224. Muñoz Caro, T., Hermosilla, C., Silva, L. M. R., Cortes, H. & Taubert, A. Neutrophil Extracellular Traps as Innate Immune Reaction against the Emerging Apicomplexan Parasite Besnoitia besnoiti. *PLoS ONE* **9**, e91415 (2014).

225. Zhou, E. *et al. Besnoitia besnoiti* bradyzoite stages induce suicidal- and rapid vital-NETosis. *Parasitology* **147**, 401–409 (2020).

226. Zhou, E. *et al.* Metabolic requirements of Besnoitia besnoiti tachyzoite-triggered NETosis. *Parasitol Res* **119**, 545–557 (2020).

227. Conejeros, I. *et al.* Histone H2A and Bovine Neutrophil Extracellular Traps Induce Damage of *Besnoitia besnoiti*-Infected Host Endothelial Cells but Fail to Affect Total Parasite Proliferation. *Biology* **8**, 78 (2019).

228. Conejeros, I. *et al.* The CAMKK/AMPK Pathway Contributes to Besnoitia besnoiti-Induced NETosis in Bovine Polymorphonuclear Neutrophils. *International Journal of Molecular Sciences* **25**, 8442 (2024).

229. Espinosa, G. *et al.* Bovine PMN responses to extracellular vesicles released by Besnoitia besnoiti tachyzoites and B. besnoiti-infected host cells. *Front. Immunol.* **15**, (2024).

230. Conejeros, I. *et al.* AMPK and CAMKK activation participate in early events of Toxoplasma gondii-triggered NET formation in bovine polymorphonuclear neutrophils. *Front. Vet. Sci.* **12**, 1557509 (2025).

231. Espinosa, G., Conejeros, I., Rojas-Barón, L., Hermosilla, C. R. & Taubert, A. Besnoitia besnoiti-induced neutrophil clustering and neutrophil extracellular trap formation depend on P2X1 purinergic receptor signaling. *Frontiers in Immunology* **14**, (2023).

232. Schindelin, J. *et al.* Fiji: an open-source platform for biological-image analysis. *Nat Methods* **9**, 676–682 (2012).

233. Otsu, N. A Threshold Selection Method from Gray-Level Histograms. *IEEE Transactions on Systems, Man, and Cybernetics* **9**, 62–66 (1979).

234. Brinkmann, V., Goosmann, C., Kühn, L. I. & Zychlinsky, A. Automatic quantification of in vitro NET formation. *Frontiers in Immunology* **3**, (2013).

235. Tanaka, K. *et al.* In Vivo Characterization of Neutrophil Extracellular Traps in Various Organs of a Murine Sepsis Model. *PLoS ONE* **9**, e111888 (2014).

236. Morales-Kastresana, A. *et al.* Labeling Extracellular Vesicles for Nanoscale Flow Cytometry. *Sci Rep* **7**, 1878 (2017).

237. Neubert, E. *et al.* Chromatin swelling drives neutrophil extracellular trap release. *Nature Communications* **9**, 3767 (2018).

238. Itakura, A. & McCarty, O. J. T. Pivotal role for the mTOR pathway in the formation of neutrophil extracellular traps via regulation of autophagy. *American Journal of Physiology-Cell Physiology* **305**, C348–C354 (2013).

239. Remijsen, Q. *et al.* Neutrophil extracellular trap cell death requires both autophagy and superoxide generation. *Cell Res* **21**, 290–304 (2011).

240. Thiam, H. R., Wong, S. L., Wagner, D. D. & Waterman, C. M. Cellular Mechanisms of NETosis. *Annual Review of Cell and Developmental Biology* **36**, 191–218 (2020).

241. Todorova, D., Simoncini, S., Lacroix, R., Sabatier, F. & Dignat-George, F. Extracellular Vesicles in Angiogenesis. *Circulation Research* **120**, 1658–1673 (2017).

242. Mulcahy, L. A., Pink, R. C. & Carter, D. R. F. Routes and mechanisms of extracellular vesicle uptake. *Journal of Extracellular Vesicles* **3**, 24641 (2014).

243. Neumann, A., Brogden, G. & Von Köckritz-Blickwede, M. Extracellular Traps: An Ancient Weapon of Multiple Kingdoms. *Biology* **9**, 34 (2020).

244. Villagra-Blanco, R., Silva, L., Conejeros, I., Taubert, A. & Hermosilla, C. Pinniped- and Cetacean-Derived ETosis Contributes to Combating Emerging Apicomplexan Parasites (Toxoplasma gondii, Neospora caninum) Circulating in Marine Environments. *Biology* **8**, 12 (2019).

245. Worku, M., Rehrah, D., Ismail, H. D., Asiamah, E. & Adjei-Fremah, S. A Review of the Neutrophil Extracellular Traps (NETs) from Cow, Sheep and Goat Models. *IJMS* **22**, 8046 (2021).

246. Miranda, F. J. B. *et al.* Toxoplasma gondii-Induced Neutrophil Extracellular Traps Amplify the Innate and Adaptive Response. *mBio* **12**, e01307-21 (2021).

247. Muñoz-Caro, T. *et al.* The Role of TLR2 and TLR4 in Recognition and Uptake of the Apicomplexan Parasite Eimeria bovis and Their Effects on NET Formation. *Pathogens* **10**, 118 (2021).

248. Omar, M. & Abdelal, H. NETosis in Parasitic Infections: A Puzzle That Remains Unsolved. *International Journal of Molecular Sciences* **24**, 8975 (2023).

249. Muñoz-Caro, T., Silva, L. M. R., Ritter, C., Taubert, A. & Hermosilla, C. Besnoitia besnoiti tachyzoites induce monocyte extracellular trap formation. *Parasitol Res* **113**, 4189–4197 (2014).

250. Borregaard, N. & Herlin, T. Energy Metabolism of Human Neutrophils during Phagocytosis. *J. Clin. Invest.* **70**, 550–557 (1982).

251. Fossati, G. *et al.* The Mitochondrial Network of Human Neutrophils: Role in Chemotaxis, Phagocytosis, Respiratory Burst Activation, and Commitment to Apoptosis. *The Journal of Immunology* **170**, 1964–1972 (2003).

252. Sadiku, P. *et al.* Neutrophils Fuel Effective Immune Responses through Gluconeogenesis and Glycogenesis. *Cell Metabolism* **33**, 411-423.e4 (2021).

253. Chacko, B. K. *et al.* Methods for defining distinct bioenergetic profiles in platelets, lymphocytes, monocytes, and neutrophils, and the oxidative burst from human blood. *Laboratory Investigation* **93**, 690–700 (2013).

254. Pelletier, M., Billingham, L. K., Ramaswamy, M. & Siegel, R. M. Extracellular Flux Analysis to Monitor Glycolytic Rates and Mitochondrial Oxygen Consumption. in *Methods in Enzymology* vol. 542 125–149 (Elsevier, 2014).

255. Jeon, J.-H., Hong, C.-W., Kim, E. Y. & Lee, J. M. Current Understanding on the Metabolism of Neutrophils. *Immune Netw* **20**, e46 (2020).

256. Idzko, M., Ferrari, D. & Eltzschig, H. K. Nucleotide signalling during inflammation. *Nature* **509**, 310–317 (2014).

257. Chen, Y. *et al.* ATP Release Guides Neutrophil Chemotaxis via P2Y2 and A3 Receptors. *Science* **314**, 1792–1795 (2006).

258. Trautmann, A. Extracellular ATP in the Immune System: More Than Just a 'Danger Signal'. *Science Signaling* **2**, pe6–pe6 (2009).

259. Junger, W. G. Immune cell regulation by autocrine purinergic signalling. *Nat. Rev. Immunol.* **11**, 201–212 (2011).

260. Bao, Y. *et al.* Mitochondria Regulate Neutrophil Activation by Generating ATP for Autocrine Purinergic Signaling. *Journal of Biological Chemistry* **289**, 26794–26803 (2014).

261. Bao, Y. *et al.* mTOR and differential activation of mitochondria orchestrate neutrophil chemotaxis. *Journal of Cell Biology* **210**, 1153–1164 (2015).

262. Weninger, W., Biro, M. & Jain, R. Leukocyte migration in the interstitial space of non-lymphoid organs. *Nat Rev Immunol* **14**, 232–246 (2014).

263. Wang, X. *et al.* Endotoxin-induced autocrine ATP signaling inhibits neutrophil chemotaxis through enhancing myosin light chain phosphorylation. *PNAS* **114**, 4483–4488 (2017).

264. Sil, P. *et al.* P2Y6 Receptor Antagonist MRS2578 Inhibits Neutrophil Activation and Aggregated Neutrophil Extracellular Trap Formation Induced by Gout-Associated Monosodium Urate Crystals. *The Journal of Immunology* **198**, 428–442 (2017).

265. Muñoz-Caro, T. *et al. Eimeria bovis*-triggered neutrophil extracellular trap formation is CD11b-, ERK 1/2-, p38 MAP kinase- and SOCE-dependent. *Vet Res* **46**, (2015).

266. Burgos, R. A., Conejeros, I., Hidalgo, M. A., Werling, D. & Hermosilla, C. Calcium influx, a new potential therapeutic target in the control of neutrophil-dependent inflammatory diseases in bovines. *Veterinary Immunology and Immunopathology* **143**, 1–10 (2011).

267. Viollet, B. *et al.* AMPK inhibition in health and disease. *Critical Reviews in Biochemistry and Molecular Biology* **45**, 276–295 (2010).

268. Steinckwich, N. *et al.* Potent inhibition of store-operated Ca $^{2+}$ influx and superoxide production in HL60 cells and polymorphonuclear neutrophils by the pyrazole derivative BTP2. *Journal of Leukocyte Biology* **81**, 1054–1064 (2007).

269. Conejeros, I. *et al.* 2-Aminoethoxydiphenyl borate (2-APB) reduces respiratory burst, MMP-9 release and CD11b expression, and increases l-selectin shedding in bovine neutrophils. *Research in Veterinary Science* **92**, 103–110 (2012).

270. Muñoz-Caro, T., Lendner, M., Daugschies, A., Hermosilla, C. & Taubert, A. NADPH oxidase, MPO, NE, ERK1/2, p38 MAPK and Ca2+ influx are essential for Cryptosporidium parvum-induced NET formation. *Dev. Comp. Immunol.* **52**, 245–254 (2015).

271. Lawson, N. D. *et al.* Modulation of a calcium/calmodulin-dependent protein kinase cascade by retinoic acid during neutrophil maturation. *Experimental Hematology* **27**, 1682–1690 (1999).

272. Watanabe, M., Kaihatsu, T., Miwa, M. & Maeda, T. Ca2+/Calmodulin-dependent Protein Kinase II Inhibitors Potentiate Superoxide Production in Polymorphonuclear Leukocytes. *Journal of Pharmacy and Pharmacology* **51**, 295–300 (1999).

273. Verploegen, S., Lammers, J.-W. J., Koenderman, L. & Coffer, P. J. Identification and characterization of CKLiK, a novel granulocyte Ca++/calmodulin-dependent kinase. *Blood* **96**, 3215–3223 (2000).

274. Verploegen, S. *et al.* Characterization of the role of CaMKI-like kinase (CKLiK) in human granulocyte function. *Blood* **106**, 1076–1083 (2005).

275. Verploegen, S. *et al.* Role of Ca2+/calmodulin regulated signaling pathways in chemoattractant induced neutrophil effector functions. *European Journal of Biochemistry* **269**, 4625–4634 (2002).

276. Zhang, B. *et al.* Transcriptomics of circulating neutrophils in dairy cows with subclinical hypocalcemia. *Front. Vet. Sci.* **9**, (2022).

277. Ong, C. W. M. *et al.* Neutrophil-Derived MMP-8 Drives AMPK-Dependent Matrix Destruction in Human Pulmonary Tuberculosis. *PLOS Pathogens* **11**, e1004917 (2015).

278. Carretta, M. D. *et al.* β-hydroxybutyrate and hydroxycarboxylic acid receptor 2 agonists activate the AKT, ERK and AMPK pathways, which are involved in bovine neutrophil chemotaxis. *Sci Rep* **10**, 12491 (2020).

279. Wang, X. *et al.* Estrogen Regulates Glucose Metabolism in Cattle Neutrophils Through Autophagy. *Front. Vet. Sci.* **8**, (2021).

280. Kim, J., Kundu, M., Viollet, B. & Guan, K.-L. AMPK and mTOR regulate autophagy through direct phosphorylation of Ulk1. *Nat Cell Biol* **13**, 132–141 (2011).

281. Abdel Malik, R. *et al.* AMP-Activated Protein Kinase α2 in Neutrophils Regulates Vascular Repair via Hypoxia-Inducible Factor-1α and a Network of Proteins Affecting Metabolism and Apoptosis. *Circulation Research* **120**, 99–109 (2017).

282. Song, Y. *et al.* Effects of Fluorine on Neutrophil Extracellular Trap Formation through Regulating AMPK/p38 Signaling Pathway. *Oxidative Medicine and Cellular Longevity* **2021**, 6693921 (2021).

283. Levine, B. & Kroemer, G. Autophagy in the Pathogenesis of Disease. *Cell* **132**, 27–42 (2008).

284. Levine, B., Mizushima, N. & Virgin, H. W. Autophagy in immunity and inflammation. *Nature* **469**, 323–335 (2011).

285. Jones, S. A., Mills, K. H. G. & Harris, J. Autophagy and inflammatory diseases. *Immunology & Cell Biology* **91**, 250–258 (2013).

286. Egan, D. F. *et al.* Phosphorylation of ULK1 (hATG1) by AMP-Activated Protein Kinase Connects Energy Sensing to Mitophagy. *Science* **331**, 456–461 (2011).

287. Herb, M., Gluschko, A. & Schramm, M. LC3-associated phagocytosis - The highway to hell for phagocytosed microbes. *Seminars in Cell & Developmental Biology* **101**, 68–76 (2020).

288. Mitroulis, I. *et al.* Regulation of the autophagic machinery in human neutrophils. *European Journal of Immunology* **40**, 1461–1472 (2010).

289. Rossi, A. & Lord, J. M. Adiponectin inhibits neutrophil apoptosis via activation of AMP kinase, PKB and ERK 1/2 MAP kinase. *Apoptosis* **18**, 1469–1480 (2013).

290. Brown, G. B. & Roth, J. A. Comparison of the response of bovine and human neutrophils to various stimuli. *Veterinary Immunology and Immunopathology* **28**, 201–218 (1991).

291. Pitale, D. M., Gendalur, N. S., Descoteaux, A. & Shaha, C. *Leishmania donovani* Induces Autophagy in Human Blood–Derived Neutrophils. *The Journal of Immunology* **202**, 1163–1175 (2019).

292. Coakley, G., Maizels, R. M. & Buck, A. H. Exosomes and Other Extracellular Vesicles: The New Communicators in Parasite Infections. *Trends in Parasitology* **31**, 477–489 (2015).

293. Fernandez-Becerra, C. *et al.* Guidelines for the purification and characterization of extracellular vesicles of parasites. *J Extracell Biol* **2**, e117 (2023).

294. Théry, C. *et al.* Minimal information for studies of extracellular vesicles 2018 (MISEV2018): a position statement of the International Society for Extracellular Vesicles and update of the MISEV2014 guidelines. *J Extracell Vesicles* **7**, 1535750 (2018).

295. Todorova, D., Simoncini, S., Lacroix, R., Sabatier, F. & Dignat-George, F. Extracellular Vesicles in Angiogenesis. *Circulation Research* **120**, 1658–1673 (2017).

296. Couper, K. N. *et al.* Parasite-Derived Plasma Microparticles Contribute Significantly to Malaria Infection-Induced Inflammation through Potent Macrophage Stimulation. *PLOS Pathogens* **6**, e1000744 (2010).

297. Mantel, P.-Y. *et al.* Malaria-infected erythrocyte-derived microvesicles mediate cellular communication within the parasite population and with the host immune system. *Cell Host Microbe* **13**, 521–534 (2013).

298. Hu, G. *et al.* Release of Luminal Exosomes Contributes to TLR4-Mediated Epithelial Antimicrobial Defense. *PLOS Pathogens* **9**, e1003261 (2013).

299. Herrera-Zelada, N. *et al.* Endothelial activation impairs the function of small extracellular vesicles. *Front. Pharmacol.* **14**, (2023).

300. Hurtado Gutiérrez, M. J., Allard, F. L., Mosha, H. T., Dubois, C. M. & McDonald, P. P. Human Neutrophils Generate Extracellular Vesicles That Modulate Their Functional Responses. *Cells* **12**, 136 (2022).

301. Díaz-Godínez, C., Ríos-Valencia, D. G., García-Aguirre, S., Martínez-Calvillo, S. & Carrero, J. C. Immunomodulatory effect of extracellular vesicles from Entamoeba histolytica trophozoites: Regulation of NETs and respiratory burst during confrontation with human neutrophils. *Front. Cell. Infect. Microbiol.* **12**, (2022).

302. Ren, X. *et al.* Macrophage–endothelial cell crosstalk orchestrates neutrophil recruitment in inflamed mucosa. *J Clin Invest* **133**, (2023).

303. Jiang, K. *et al.* Peripheral Circulating Exosome-Mediated Delivery of miR-155 as a Novel Mechanism for Acute Lung Inflammation. *Molecular Therapy* **27**, 1758–1771 (2019).

304. Liu, Z. *et al.* Exosomes derived from mesenchymal stem cells inhibit neointimal hyperplasia by activating the Erk1/2 signalling pathway in rats. *Stem Cell Res Ther* **11**, 220 (2020).

305. Zhang, J. *et al.* Exosomes Derived from Human Endothelial Progenitor Cells Accelerate Cutaneous Wound Healing by Promoting Angiogenesis Through Erk1/2 Signaling. *Int J Biol Sci* **12**, 1472–1487 (2016).

306. Chen, Z., Larregina, A. T. & Morelli, A. E. Impact of extracellular vesicles on innate immunity. *Curr Opin Organ Transplant* **24**, 670–678 (2019).

307. Li, Y. *et al.* Characterization of exosomes derived from Toxoplasma gondii and their functions in modulating immune responses. *IJN* **Volume 13**, 467–477 (2018).

308. Silverman, J. M. *et al.* Leishmania exosomes modulate innate and adaptive immune responses through effects on monocytes and dendritic cells. *J Immunol* **185**, 5011–5022 (2010).

309. Aline, F., Bout, D., Amigorena, S., Roingeard, P. & Dimier-Poisson, I. Toxoplasma gondii antigen-pulsed-dendritic cell-derived exosomes induce a protective immune response against T. gondii infection. *Infect Immun* **72**, 4127–4137 (2004).

310. Jebbari, Roberts, Ferguson, Bluethmann, & Alexander. A protective role for IL-6 during early infection with Toxoplasma gondii. *Parasite Immunology* **20**, 231–239 (1998).

311. Lima, T. S., Gov, L. & Lodoen, M. B. Evasion of Human Neutrophil-Mediated Host Defense during Toxoplasma gondii Infection. *mBio* **9**, 10.1128/mbio.02027-17 (2018).

312. Hong, C.-W. Extracellular Vesicles of Neutrophils. *Immune Netw* **18**, e43 (2018).

313. Gierlikowska, B., Stachura, A., Gierlikowski, W. & Demkow, U. The Impact of Cytokines on Neutrophils' Phagocytosis and NET Formation during Sepsis—A Review. *Int J Mol Sci* **23**, 5076 (2022).

314. Keshari, R. S. *et al.* Cytokines Induced Neutrophil Extracellular Traps Formation: Implication for the Inflammatory Disease Condition. *PLOS ONE* **7**, e48111 (2012).

315. Mulcahy, L. A., Pink, R. C. & Carter, D. R. F. Routes and mechanisms of extracellular vesicle uptake. *Journal of Extracellular Vesicles* **3**, 24641 (2014).

316. Morales-Kastresana, A. *et al.* Labeling Extracellular Vesicles for Nanoscale Flow Cytometry. *Sci Rep* **7**, 1878 (2017).

8. EHRENWÖRTLICHE ERKLÄRUNG

Ich erkläre: Ich habe die vorgelegte Thesis selbständig, ohne unerlaubte fremde Hilfe und nur mit den Hilfen angefertigt, die ich in der Thesis angegeben habe. Alle Textstellen, die wörtlich oder sinngemäß aus veröffentlichten oder nicht veröffentlichten Schriften entnommen sind, und alle Angaben, die auf mündlichen Auskünften beruhen, sind als solche kenntlich gemacht. Bei den von mir durchgeführten und in der Thesis erwähnten Untersuchungen habe ich die Grundsätze guter wissenschaftlicher Praxis, wie sie in der Satzung der Justus-Liebig-Universität Gießen zur Sicherung guter wissenschaftlicher Praxis niedergelegt sind, eingehalten.

Gabriel Rodolfo Espinosa Espinoza

9. FUNDING

The present work was financed by the “Deutsche Forschungsgemeinschaft” (DFG project: TA291/4-3). I was funded by a DAAD/BECAS Chile, 2021 (57559515). The publication fees were partially funded by the Open Access Publication Fund from JLU Giessen.

10. ACKNOWLEDGMENTS

First and foremost, I would like to express my deepest gratitude to **Prof. Dr. Anja Taubert**, my supervisor, for her invaluable support, insightful guidance, and constant encouragement throughout my doctoral studies. Her mentorship has shaped both my scientific and personal development.

I am also sincerely thankful to **Prof. Dr. Carlos Hermosilla** for his co-supervision, thoughtful advice, and ongoing support during my time at the Institute of Parasitology, JLU Gießen. Working within the inspiring team led by Prof. Taubert and Prof. Hermosilla has been an incredible privilege.

A special thanks goes to **Dr. Conejeros**, who led the project and guided me closely throughout the research. His patience, expertise, and mentorship were essential in bringing this work to life.

I am also grateful to my colleagues and friends who made the journey more collaborative, joyful, and intellectually stimulating. In particular, I thank **Dr. Grob**, **Dr. Larrazábal**, **Dr. Rojas**, and **Frau Salinas** (soon to be Dr. Salinas) for their camaraderie, support, and scientific input. Special acknowledgement to my future wife **Dr. Segeritz**, for her invaluable and unconditional support throughout much of my personal life during my PhD. I also extend my appreciation to the **technical staff** at the institute, whose dedication and assistance were crucial for the smooth progress of my experiments.

A heartfelt and slightly humorous thank you goes to the **cows at the university farm**, whose weekly blood donations were indispensable for my research. I owe a good part of my thesis to their generous contributions.

Most importantly, I want to express my profound gratitude to my family in Chile. To my father **Gabriel**, my brother **Roberto**, and in loving memory of my mother **Soledad**, who passed away in 2013 but continues to live in my heart and inspire me every day. I would also like to warmly thank **Carmen**, my father's wife and my "new mom," for her love and kindness. She has become a special part of my life, and I truly appreciate the care and support she has given me and our family.

Although I have been living in Germany since 2021, the love, strength, and unshakable belief of my family have been my guiding light throughout this journey. This accomplishment belongs to them as much as it does to me.

Thank you all for being part of this journey.

édition scientifique
VVB LAUFERSWEILER VERLAG

VVB LAUFERSWEILER VERLAG
STAUFENBERGRING 15
D-35396 GIESSEN

Tel: 0641-5599888 Fax: -5599890
redaktion@doktorverlag.de
www.doktorverlag.de

ISBN: 978 3 8359 7273 5

Cover graphic: © Author